Self-Powered Sensor System Design in Dynamic Low Harvesting Environments

by

Luis Javier Lopez Ruiz

A dissertation presented to

The Faculty of the School of Engineering and Applied Science

University of Virginia

In partial fulfillment of the requirements for the degree

Doctor of Philosophy in Electrical Engineering

December 2021

APPROVAL SHEET

This

Dissertation

is submitted in partial fulfillment of the requirements
for the degree of

Doctor of Philosophy

Author: Luis Javier Lopez Ruiz

This Dissertation has been read and approved by the examining committee:

Advisor: John Lach

Advisor: Daniel Quinn

Committee Member: Benton Calhoun

Committee Member: Joanne Dugan

Committee Member: Mark Sochor

Committee Member:

Committee Member:

Committee Member:

Accepted for the School of Engineering and Applied Science:

Jennifer L. West, School of Engineering and Applied Science

December 2021

"If we knew what we were doing,

we wouldn't call it research."

-John Lach

Abstract

The internet of things (IoT) covers a wide umbrella of applications that range from smart environments, transportation, to even healthcare. However, challenges in interoperability, security and privacy, resilience, and reliability need to be overcome for the full realization of the IoT. To improve reliability, energy harvesting and self-powered operation are promising alternatives to sustainably and efficiently power remote sensing devices by harnessing energy from ambient energy sources while ensuring continuous operation. Although successful demonstrations of self-powered sensing have been presented in the literature, applications with very low energy harvesting levels and high energy fluctuations continue to be a challenge for researchers and designers.

Current works in self-powered sensing have focused on developing more efficient harvesters, ultra-low power electronics, and new dynamic power management strategies. However, the synergistic integration of these individual efforts is necessary to enable self-powered operation in dynamic low harvesting environments. Furthermore, the dynamics of energy harvesting under these conditions are not yet well understood, resulting in not so efficient and/or heavily duty-cycled systems that can miss relevant information. Thus, this work proposes a framework for the design of self-powered sensors intended to operate in dynamic low harvesting environments. The framework integrates three components: energy harvesting profiling, system-level power optimizations, and application-specific quality of information (QoI) metrics. The methods in the framework are implemented in two medical applications as case studies: vigilant cardiac monitoring and continuous respiratory health monitoring.

In the case of energy harvesting profiling, an energy harvesting and data collection (EHDC) system was developed to provide a deeper understanding of energy harvesting dynamics in real-world scenarios. The EHDC platform monitors and records the instantaneous usable power

generated by body-worn harvesters, while also collecting human activity and environmental data to provide a comprehensive real-world evaluation of two energy harvesting modalities common to wearable sensors: solar and thermoelectric. Additionally, a mathematical model for piezoelectric cantilevers that correlates fluid flow characteristics with energy harvesting availability was created. The model incorporates principles from fluid dynamics, elasticity theory, piezoelectric science, and circuit design. These techniques aim to provide real-world energy harvesting information under dynamic low harvesting environments to assist in the design and selection of harvesters and low power electronics.

In regards to system-level power optimizations, system power modeling was used as a tool to identify potential variables for power optimizations and analyze their impact in the total system's power consumption to meet specific power budgets defined by the harvesters or sensing requirements. Similarly, energy storage sizing was conducted as a mechanism to deal with energy harvesting fluctuations and to guarantee the system operation during prolonged energy harvesting draughts. Furthermore, the effect of piezoelectric cantilever shape and size was investigated to determine the best form factor for self-powered fluid flow sensors that operate under non-resonance and sub-Hz conditions. This evaluation was complemented by an assessment of two common energy harvesting circuits for piezoelectric harvesters in dynamic low harvesting environments.

Finally, the definition of application-specific information metrics as an alternative to traditional digital signal metrics to determine the relation between system power consumption and quality of information is proposed. This technique aims to assist in the formalization of specifications for sensing systems during the design process to achieve self-powered operation while providing useful information. The successful implementation of the proposed methods resulted in the demonstration of functional prototypes of self-powered health monitoring systems for the two case studies discussed in this dissertation.

Acknowledgments

First and foremost, I would like to express my sincerest gratitude to my advisor Prof. John Lach for giving me the opportunity to come to UVA to pursue my Ph.D. studies. Prof. Lach has not only taught me how to be a good researcher, but also has showed me firsthand how to be a great mentor. One that cares for their students' academic success and also their wellbeing as a person. Prof. Lach has always showed great support to me and knows better than anyone perhaps, the personal challenges I have faced to be at this point in my career. He has believed in me even at moments when I have doubted myself. I am very fortunate to have him as my advisor, and for that I am extremely thankful.

I would also like to thank professors Dan Quinn, Ben Calhoun, Joanne Dugan, and Dr. Mark Sochor for being part of my Ph.D. committee and their feedback to bring together this dissertation. I want to extend a special thanks to Prof. Quinn who has also been my co-advisor, formally and informally since Prof. Lach became the Dean of Engineering at GWU. His way of conducting research, leading his group, and teaching have made him a role model to me as a young researcher. If I were to become a PI, I would strive to be like Prof. Quinn during his time at UVA.

I also want to thank Prof. Calhoun for being a great resource during my time at the university. The close collaboration between our research groups gave me the opportunity to learn from him as a researcher, project manager, and professor. The best teaching moments with Prof. Calhoun were always the days before the ASSIST site visit. By asking me to describe step by step how we reached a problem with the SAP and making me think about the next steps before conducting any testing or debugging, help me sharpen my problem-solving skills.

There are many research groups, but there will be only one INERTIA team. To everyone and each one of the students that belonged to our team at any extent, I am thankful for all we shared during our journeys at the university. A special thanks to Josh Dugan, Philip Asare, Dawei Fan, Sriram Dandu, Ridwan Alam, Victor Sobral, Matthew Rider, Nutta Homdee, Matt Engelhard, Jamie Hayes, Ahmad Mansouri, Tamanna Hammid, Ben Gahemmaghami, Neeraj Gandhi, Alyson Irizarry, Renee Mitchell, Phillip Seaton, Sean Wolfe, Seth VanderBraak, Will Define, Yudel Martinez, Noelle Law, Emmanuel Ogunjirin, and Vivian Lin. To Terry Tigner for all she did for our group.

I want to thank Prof. Jiaqi Gong for all his mentorship and support during his time as a Research Scientist at UVA. He helped me establish a foundation to start my research and become a leader in our research group. Prof. Gong became a great friend to me.

Another special mention I need to do is for Chris Lukas and Farah Yahya. Although they were part of a different group, they were great senior students that had an important role in my formation as a researcher. Similarly, I am thankful for sharing the pains and glories of ASSIST with Jacob Breiholz. We made a great team during the multiple site visits and as leaders for the SAP testbed. We were so lucky that our demo system always broke down the night before the site visit, and when everyone wanted to leave or give up, Jacob was as persistent or stubborn as me to stay and figure out any problem that came up. Together we could fix anything. Thank you to Lucy Fitzgerald for embarking in an unknown journey when we started the implantables project. Without her, the project would have not developed to the level it is today.

I would not have been able to complete my studies without the support of my family. Muchas gracias papás por todos los sacrificios que hicieron y siguen haciendo por mí y por mi hermana. Sin ustedes nunca habríamos llegado hasta acá. No hay palabras ni forma de expresar lo mucho que les debo. Este título es tan suyo como lo es mío. Gracias hermana, Paty, por siempre estar orgullosa de mí cuando en verdad es lo opuesto. Lo mismo para mi Sirena. Lo escribo en español porque ella es Zamorana. Por muchas aventuras mas juntos. ¡Gracias por todo!

Finally, I would like to thank the ASSIST Center for supporting my graduate studies and for the opportunity to meet great collaborators.

Contents

List of Figures

List of Tables

Chapter 1

Introduction

The rapid evolution of the internet, the continuous development of new devices with wireless communication capabilities, along with the reduction in cost of these technologies have enabled the conception of the Internet of Things (IoT) [1]. The IoT encompasses the realization of connecting any device, wired or wirelessly, to the internet and to other devices, creating a network for continuous exchange of information about people and their environment. The extent of the IoT and its application covers multiple sectors that go from smart cities and infrastructure, as well as smart manufacturing and automation, to wearables and smart connected health [2], [3].

Even though the number of interconnected devices has been growing rapidly [4], challenges in interoperability, security and privacy, and resilience and reliability remain to be addressed in order to achieve a successful realization of the IoT [5]. Given that most devices will require to operate wirelessly due to accessibility constraints dictated by the application, *sustainably* and *efficiently* powering these devices becomes a relevant issue. Aware of this limitation, researchers have looked into multiple alternatives, with a special focus in the design of ultra-low power hardware, the development of more efficient power management techniques, and the possibility of harnessing energy from the ambient [6]. In the case of ultra-low power hardware, new designs of computation elements such as microcontrollers, microprocessors and system-on-chip (SoC) devices have been able to bring the power consumption down to single-digit μW [7], [8]. Novel approaches for power management looking at the system from the energy source or the energy consumer point of view have been presented in the literature [9]. Similarly, harvesters to harness

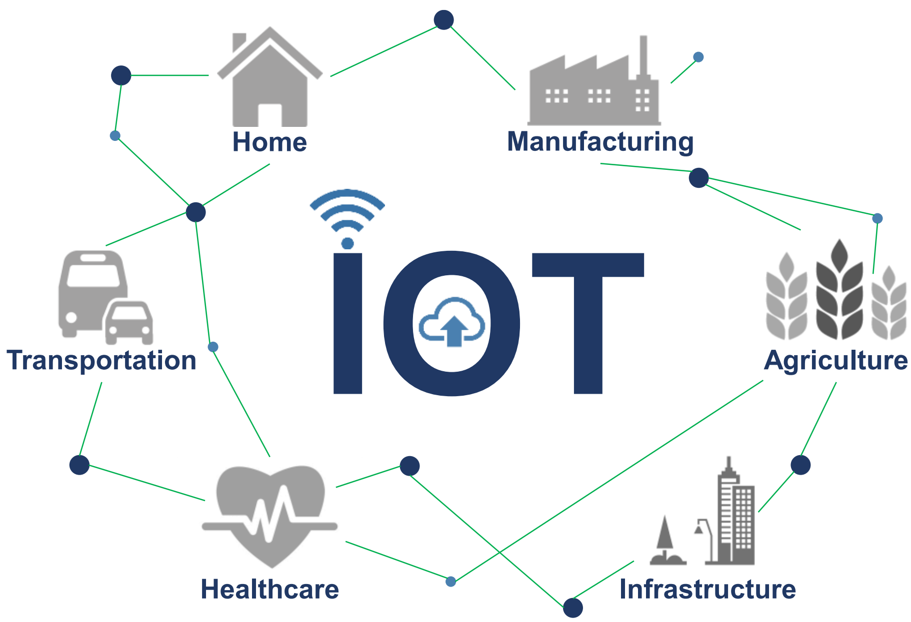

Figure 1.1 | The Internet of Things (IoT). The IoT refers to a network of interconnected devices sharing information about ourselves and our environment that covers a wide umbrella of applications that are part of our daily lives for an enhanced life experience.

energy from light, radio frequency (RF), motion and heat have been developed as potential alternatives to batteries [10]. In conjunction, these efforts have brought to life the idea of a new type of self-powered device that can operate quasi-perpetually to move toward the conception of a better, smarter, and more connected world.

1.1. Motivation

Conquering disease has been identified by several health leader organizations as one of the twenty-first century challenges [11]. Globally, chronic diseases and neonatal conditions are the leading causes of death worldwide, with the former being a major driver of health costs and impacting workforce patterns [12], [13]. According to the Centers for Disease Control and Prevention, 6 in 10 adults in the United States present a chronic condition, and 90% of the nation's $3.8 trillion in annual health care expenditures are used to provide care for these patients. Chronic conditions such as heart disease, chronic lower respiratory diseases, and stroke are at the top of the list of causes of death in the country, alongside cancer and accidents [14]–[18].

Condition	Total Cases (Millions)	Associated Cost ($ USD Billions)	Deaths per 100 000 Population
Heart Disease	30.3	219	161.5
Cancer	1.8[1]	50	146.2
Chronic Lung Disease	35	12	47.8
Diabetes	34.2	327	21.6
Stroke	0.795[2]	8	37

Table 1.1 | Leading causes of death in the U. S. Top five chronic conditions in the U. S. as leading causes of death and their associated cost per year [14]-[18]. [1]New diagnosed cases in 2020. [2]Estimated number of strokes per year.

In parallel, wearable sensing technology has become ubiquitous in our daily lives, providing insights in our health with the aim of improving quality of life. According to recent data from Statista, the number of connected wearable devices around the world went from 325 million in 2016 to 722 million in 2019 [150]. In the United States alone, 32% of the population that participated in the Statista Global Consumer Survey 2021 responded to personally use a wearable device on a daily basis, with Fitbit fitness trackers and Apple smart watches being predominant among users [151]. Having the ability to continuously monitor users' physiological and environmental data presents the opportunity to better diagnose, treat, and prevent diseases in ways that previously were never conceived [19]. Furthermore, as wearables follow the trend of other technologies and the manufacturing costs are being reduced while the robustness and maturity increases, these systems have the potential to help with the disparities in healthcare by bringing health equity at a global scale and bridging the gaps between developed countries and in development or sub-developed countries [20]–[23].

Multiple studies have shown evidence that wearable technology has the potential to transform healthcare [24]–[26]. However, its widespread adoption in this domain has been prevented given the general challenges of IoT technologies. In addition, by the nature of wearable devices, human factors define specific constraints that need to be addressed in conjunction with the more generalized issues. A study presented in 2015 looking into challenges for use and adoption of wearable activity trackers identified battery-related issues such as difficulty incorporating the devices into a daily routine (e.g., irregular charging patterns) and physical design and aesthetics

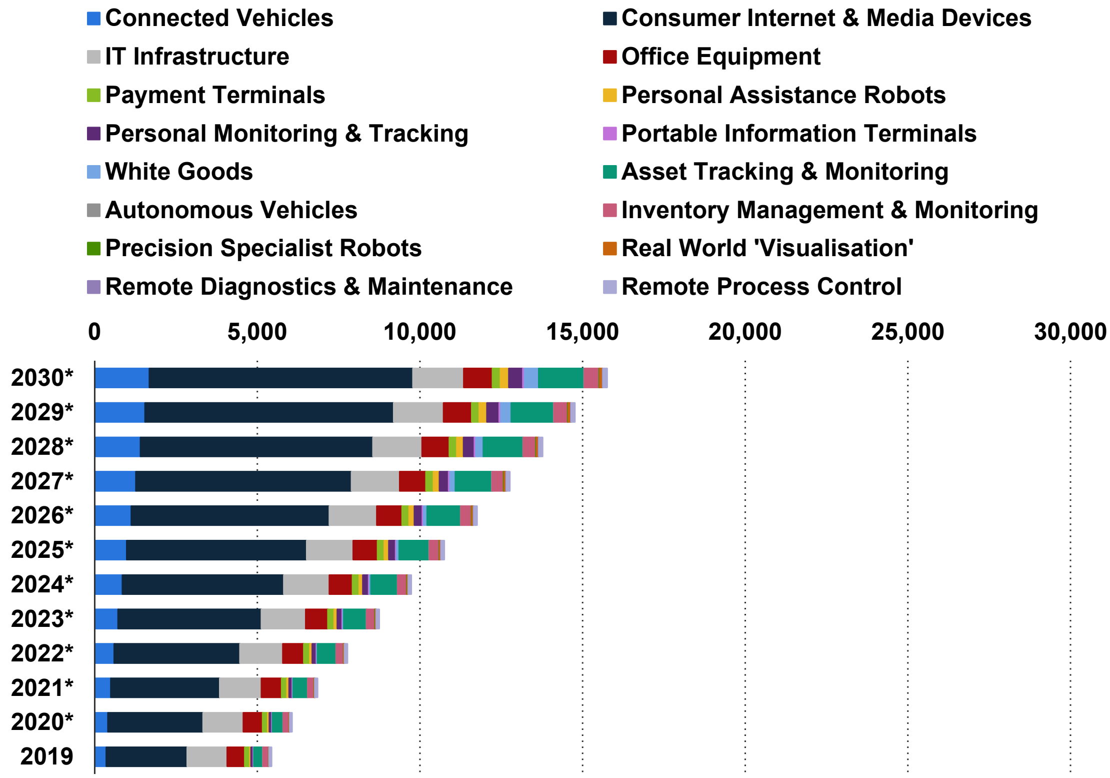

Figure 1.2 | Connected IoT devices worldwide. Growth of IoT connected devices worldwide from 2019 to 2030 (*forecasted) by use case (adapted from [150]).

(e.g., form factor) as two main challenges for users when wearing the devices for the six weeks period that the study was conducted [27]. Conversely, the researches recognized that data management (e.g., privacy and security) as well as accuracy were equally important concerns for the participants. A couple more studies motivated by the slow integration of wearable and implantable technologies into clinical care presented a comprehensive patient data set about mobile medical technology. The authors concluded that in order to improve acceptance and compliance, the system needed to be small, discreet, unobtrusive, and preferably incorporated into everyday objects. Additionally, they made a recommendation about considering the target user groups at an early stage of the design process and the need for bigger data sets regarding user preferences that can inform the development of future wearable technology [28], [29].

1.2. Thesis

The main objective of this work is to provide a framework for the design of self-powered sensors intended to operate in dynamic low harvesting environments (i.e., low power energy harvesting and high energy fluctuations), such as wearable and implantable conditions. A self-powered sensing system for long term monitoring can generate more data and capture more critical events than battery-powered devices, allowing for better decision making in the respective target application. Additionally, eliminating the need for batteries can help address challenges related to reliability, sustainability and maintenance costs to help in the full realization of the IoT. The framework presented in this dissertation incorporates three elements: energy harvesting profiling, system-level power optimizations, and the use of application-specific Quality of Information (QoI) metrics.

Energy harvesting profiling is a process that correlates energy harvesting levels with environmental parameters relevant to the energy source. An energy harvesting profile is a graphical representation of that correlation over time, and has the value of filling up the gaps that exist from limited information normally presented in the harvesters' datasheets. In this same context, power optimizations refer to the process of boosting the energy harvesting levels and minimizing energy losses for an overall improved energy efficiency. At a system level, these optimizations are done through the appropriate selection of components and implementation of techniques used for the system's power management. Finally, QoI is the value that the information from the sensor provides. A higher value means a higher quality. Traditional sensor systems use digital signal metrics (e.g., sampling frequency following Nyquist theory, etc.) to evaluate QoI. However, for several applications, these metrics tend to lack appropriateness (i.e., the suitability of the information and the receiver, and the objective of the information), which leads to the generation of massive amounts of data that require further processing before they can be converted into actionable information.

With these considerations, the thesis statement of this dissertation is that *while individual technological advances for self-powered sensing are necessary, a framework that enables their synergistic integration can help achieve self-powered operation in dynamic low harvesting environments.*

1.3. Contributions

This dissertation incorporates multiple elements of circuit design, circuit modeling, and system modeling and implementation for self-powered sensors. These techniques are intended to support a proposed framework for the design of wireless sensing systems that can operate long-term from ambient energy sources while providing useful information to the user. The specific work is developed around two case studies – vigilant cardiac monitoring for atrial fibrillation (AFib) and continuous respiratory health monitoring in the airway. These two case studies are discussed in further detail in Chapter 2. The methodologies supporting the proposed framework for the design of self-powered sensors in each case study use different elements of energy harvesting profiling, system power optimization, and QoI application-specific metrics and their successful implementation is demonstrated with two functional systems for health monitoring.

The specific contributions within the proposed framework are as follow:

1. Design and implementation of an energy harvesting and data collection (EHDC) platform for energy harvesting profiling of solar cells and thermoelectric generators (TEGs) on the human body. Previous characterizations of these type of harvesters have been done to show the potential of energy harvesting from these devices. However, these studies have been done in their majority for scenarios where energy fluctuations are reduced an energy availability is relatively high. Furthermore, the few studies looking at wearable conditions present experiments conducted for short periods of time and limited number of activities. With this platform, long-term energy harvesting profiling can be conducted to capture energy harvesting dynamics in real-world conditions. The information that this platform

provides can aid researchers in the selection and sizing of harvesters for self-powered systems.

2. A characterization and mathematical model of piezoelectric cantilevers in oscillating complex flows, operating at sub-Hz and non-resonance conditions. Energy harvesting using piezoelectric cantilevers for fluid flow applications has been previously demonstrated. However, these demonstrations have been limited to scenarios where ideal conditions for the cantilevers are met (e.g., resonance conditions). Through this characterization, we show the potential of energy harvesting using these devices even in non-ideal harvesting conditions, expanding the potential applications of piezoelectric cantilevers in self-powered systems. In addition, the mathematical model represents a mechanism to quickly evaluate different physical parameters of the cantilever and their impact in energy harvesting.
3. An information-driven approach for self-powered sensor system design in dynamic low harvesting environments. The premise of this design approach is to deliver a specific QoI that the application of interest requires. Therefore, the sensing requirements of the application define the power consumption constraints in the system and guide the additional power optimizations to achieve self-powered operation.
4. A harvesting-limited approach for self-powered sensor system design in dynamic low harvesting environments. A system that is designed with this approach aims to expand the sensing opportunities to applications where other type of systems or approaches are not feasible.
5. A demonstration of self-powered sensor systems operating in dynamic low harvesting environments. This demonstration is the result of the integration of the different approaches presented in this dissertation and show the potential of the proposed framework to assist in the design of self-powered sensors for dynamic low harvesting environments.

While this work is presented in the domain of healthcare, the contributions defined above can be generalized to other IoT applications for remote monitoring that require long-term operation such as infrastructure and environmental monitoring. For instance, the EHDC platform -publicly available on GitHub – could be deployed near water monitoring stations to create a database of solar energy harvesting availability to develop better power management strategies for this type of sensors. Similarly, the characterization and model for piezoelectric cantilevers could be used in other flow systems such as HVAC to monitor air leakage and the overall system efficiency.

1.4. Dissertation Outline

The remaining chapters of this dissertation are organized as follows. Chapter 2 presents a general classification of energy harvesting systems based on energy neutrality between the amount of energy that is being harvested and the amount of energy that is being consumed. This classification is intended to assists in the definition of the scope of this work, but not necessarily be a canonical classification of energy harvesting systems. Next, a definition of dynamic low harvesting environments with respect to energy neutrality is introduced. Additionally, a definition of vigilant sensing and continuous sensing in the context of sensor systems as well as their differences are included. Finally, the two medical case studies supporting the development of methodologies for self-powered system design are outlined.

Chapter 3 presents the design and implementation of the EHDC platform and shows the collected energy harvesting profiles for two different deployments in the real world. The profiles show the highly dynamic behavior of energy harvesting, which contrasts with the more static behavior that can be obtained using available information from datasheets. The second half of the chapter is dedicated to the characterization and modeling of the piezoelectric cantilevers in oscillating flows under non-ideal harvesting conditions. The characterization is done using a custom rig integrated by a lung simulator, a cylindrical tube, a full bridge energy harvesting circuit, and a data acquisition system. This same setup is used in the development and validation of the mathematical model.

Chapter 4 explores different system power optimizations that aim to improve the energy harvesting levels, help in the selection of components during the definition of the system architecture to meet specific power budgets, and it also discusses the need for appropriate energy storage as a mechanism to deal with energy harvesting droughts. These optimizations are presented within the medical case studies for a better illustration and understanding. First, system power modeling and supercapacitor sizing for the cardiac monitoring system, and second, harvester selection and sizing for the respiratory monitoring system.

Chapter 5 is dedicated to the discussion about application-specific QoI metrics. QoI is the value that the information from the sensor provides. A higher value means a higher quality. Traditional sensor systems use digital signal metrics (e.g., sampling frequency following Nyquist theory, etc.) to evaluate QoI. However, for several applications, these metrics tend to lack appropriateness (i.e., the suitability of the information and the receiver, and the objective of the information). In this chapter, first we present how lower sampling frequencies and bit depth can provide enough information in the detection of AFib for the cardiac case study. We illustrate the impact in power savings when appropriate sensing specifications are used and the benefits of this type of analysis for self-powered operation when following an information-driven approach. Next, in the case of harvesting-limited systems, we discuss the relationship between energy harvesting levels and information through a transfer function that correlates both variables. This discussion presents a first order transfer function for the respiratory monitoring system and its limitations, as well as an exploration of the concept of broadband sensing using multiple harvesting-limited systems to increase QoI.

Chapter 6 demonstrates the potential and benefits of the proposed framework to assist in the design of self-powered systems by introducing two systems for health monitoring, one for each case study, which were implemented following the techniques discussed in this dissertation. The first system used for long-term cardiac monitoring is powered solely by body heat and integrates different novel sensors, ultra-low power electronics, and energy storage elements into an e-textile shirt with printed dry-electrodes to improve comfort and user compliance. The second system is a prototype for an implantable device that could be attached to the trachea for continuous respiratory monitoring. The system is powered by piezoelectric cantilevers excited by the airflow in the airway, and it demonstrates the relation between energy harvesting levels and flow conditions.

Lastly, Chapter 7 presents the conclusion of this dissertation with a summary of the contributions, and a discussion about open problems, as well as potential future directions for this research.

Chapter 2

Background and Case Studies

2.1. Energy Harvesting Systems

Energy harvesting is the process of converting ambient energy (e.g., solar energy, thermal energy, mechanical energy, etc.) into electrical energy, as shown in Figure 2.1. This concept of energy harvesting shares the same principle as the large-scale renewable energy generation. In the general sense, the purpose of an energy harvesting system is to harness ambient energy and store it or deliver it to a load to perform a task.

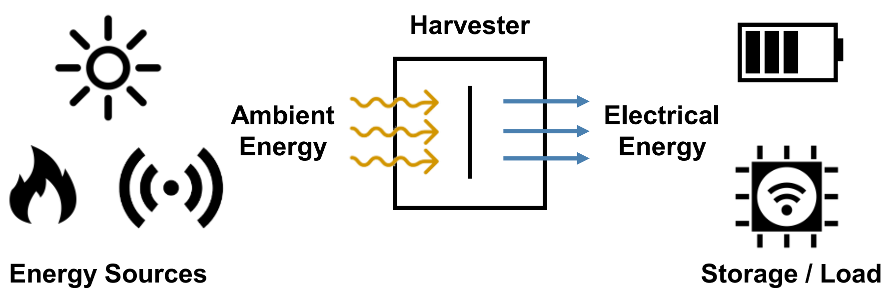

Figure 2.1 | Energy harvesting. The process of energy harvesting refers to the conversion of ambient energy into electrical energy for storage or to supply power to a load.

In order to define the scope of this work, we classified the energy harvesting systems based on the energy balance between the amount of energy that is being harvested and the amount of energy that is being consumed. Using this relationship, energy harvesting systems can be grouped into three different categories: energy negative systems, energy neutral systems, and energy positive systems.

An energy negative system is one that does not use energy harvesting as the main energy source. The purpose of energy harvesting is then to supplement the main energy source in emergency situations where, for any given reason, the main source is not available. Thus, in this type of systems, the amount of energy that is being consumed is higher than the energy that is being harvested and, the majority of times, the harvested energy is stored for later use. An example of this type of system is a battery-powered sensor that uses the stored harvested energy to perform some data backup when the main source is interrupted to avoid losing information or to extend the battery life of the system. In contrast, an energy positive system operates in such a way that the amount of energy that is being harvested is higher than the energy that is being consumed. One can think of a renewable energy generation system such as a solar farm as an energy positive system. Finally, we define the energy neutral systems as those where the harvested energy is equal to the amount of energy that is being consumed. This is where most self-powered sensors aim to operate and where the efforts of this work will focus.

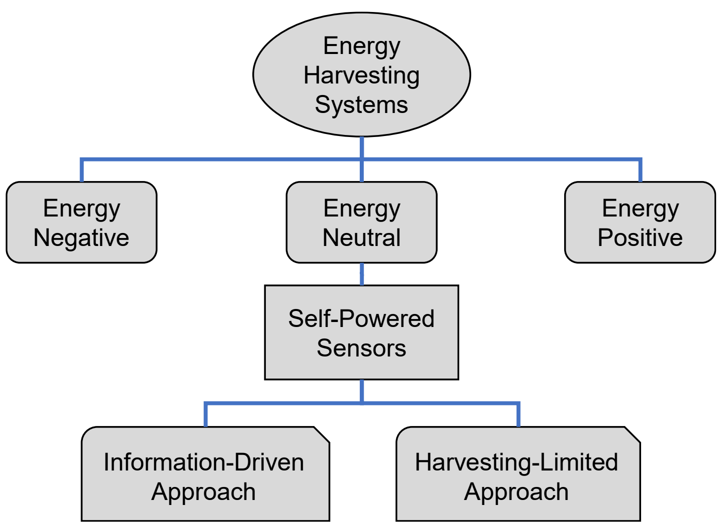

Figure 2.2 | Energy Harvesting Systems. Proposed classification of energy harvesting systems based on the energy balance between harvested energy and consumed energy – the central branch defines the area of interest for this work.

It is important to recognize that not all self-powered sensor systems are meant to operate under equal conditions, and therefore, there is no single *recipe* for their design. In this thesis, we present two different approaches for self-powered sensor design in dynamic low harvesting environments – an information-driven design approach, and a harvesting-limited operation approach. Even though the two design approaches are different, they are developed using the same framework introduced in Chapter 1. For each approach, different elements of energy harvesting profiling, system-level power optimizations and QoI metrics are defined, and used in different stages of the design process according to the premise of each approach -i.e., to meet specific sensing requirements or to operate with a predefined energy budget.

In the information-driven design approach, we determine what specific information the sensor needs to provide as the first step. Then we correlate this information to system requirements and derive the system design and power optimizations. Finally, we determine the appropriate harvester based on the energy harvesting profiles. In contrast, for the harvesting-limited operation approach, we first determine the energy harvesting levels based on application-specific constraints such as form factor and harvesting conditions through energy harvesting profiling. Then we define the system architecture using the energy profiles, perform system-level power optimizations, and we conclude by deriving what type of useful information the sensor provides. The goal of this approach is not to meet specific sensing requirement but instead to enable sensing capabilities in applications where otherwise it would not be possible or where a different type of sensing results impractical.

By establishing these design approaches, we demonstrate that the proposed framework can be applied in multiple scenarios, illustrating the generalizability of these methods in the realization of self-powered sensors. Figure 2.2 shows the proposed approaches within the classification of energy harvesting systems and Figure 2.3 presents a complete illustration of the proposed framework and the two design approaches for self-powered sensor design. The intersection areas between each approach and the elements comprising the framework are intentionally represented with different sizes to indicate that when developing a design approach, there are no constraints regarding the use of the methods in the framework.

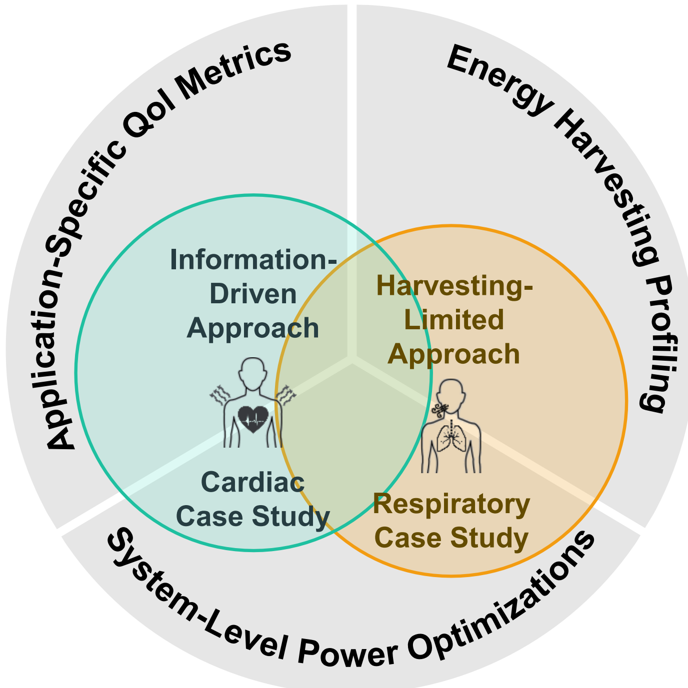

Figure 2.3 | Proposed framework for self-powered sensor design. The proposed framework is integrated by three fundamental methods: energy harvesting profiling, system-level power optimizations, and application-specific QoI metrics. These methods can be applied to create different design approaches for self-powered systems.

2.2. Dynamic Low Harvesting Environments

The harvesting conditions where wireless sensor nodes operate are as diverse and dynamic as the applications themselves. The work presented in this dissertation aims to support applications where energy harvesting levels are low, and therefore a definition of low harvesting environments is necessary.

A search in Google Scholar with the words “energy harvesting systems” shows about 2, 530, 000 results. Although not all of those results are about specific individual sensor systems, the big majority of the papers present some prototype demonstrating the operation of the system using a modality of energy harvesting. In general, the energy harvesting levels in these applications range from micro- to milli-watts, and even in some cases watts [30]–[39]. With this wide range of energy harvesting levels, it is difficult to establish a deterministic value to identify low harvesting environments. However, we try to illustrate the concept using some of the studies and applications found in the literature, one at the μW level and another one at the W level.

The approximate harvested power with a thermoelectric harvester of 1 cm^2 using body heat can produce on average 9 μW to 25 μW [40]. A state-of-the-art, low-power, wearable ECG system using commercial of the shelf (COTS) components has an average power consumption of approximately 12 mW [41]. In order to power this device from the body using a TEG, the harvester would require a surface area of 480 cm^2, which results impractical in a wearable application. Under these circumstances, one can say that the ECG system will be operating in a low harvesting environment. Yet, a custom ultra-low power system for ECG monitoring only consumes 1.02 μW [8]. Then using 1 cm^2 of the same thermoelectric harvester, the custom system can be powered without any constraints. In this scenario, even though the harvesting conditions are similar, one cannot consider this a low harvesting environment for such ECG system.

A commercial hydro-turbine for energy harvesting from a streamflow can generate about 1 W of power at an average flow velocity of 1 m/s, while a typical set of sensors for water quality monitoring consumes approximately 1.5 W [42]. If an energy harvesting system for water quality monitoring were to use those devices – the harvester and the sensors – in a stream where the average velocity is below the 1 m/s flow velocity, that harvesting scenario can be considered a low harvesting environment. In contrast, in a scenario where the same set of devices are deployed for the same application but in a different stream where average flow velocities are 2 m/s, this cannot be considered a low harvesting environment.

Using this rationale of only looking at the power generated and power consumed by a system makes easier to identify a low harvesting environment. However, this is a limited approach that does not consider other important elements of energy harvesting systems, which are application-specific. A more comprehensive approach needs to examine other constraints such as the presence of storage elements, form factor, device availability, etc. Therefore, the designer must analyze each system and application in a case-by-case basis.

2.3. Continuous Sensing and Vigilant Sensing

In the context of sensor systems, continuous sensing refers to the concept of acquiring data periodically, oftentimes with a predefined time interval. Continuous sensing is the most common type of sensing for wireless sensor nodes as it creates an uninterrupted stream of data from the sensor to the aggregator or the user during the battery lifetime of the node. The generation of data is the biggest benefit of this type of sensing, and it is better suited for application where no data or limited amounts of data previously exist. This was the case at the early stages of wireless sensing technology [43]–[46]. However, this type of sensing has several limitations that affect the sensing devices and the overall information systems. In the case of the sensing nodes, each sensing operation decreases the battery lifetime of the device, thus the faster the data is sensed, the faster the node will run out of power. Regarding the overall information system where the sensor has been incorporated, the extensive and nonselective generation of data creates the need of additional infrastructure for the analysis and interpretation of data before the decision making process – a major challenge in the field of big data [47], [48].

In contrast, the term vigilant in the same context has a specific meaning – a vigilant monitoring system is one that operates in a mode such that no critical events are missed. The definition of a critical event is inherently application dependent and it must be established for each case. In a vigilant sensing system, events may be missed due to noise or user error, but not due to

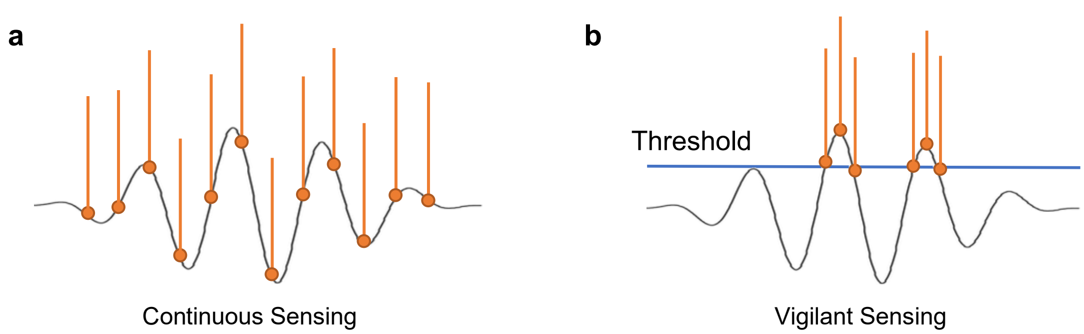

Figure 2.4 | Comparison between continuous sensing and vigilant sensing. a) In continuous sensing the data is acquired periodically with a predefined time interval. **b)** Vigilant sensing is inherently application-dependent and it requires the definition of a *critical event.*

operational mode. It is important to note the difference between vigilant sensing and continuous sensing, as a continuous sensing system may not include all of the necessary sensors or operate at the minimum sampling frequency and/or quantization bit depth to ensure that all critical events will be detected. Conversely, not all vigilant systems perform continuous sensing, as critical events may only happen during certain times, activities, etc., and the system does not need to operate otherwise. By definition, vigilant sensing has the advantage of only generating relevant information for the application of interest and in several cases, reducing the average power consumption of the sensing system during operation. Nonetheless, having the definition of a critical event as a requirement limits the use of this type of sensing to applications where enough information has been previously generated and analyzed such that the events of interest have been identified and mechanisms for the extraction of information have been studied.

2.4. Case Study 1: Vigilant Cardiac Monitoring

In a 2018 study, the American Heart Association reported Cardiovascular Diseases (CVDs) as a leading cause of death in the United States and an associated cost of $555 billion driven by the elevated number of hospitalizations and re-hospitalizations of patients with CVD due to the aggravation of symptoms [49], [50]. In response to this, researchers and physicians have looked at remote patient monitoring as a potential solution to provide affordable and effective care by eliminating unnecessary visits, improving communication and treatment, and optimizing the allocation of resources in the clinic [51]. Furthermore, specific recommendations have emphasized the integration of telehealth and mobile health technologies as part of this effort [49].

A variety of home health technologies have seen some success, but the associated user burden often results in infrequent samples of physiological status. Wearable technology can alleviate many of the issues found in current remote patient monitoring methods by collecting,

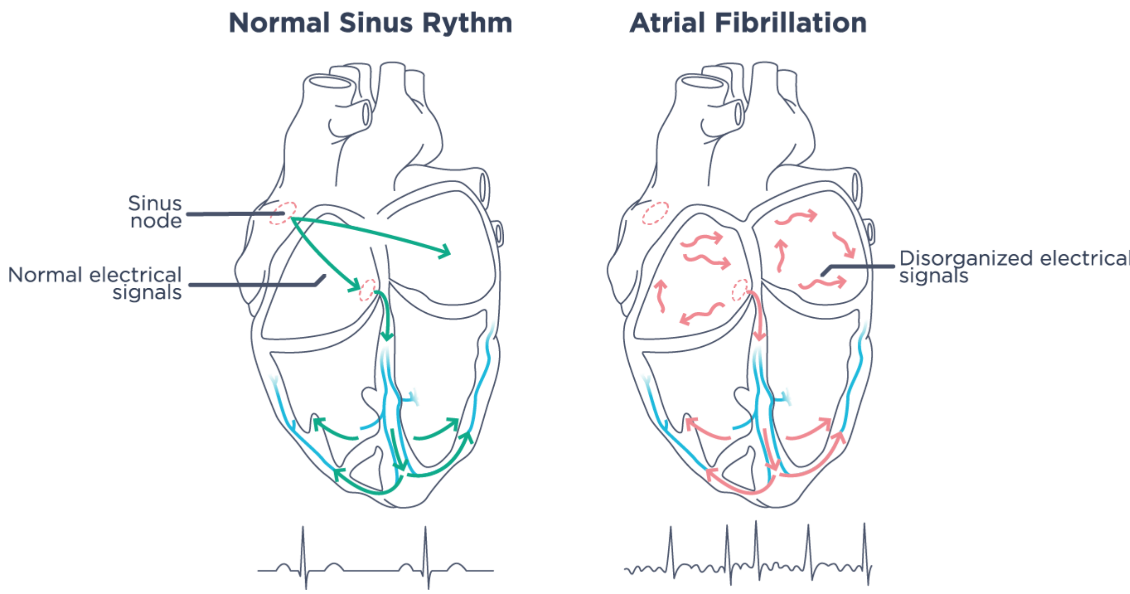

Figure 2.5 | Atrial fibrillation. Afib is a cardiac condition characterized by an abnormal heart rhythm. Image extracted from [152]

processing and transmitting high quality physiological, activity, and environmental data to physicians and/or users in real-time.

AFib is a cardiac condition characterized for an abnormal heart rhythm commonly associated with heart diseases such as cardiac failure. The early detection and diagnosis of AFib could help to prevent heart failure and stroke, but vigilant monitoring is necessary to capture transient periods of AFib. In a patient with AFib, the irregularly rapid action potentials produced in the atrium manifest in the electrocardiogram (ECG) as low amplitude potentials that alter the ECG baseline, often masking the P-wave. As these irregular atrial action potentials travel through the heart's electrical system, they reach the AV node and generate ventricular activity that is presented in the ECG as a QRS complex. Given the refractory period of the AV node, not all of the irregular atrial action potentials can trigger ventricular activity. As a result, the ECG of an AFib patient is commonly characterized by the absence of P-waves and irregular QRS complex.

For our first case study, we developed a self-powered system for cardiac monitoring with vigilant AFib monitoring as the target application. To accomplish this, we present and follow an information-driven approach based on the analysis of the effects of sampling frequency and bit-depth quantization in ECG monitoring to determine the optimal sensing specifications for vigilant operation. The system is powered by body heat, and integrated into an e-textile garment with dry electrodes. Additionally, the sensor system integrates custom ultra-low power electronics to acquire and transmit the data wirelessly to the user's mobile device. At the same time, the data is uploaded to a web server for remote access by researchers and physicians. Figure 2.6 shows the concept of the self-powered vigilant cardiac monitoring system.

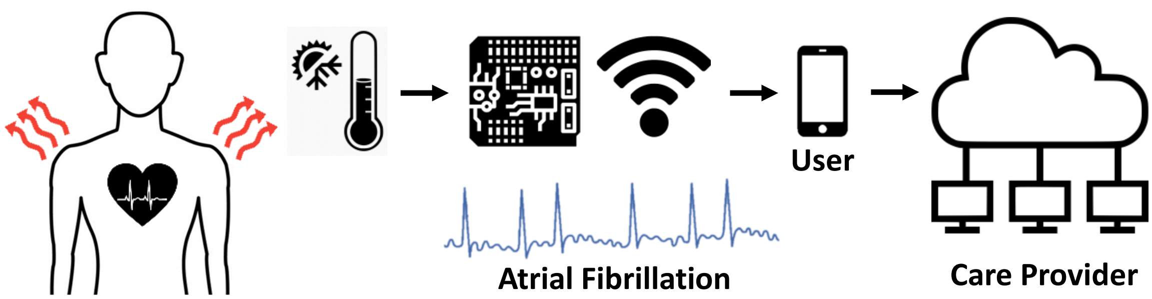

Figure 2.6 | Concept of the vigilant cardiac monitoring system for AFib patients. The cardiac system is powered by body heat and continuously transmits vigilant ECG data to a mobile phone and web server for further analysis.

2.5. Case Study 2: Respiratory Health Monitoring

In the moments leading up to respiratory arrest, many asthma patients experience a sense of chest "tightness". Some severe asthmatics, however, feel no such sensation, leading to sudden arrest with little or no warning [52]. Early detection of an asthma exacerbation is possible – even for severe asthmatics – but it requires professionally supervised monitoring in a controlled setting or pneumotachometer-instrumented masks that are bulky and not conducive to real-world use. Airflow sensors embedded in the trachea and/or bronchi that could automatically detect an impending arrest would therefore have considerable clinical impact for severe asthmatics. Such a sensor could offer early warning to asthmatics during their day-to-day life, thus triggering medical interventions that prevent the need for urgent care.

An increasingly popular choice for making sensors invisible, reliable, and easy to use is to implant them inside the body. The pitfall of many implantables is that their small size requires small batteries, which reduces operational lifetime and/or functionality. While cardiac pacemakers are able to fit a large battery in the chest cavity, the trachea and bronchi do not provide such area, especially since the implantable cannot impede airflow. One solution is to design sensors that harvest their own energy from the user's body. Implantable energy harvesting is in its nascent stages and currently focuses on inertial and thermal energies [37], [53]. An unexplored power source for implantables is the kinetic energy of the fluids (gases and liquids) in a user's body. Using typical air densities and flow rates in the lung, one can estimate the kinetic power of airflow in the trachea to be ~ 6 mW during normal breathing. It would take only a fraction of that power to run ultra-low power electronics, some of which can run on < 1 μW, especially when duty-cycled for scheduled or on-demand use [54].

A key advantage of harvesting energy from airflow in the lung is that the harvester could double as the sensor. Because the airflow itself is the signal to be measured, a device implanted in the trachea may be able to use the same components to measure airflow and harvest its own energy. Implantables need to be as small and minimalist as possible, so combining sensing and harvesting into a single element is a transformative design concept.

This second case study intends to set the foundation for self-powered implantable technology in the airway. To do this, we developed a self-powered system powered by human breathing capable to provide information regarding the airway conditions. The current version of the sensing system is a prototype of the implantable device we envision and serves the purpose of demonstrating the usefulness of the harvesting-limited design approach, as well as proving the hypothesis that the harvester can be used as the sensor to obtain useful information for applications that operate in low harvesting environments. The system was validated in a laboratory environment emulating the respiratory system using a custom test rig that offers the advantage of quick iteration for the testing and refinement of the sensing system. Figure 2.7 illustrates the concept of the harvesting-limited design approach within the respiratory case study.

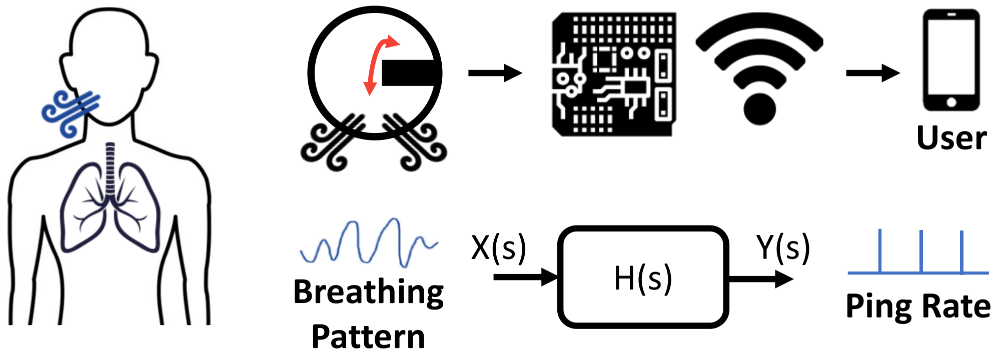

Figure 2.7 | Concept of the continuous respiratory monitoring system. The system is powered by airflow in the airway, and it generates data-less transmissions that correlate with the flow conditions.

Chapter 3

Energy Harvesting Profiling

A critical challenge encountered when designing self-powered energy harvesting systems is the discontinuous nature of the energy sources. These dynamic characteristics of energy harvesting in real-world scenarios and their implications on the design of self-powered sensors have not been fully explored. In this dissertation, we expand the exploration of those dynamics using energy profiling for three energy harvesting modalities: solar, thermoelectric and mechanical energy. The studies are conducted under wearable and implantable conditions following the case studies discussed in Chapter 2.

3.1. EHDC Platform for Solar and Thermal Energy Harvesters

3.1.1. Introduction[1]

Considering the principles of operation of solar and thermoelectric harvesters and the nature of their corresponding energy sources, the amount of energy that can be harvested must have a particular correlation with human activity and ambient conditions [36]. For instance, in the case of solar cells, it is clear that the ambient illumination level defines the maximum amount of harvested energy, but it also has been studied how the angle of incidence of light impacts the efficiency [55]. In a wearable application where the cell is attached to the body in some manner, both the illumination and the angle of incidence changes as the person moves around during a typical day.

Furthermore, for wearable applications that use solar cells for energy harvesting, it is important to note that users spend the majority of the day indoors, and the indoor solar energy

[1] The work in this section was done in collaboration with Dawei Fan.

harvesting conditions are quite different from the outdoor environment. First, indoor light is usually incandescent light, fluorescent light, LED, etc., rather than the sun. The radiant spectra of these light sources differ and therefore affect the efficiency of solar cells. Second, the indoor light has lower illumination levels, usually less than 1000 lux, compared to outdoor sunlight, which is 10000-200000 lux. Third, the illumination levels indoor can be controlled by people and have less dependence on weather or seasonal changes.

Similarly, for a TEG, the temperature difference across the device determines the available power. For a wearable system powered by TEGs, this delta in temperature relates to the difference between the skin temperature and the ambient temperature, most specifically the microclimate surrounding the device. Air flow is a factor that influences this microclimate, and it is also highly dependent on human activity. If the wearer is relatively static, the airflow is practically zero, but while the person is active, the airflow can be high enough to increase the amount of harvested energy considerably.

Even though certain information can be retrieved from the datasheets of these devices, the data presented corresponds to static, controlled conditions in a laboratory setting. Accordingly, having a mechanism to understand the relation of human behavior, environmental parameters and energy harvesting can bring valuable insights to help researchers and designers solve key issues for the development of self-powered sensor systems.

3.1.2. Related Work

The concept of energy profiling as a mechanism to study the dynamics of energy harvesting has been presented previously in the literature. However, the most extensive studies have focused on non-wearable applications where the fluctuations of energy harvesting levels are reduced. For instance, in [56], power profiles for indoor solar energy harvesting are presented. The profiles were elaborated with data collected over one year, and a simulation for a particular load is designed to show the application of these profiles. The limitation of this work relies on the fact that the energy transducer was fixed next to a window, and as mentioned before, the interest for wearable sensors is to have profiles that consider human activity.

Since human beings are warm-blooded, they can be used as a heat source for TEGs attached to the skin. Wearable applications that use TEGs for energy harvesting commonly attach the device on the wrist or the arm. A prototype energy harvesting system using TEGs attached to the arm was presented in [57] to demonstrate that TEGs are comparable and even better than solar energy harvesting. The results show that the system can harvest up to 250 μW during daytime, corresponding to 20μW/cm^2. In [58] a system for fall detection powered by thermal energy harvested from the body was introduced, and for this application the authors reported a peak power of 520μW. A hybrid system that incorporates indoor ambient light and thermal energy harvesting was reported in [36], The results of this multimodal approach show that higher average power levels of up to 621 μW can be achieved in environments with an indoor illuminance of 1010 lux and a thermal gradient of 10 K.

Regarding profiling, there is little work studying on-body thermoelectric energy harvesting, with one of the few studies presented in [59]. This work shows the correlation of the power generated for one activity (cycling) over one hour, and mentions the average amount of energy harvested while working in the office, but it does not present a full profile for different activities over long periods of time. One of the contributions of this dissertation is the generation of energy profiles over several hours for various typical daily activities, both at work and at home.

3.1.3. EHDC Architecture and Implementation

The architecture of the EHDC platform is integrated by three main blocks: energy harvesting, sensing and monitoring, and data logging. The energy harvesting block integrates the harvester of interest, whether solar or thermal harvester, a DC-DC converter that boosts and regulates the voltage coming form the harvester, and a supercapacitor that serves as the energy storage. For sensing and monitoring, different environmental sensors relevant to the corresponding harvesting modality were incorporated. In the case of solar harvesting, an illumination sensor was included, whereas two temperature sensors were used to sense the skin and ambient temperatures relevant to thermal harvesting. Additionally, a current shunt monitor and an analogue to digital converter (ADC) are used to monitor the instantaneous usable power coming from the energy circuit and stored in the supercapacitor.

The platform went through two iterations. The first version served the purpose of validating the hypothesis that human behavior drastically affects the energy harvesting levels of harvesters on the body and that energy profiles were good representations of such phenomenon. The biggest limitation of this version was the level of integration, which affected the capacity of the system to be deployed, as can be seen in Figure 3.1. As a result, the second version of the system had the main goal of increasing the system integration and reducing the form factor to improve wearability and enable the collection of more energy profiles. A detailed diagram of the architecture of the second iteration is presented in Figure 3.2.

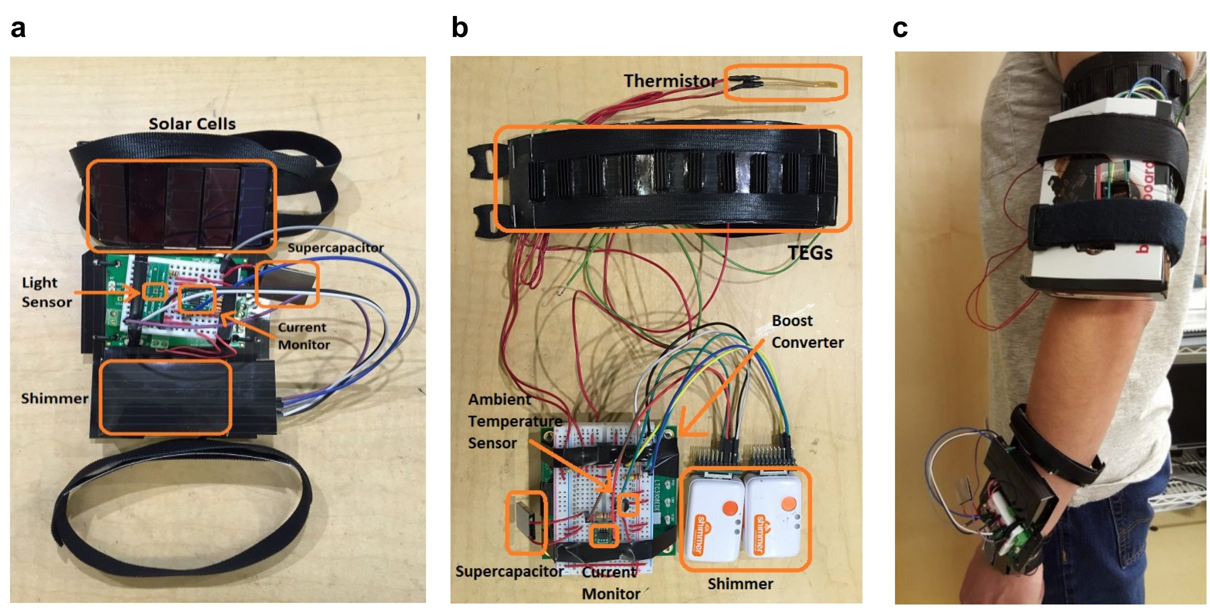

Figure 3.1 | First iteration of the EHDC. Although functional, the first iteration of the EHDC suffered from a very bulky design that affected its wearability and usability for deployments. **a)** EHDC subsystem for solar energy harvesting profiling. **b)** EHDC subsystem for thermal energy harvesting. **c)** A subject wearing the EHDC during a deployment.

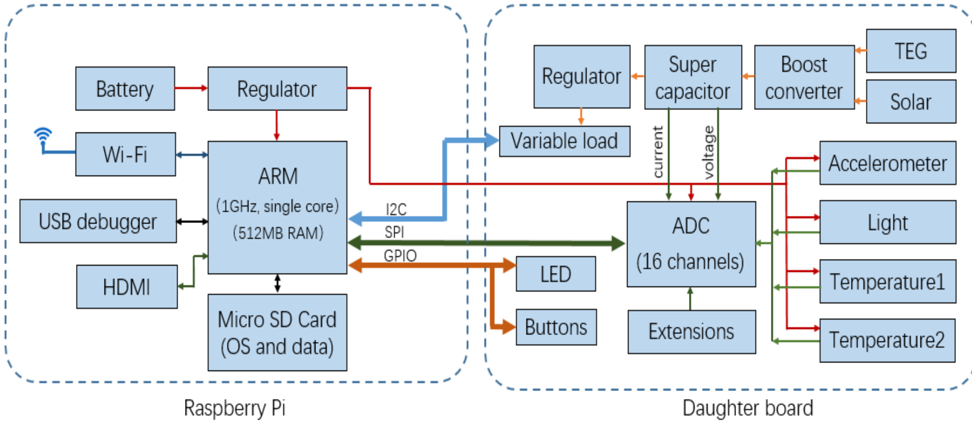

Figure 3.2 | Architecture of the second iteration of the EHDC. This second iteration of the platform presents great improvements on system integration by combining all the energy harvesting circuitry and sensors on a single board that attaches to a Raspberry Pi.

For the implementation of the second iteration, we selected amorphous solar cells from Sanyo (AM-1417CA) and thermoelectric generators (TEGs) from Marlow Industries (SP5424-04AC). A heatsink was attached to the cold side of each TEG to maximize the temperature difference across the device. For the power management unit, we used a boost converter from Texas Instruments (BQ25504) for solar energy harvesting, and a boost converter from Linear Technology (LTC3108) for thermoelectric energy harvesting. The BQ25504 has a maximum power point tracking (MPPT) function and can be cold-started from 330 mV. The LTC3108 does not include an MPPT circuit but can operate from inputs as low as 20 mV, which makes it suitable for thermal energy harvesting from the body. The harvested energy was stored in an 82 mF supercapacitor from AVX (BZ155B823ZNB), and a low-droput (LDO) regulator from Linear Technology (LT3009) was used to adjust the voltage from the boost to power a variable load.

For the selected harvesting modalities, light intensity, skin temperature, and ambient temperature represent the environmental variables of interest. To measure the illumination levels at which the solar cells were exposed, an illuminance sensor from On Semiconductor (NOA1212) was attached close to the solar cells. The range of light intensity could be adjusted up to 100000 lux, making it appropriate for indoor and outdoor conditions. To measure the temperature difference across the TEGs, two temperature sensors from Maxim Integrated (MAX6605) were used. One was placed on the skin, next to the TEG hot side, and the other one was attached close to the heatsink to measure the temperature of the TEG cold side.

To measure the instantaneous usable power, we monitored the output current and voltage delivered by the boost converter to the supercapacitor. For currents sensing, we used a current shunt monitor from Texas Instruments (INA285). An analog to digital converter (ADC) from Analog Devices (AD7490) was used to sample the signals from the environmental sensors, the accelerometer, and current and voltage from the respective energy harvesters. To track human activity levels, an accelerometer from Analog Devices (ADXL326) was included in the system.

For data logging, we used a Raspberry Pi 0 interfacing with the ADC to retrieve the data and also control a variable load that intends to expand the usability of the EHDC providing the opportunity to evaluate power management strategies. The Raspberry Pi 0 uses Linux as the operating system (OS), and we designed a Java application for control, data logging, and data compression. The collected sensor data is stored in a micro-SD card and to reduce the power consumption with each logging, the data is compressed into binary files. Additional software was

a

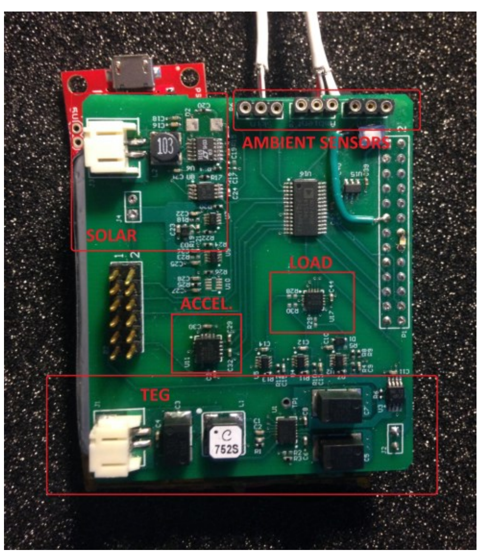

b

Figure 3.3 | Second iteration of the EHDC. a) Integrated EHDC on a single PCB (daughter board). **b)** Deployment of the newest EHDC platform.

developed to enable uploading the sensor data to a custom cloud server for data visualization and storage in real time.

3.1.4. Wearable Data Collection

For the data collection under wearable conditions, the EHDC system was deployed on two healthy subjects across multiple days and the duration of the deployments lasted at least 6 hours for the majority of the cases. The system was placed in a 3D printed case and attached to the upper arm using Velcro straps. Similarly, the TEGs and solar cells were incorporated into two armbands that attach to the upper arm and forearm respectively. Figure 3.3b showcase the platform inside the 3D printed case and the two harvesting armbands during a deployment.

During the data collection, the subjects were asked to do their normal daily activities and manually record the activities they were performing and the corresponding timestamp. The activities performed include working at a desk, walking around, eating, cooking, and driving. With this information, it was possible to create annotated profiles that display the effect of human behavior in the energy harvesting levels during normal daily activities.

3.1.5. Energy Harvesting Profiles

The generated energy harvesting profiles present activity levels (Teager Energy Operator on accelerometer data), light intensity, average solar power (μW), temperature difference between skin and ambient air (°C), average thermoelectric power (μW), and total power (μW). In order to fit all the data series in a single figure, the light intensity was normalized to 100 lux, and the Teager energy was similarly scaled. Four different annotated energy harvesting profiles are shown in Figure 3.4 that correspond to four different deployments using the second iteration of the EHDC platform.

The profiles in Figure 3.4a and 3.4b were generated from data collected mainly indoors, at home and in the office. Some of the performed activities included working at the desk, walking around, eating, and doing housework (sweeping, mopping floor, cleaning, etc). The average light intensity for the two different days was 469 lux and 101 lux, respectively. The ambient temperature was approximately 25 °C, and the average temperature difference between the ambient and the body was 5~6 °C for both days. The total average power was 5.1 μW and 1.7 μW respectively.

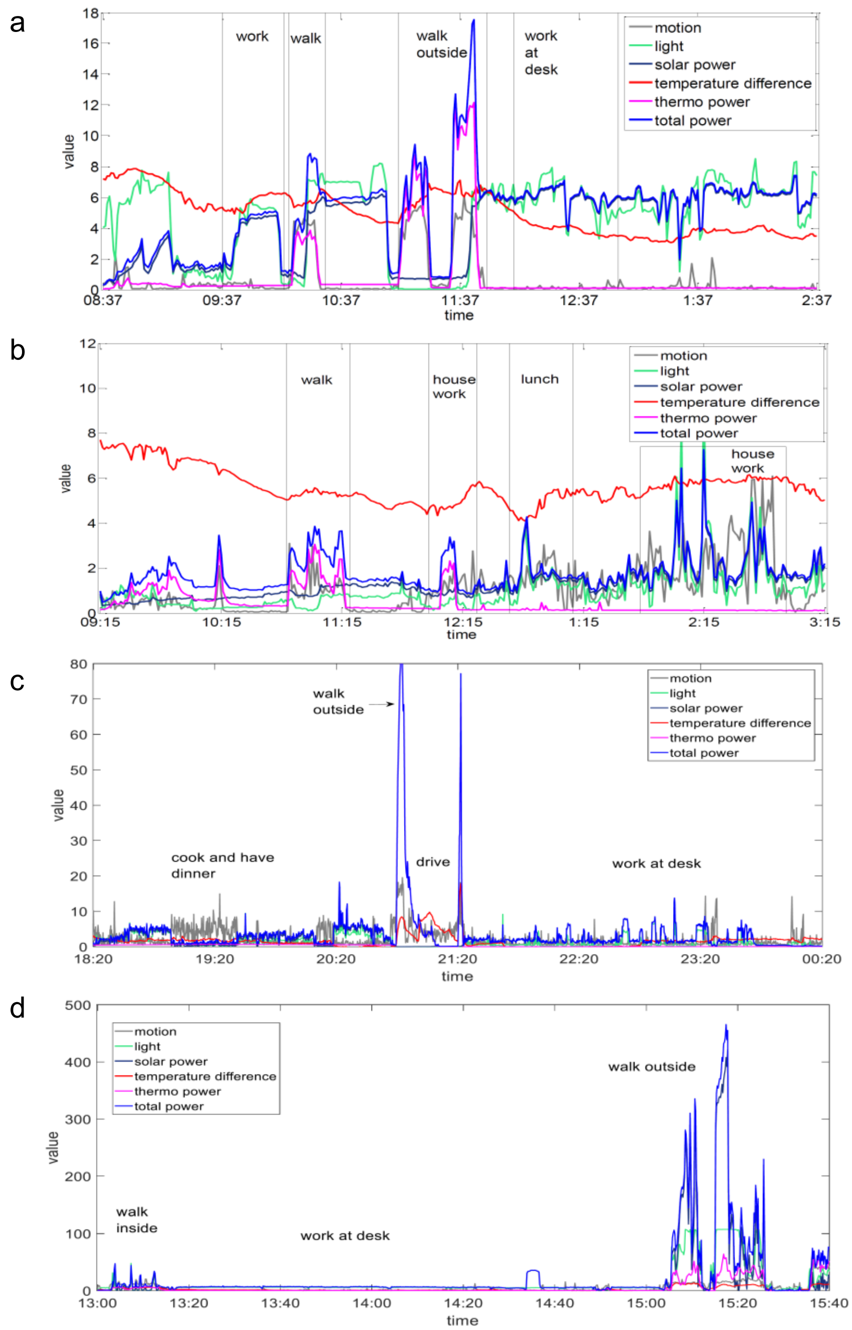

Figure 3.4 | Collected energy profiles. Energy harvesting profiles of TEGs and solar cells on the body across multiple deployments.

The profiles in Figure 3.4c and 3.4d were generated with data from both indoor and outdoor activities. For Figure 3.4c, the data was collected at night. The average indoor light intensity was 209 lux indoors, and approximately 0 lux outdoors. The average temperature difference indoor was 1.1 °C, and 6.1 °C when walking outside. The average indoor power was 3.6 μW, and the average outdoor power was 41.7 μW. This increase in power comes mostly from thermal energy given the higher temperature difference and the heat dissipation from walking. Figure 3.4d shows a profile created for activities mostly in the office. The average light intensity indoors was 537 lux, and more than 10000 lux outdoors. The average temperature difference was determined to be 5.0 °C when the subject was walking indoors, and only 0.9 °C when sitting at a desk. In contrast, when walking outdoors, the average temperature difference was 9.7 °C. The average indoor power was 7.1 μW, and the average outdoor power was 171.4 μW, mainly from the exposure of the solar cells to sunlight.

From these deployments, we found that in an indoor environment, solar power dominates the total power profile in its majority. In certain situations, such as walking, the thermoelectric power dominates due to the airflow produced by the arm movement, creating a cooling effect on the cold side of the TEG. In an outdoor environment, since the ambient air temperature is lower than the body temperature in the winter, there is much more potential for thermal energy harvesting than indoors. It is also possible to observe that the light intensity and harvesting power show a linear relationship. On the other hand, the temperature difference and harvested thermoelectric power presents a non-linear relationship. Instead, the thermoelectric power showed to be related with human motion for some time. This indicates that human activity levels, which are reflected in the airflow surrounding the microenvironment of the TEG, have a significant influence on thermoelectric energy harvesting.

3.2. Piezoelectric Cantilevers for Energy Harvesting in Oscillating Flows

3.2.1. Introduction[2]

Piezoelectric devices have a wide range of applications, both for sensing and harvesting purposes. These devices are typically used in either a sensing capacity, by generating an electric output that correlates to deformation [60], [61], or in a harvesting capacity, by using that output to charge a storage element [62]–[67]. The operating conditions for each scenario are different enough that the tradeoffs between sensing and harvesting usually prevent simultaneous sensing and harvesting by the same device.

In special cases, the sensing and harvesting functionality of a cantilever can overlap: if the harvesting rate scales with a variable of interest (e.g., flowrate), then the duty cycle at which the system operates is itself a proxy for the variable of interest. A piezoelectric energy harvester on a fish fin, for example, can act as a self-powered biotag [68]. As the fish swims, the harvester powers a transmitter, and the ping rate is a proxy for the fish's activity. This operational mode aligns with the harvesting-limited approach introduced in Chapter 2.

3.2.2. Related Work

Self-powered sensing using piezoelectric cantilevers has been previously explored under resonance, in turbulent flows. Following this principle, several sensor systems have been introduced in the literature. In [62], a piezoelectric film made of ZnO nanowires grown on an ultra-thin Al-foil was used to measure deformation in fluttering flags excited by gentle wind. Li et al. demonstrated a self-powered acoustic tag for aquatic animal tracking using a piezoelectric beam implanted sub-dermally in a fish [68]. As the fish moves through the water, energy is produced by the deformation on the beam caused by the swimming motion of the fish, and stored in a capacitor that powers an acoustic transmitter to signals the location of the fish.

[2] The work in this section was done in collaboration with Prof. Dan Quinn and Lucy Fitzgerald.

A common application for piezoelectric devices is measuring flow speeds of different fluids. In [69], a piezoelectric microcantilever measures the flow speed of wind, with a sensitivity of 0.9 mV/m/s. Similarly, a flow sensor for water faucets was introduced in [70]. The sensor utilizes a piezoelectric device made of BTZO embedded into a polyvinylidene fluoride (PVFD) matrix that produces an average peak power ranging from 0.2 to 15.8 nW for water velocities that go from 31.43 m/s to 125.7 m/s. Finally, Wang and Shan built a hybrid piezoelectric-electromagnetic system for energy harvesting as a way to improve the harvesting performance of piezoelectric devices [71].

Although the exploration of piezoelectric devices for breath-inspired applications has not been fully explored, some efforts have been reported in the literature. For instance, a stopwatch powered by driving a PVDF beam to resonance in a testbench that emulates deep inspiration/expiration flows [72]. Similarly, piezoelectric films deformed by breath have been demonstrated in inhale/exhale tests for spirometry applications [73], or to identify breathing patterns of normal and impaired breathing [74].

Designing piezoelectric-based systems for resonance is effective because at resonance the energy harvesting efficiency of the device is maximized. In contrast, a self-powered system using piezoelectric devices driven by laminar flows such as tidal breathing may be forced well below its resonance frequency. Therefore, the rest of this chapter is dedicated to expand the exploration of energy harvesting using piezoelectric cantilevers driven at sub-Hz frequencies, far from resonance conditions.

3.2.3. Piezoelectric Cantilevers in Nonoptimal Harvesting Conditions

Several flow sensing applications do not have the option to accept wake-driven approaches when using piezoelectric cantilevers. Instead, the flow environments present a purely laminar behavior. Such is the case of airflow in the human airway. Motivated by the respiratory case study presented in Chapter 2, here we explore the energy harvesting capabilities of PVDF piezoelectric cantilevers excited by human beathing.

For this study, we built an apparatus for testing piezoelectric devices embedded in time-varying air flows. These flows are produced by a servo-driven piston pump that acts as a lung simulator (Hans Rudolph Series 1120). The airflows pass through an acrylic tube with a 16.5 mm diameter, which is comparable to that of a typical human airway in adults (tracheal diameter ≈ 15 mm [LF24]). To avoid entrance/exit effects, the cantilever was placed more than 10 diameters from either end of the tube. We measured both the voltage output of the piezoelectric cantilever and the voltage across a storage element being charged by the device. Additionally, the apparatus supports the integration of a hotwire anemometer (Dantec 9055H0211) that gives the opportunity to measure flowrate and turbulence intensity directly. These data provide the actual flow properties of the flow pattern that is being considered.

The setup was completed with a full-bridge rectifier as part of the energy harvesting circuit. The rectifier is made of four discrete diodes (1N4001), and it is interfaced with a ceramic capacitor that stores the harvested energy from the cantilevers. To collect the data, we used a data acquisition (DAQ) system from National Instruments (DAQ-6259) given its high probe impedance (>100 GΩ) to avoid loading the harvester. Figure 3.5 shows a diagram of the testing apparatus, including the energy harvesting circuit.

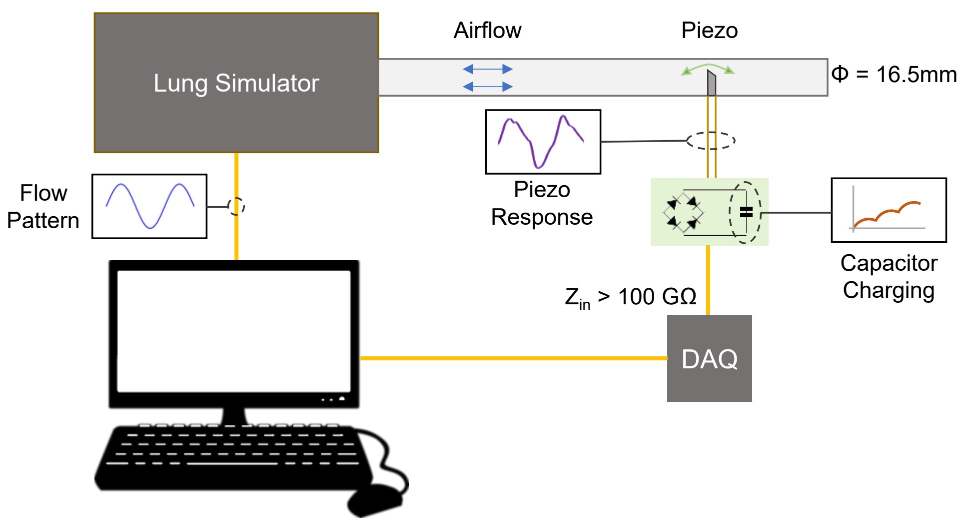

Figure 3.5 | Apparatus for characterization of piezoelectric cantilevers. The rig allows for a quick evaluation of piezoelectric-based systems excited by oscillating flows. In our testing, the flow patterns corresponded to human breathing conditions for different activities.

For our experiments we used a PVDF piezoelectric film (TE Connectivity 1-1003702-7) with a thickness of 28 μm to fabricate a rectangular cantilever with dimensions of 12 mm by 7 mm. Thinner materials produce larger deflections at low speeds, and PVDF material has a

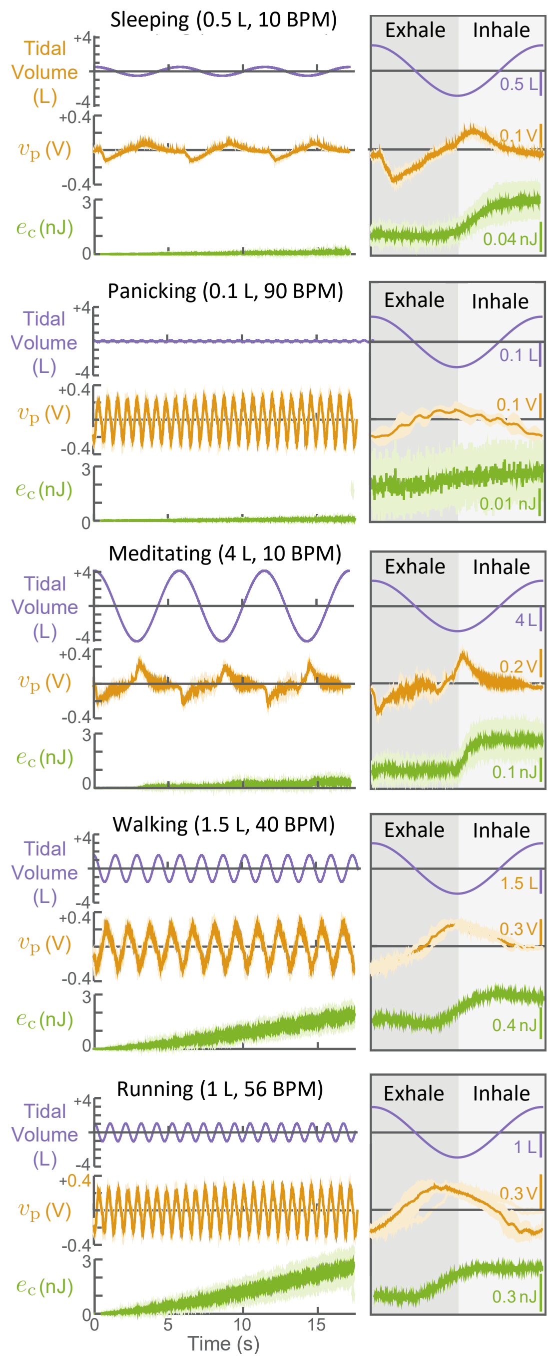

Figure 3.6 | Cantilever output voltage and stored energy in the capacitor for 5 sample breath types. The input oscillating tidal volume is shown for reference. Solid curves and shaded bands show mean ±σ based on 5 trials. Zoomed inserts on the right show data for the final breath only.

biocompatibility advantage over materials like PZT [75]. To finish the fabrication of the cantilever, we placed copper tape at the base of each face and soldered a lead wire to the tape. In this way, the cantilever could be connected to the harvesting circuit and inserted in the tube for experimentation.

The piezoelectric cantilever was evaluated in different sinusoidal flows whose characteristics represented those similar to human breathing for different activities in terms of breaths per minute (BPM) and tidal volume. The full set of testing flows included 197 waveforms with frequencies ranging from 0.13 Hz (~8 BPM) to 1.67 Hz (~100 BPM) and tidal volumes ranging from 0.1 L to 7 L. The DAQ recorded the voltage across the cantilever and the voltage in a 1 μF capacitor for 20 s during each trial. To ensure that the capacitor started fully discharged, an N-channel MOSFET connected to a load resistor grounded the capacitor for 5 s before each trial. Each trial was repeated 5 times to estimate the mean and variability of voltages and harvesting rates (Figure 3.6). This experimentation led to the generation of plots (Figure 3.7b) that correlate the characteristics of the flow to the energy harvesting levels, which are used to inform the harvester design used in the continuous respiratory health monitoring system discussed in Chapter 6.

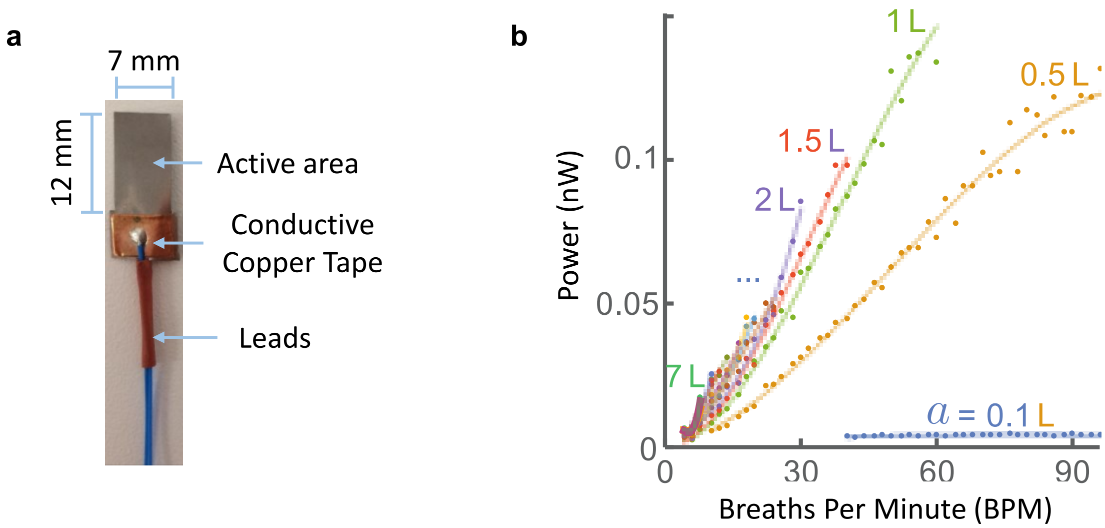

Figure 3.7 | Characterization of piezoelectric cantilevers. a) Fabricated piezoelectric cantilever. **b)** Power output for the fabricated cantilever under multiple breathing conditions.

3.2.4. Piezoelectric Harvesting Modeling

Our base model combines first principles from fluid dynamics, elasticity theory, piezoelectric science, and circuit design. The model is inspired by previous work [66], [67], [76], [77], and the difference of this dimensionless model is the addition of a user-defined circuit impedance, which makes the model more generalizable to other piezoelectric harvesting systems, including those that operate far from resonance. Oscillating fluid flows produce deformation and thus strain in a piezoelectric structure. The deformation δ driven by forcing with magnitude Q is governed by elastic beam theory:

$$\frac{\partial^4 \Delta}{\partial X^4} = -\lambda^4 \frac{\partial^2 \Delta}{\partial T^2} + Q\mathrm{e}^{\mathrm{j}T}, \tag{3.1}$$

with dimensionless variables

$$X \equiv \frac{x}{l},\ T \equiv \omega t,\ \Delta \equiv \frac{\delta}{l}\ \ \lambda \equiv \left(\frac{12m\omega^2 l^4}{ewh^3}\right)^{\frac{1}{4}},\ Q \equiv \frac{12ql^3}{ewh^3,} \tag{3.2}$$

where x is distance along the beam, t is time, q is the magnitude of the forcing, ω is the angular frequency of the forcing, j is the square root of -1, and δ, l, w, h, e, and m are the lateral displacement, length, width, thickness, elastic modulus, and mass per length of the beam, respectively. This formulation assumes that the beam's cross-sectional area moment of inertia is that for a rectangle: $wh^3/12$. The dimensionless groups λ and Q represent ratios of inertial and drag forces to elastic forces. Due to the complex forcing, the solution for deflection is a complex phasor that can be evaluated by, for example, considering its real component. Using the boundary conditions for a fixed-free cantilever ($\Delta(0,T) = \Delta_x(0,T) = \Delta_{xx}(1,T) = \Delta_{xxx} = (1,T) = 0$) leads to an exact solution for Δ:

$$\Delta = \frac{Q}{\lambda^4} e^{jT}(c_1 \sin(\lambda X) + c_2 \cos(\lambda X) + c_3 \sinh(\lambda X) + c_4 \cosh(\lambda X) - 1), \tag{3.3}$$

where the coefficients c_n are given in ... Based on linear theory, higher loading (Q) causes higher deflection (Δ), without bound. In reality, the beam cannot deflect more than $O(l)$ distances. Anticipating potential large deflections at l:

$$\Delta' = \Delta\left(\frac{l\left(1-\exp\left(-\frac{|\Delta(1,0)|}{l}\right)\right)}{|\Delta(1,0)|}\right). \tag{3.4}$$

The modified dimensionless deflection (Δ') converges to linear beam theory as $Q \rightarrow 0$ and converges to 1 as $Q \rightarrow \infty$.

In the case of a bimorph piezoelectric beam, the average stress in the device is the stress halfway between the neutral axis and the beam's surface, averaged over the length of the beam:

$$\overline{\epsilon}_{xy} = \int_0^1 \left(\frac{1}{2}\frac{h}{l}\frac{\partial^2 \Delta'}{\partial X^2}\right) dX = Q\hat{\lambda}\frac{h}{l}e^{jT}, \tag{3.5}$$

where $\hat{\lambda}$ is a dimensionless ratio involving λ introduced for notational convenience: $\hat{\lambda} \equiv (\sin\lambda - \sinh\lambda)/(2\lambda^3(1+\cos\lambda\cosh\lambda))$.

The deformation in the structure feeds into the piezoelectric constitutive equations reformulate to include macroscopic properties like current [LF23] to produce an equation governing the voltage across the piezoelectric device (v_p):

$$\frac{dV_p}{dT} = \frac{d\overline{\epsilon}_{xy}}{dT} - I, \tag{3.6}$$

with dimensionless variables

$$V_P \equiv \frac{v_p}{\gamma l/c_p} \text{ and } I \equiv \frac{i}{\gamma\omega l}, \tag{3.7}$$

where i is the current induced by the piezoelectric device, γ is the generalized electromechanical coupling factor, and c_p is the piezoelectric output capacitance. To be consistent, we similarly defined the dimensionless impedance (z), resistance (r), and capacitance (c) as $Z \equiv z\omega c_p$, $R \equiv r\omega c_p$, and $C \equiv c/c_p$.

Solving Eq. 6 requires a model current (I) based on the circuit to which the device is attached. Specifically, the current can be replaced by the voltage across the piezoelectric structure divided by the effective impedance of the total circuit ($I \rightarrow V_p/Z$). Making this substitution in Eq. 6 and solving for V_p leads to a model for the voltage across the piezoelectric device:

$$V_p = \alpha\,\overline{\in}_{xy}\left(\frac{jZ}{1+jZ}\right) = \alpha Q\hat{\lambda}\frac{h}{l}e^{jT}\left(\frac{jZ}{1+jZ}\right), \tag{3.8}$$

where the coefficient α has been added as an empirical constant to be fitted. The constant α helps to account for unmodeled losses, such as those resulting from the diodes of a voltage bridge rectifier or the vortex-induced vibration of the piezoelectric beam. Note that in the open circuit case ($Z \rightarrow \infty$), the voltage follows the strain in magnitude and phase.

In this work, we consider the harvesting circuit described in the experimental setup (i.e., full bridge rectifier with storage element), where the impedance is the sum of the internal impedance of the piezoelectric device (Z_p) and the impedance of the storage element (Z_c). The transfer function from voltage across the piezoelectric device to voltage across the storage element is Z_c/Z. The model therefore predicts a dimensionless voltage across the storage element of

$$V_c = \mathcal{L}^{-1}\left\{\mathcal{L}\left[\alpha Q\hat{\lambda}\frac{h}{l}e^{jT}\left(\frac{jZ}{1+jZ}\right)\right]\left(\frac{Z_c}{Z}\right)\right\}, \tag{3.9}$$

where $\mathcal{L}$ and $\mathcal{L}^{-1}$ denote the Laplace and inverse Laplace transforms.

We modeled the storage element as a capacitor with capacitance C and the resistor with resistance R_2 in parallel ($Z_c = R_2/(R_2 + SCR_2)$), where S is the complex frequency parameter divided by ω, and the total impedance as the impedance of the storage element plus the internal resistance of the piezoelectric device ($Z = Z_c + R_1$). Making these substitutions into Eq. 9 leads to

$$V_c = \alpha Q\hat{\lambda}\frac{h}{l}\frac{R_2(R_1+R_2)}{2[1+(R_1+R_2)^2]}\left[K_1\sin(2T+\phi_1) + 1 + K_2 e^{-T\frac{1+R_1(R_1+R_2)}{R_2C({R_1}^2+1)}}\sin\left[\frac{T}{C(1+{R_1}^2)}+\phi_2\right]\right], \tag{3.10}$$

where K_1, K_2, ϕ_1, and ϕ_2 are constant coefficients that include R_1, R_2, and C. The term scaled by K_1 models a fluctuating component of the capacitor's voltage due to the oscillating piezoelectric beam, and the term scaled by K_2 models the energy accumulating on the capacitor

($e_c = (1/2)cv_c{}^2$). Eq. 10 can be used, for instance, to estimate the initial harvesting rate by calculating $de_c/dt|_{t=0}$ with $K_1 = 0$.

These set of equations offer a platform for studying energy harvesting given different geometries (defined by ℓ, h, etc.), materials (defined by λ, γ, etc.), or flow environments (defined by Q, ω, etc.).

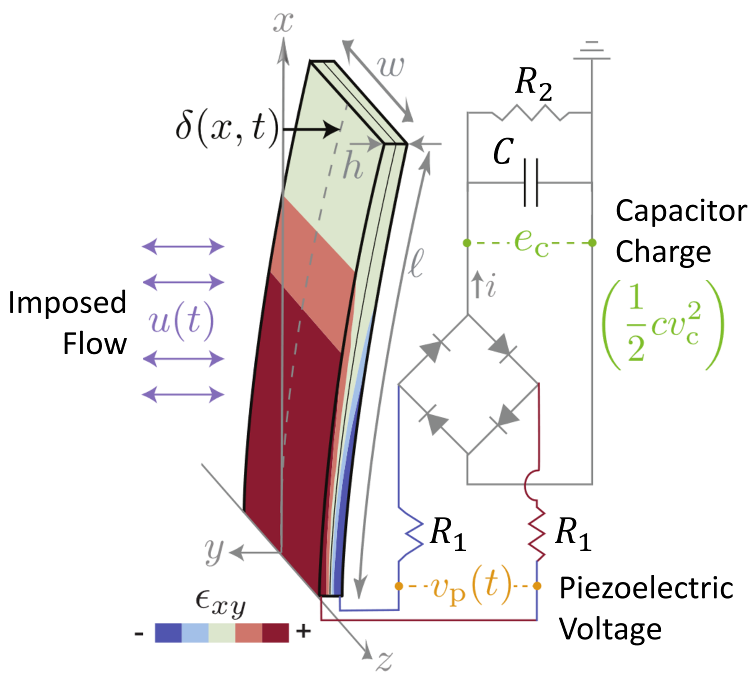

Figure 3.8 | Model setup. A similar setup to that in the piezoelectric characterization was assumed during the modeling process. An oscillating flow causes an oscillating strain field and therefore an oscillating voltage. The AC signal passes through a rectifier, causing charge to accumulate on the capacitor.

3.2.5. Piezoelectric Model Validation

To validate our model, we used the characteristics of the sinusoidal flows from the previous energy profiling evaluation as inputs to the model and used physical constants that matched those for our setup. The output of the model was then compared to the observations in the profiling experiments. The model was able to capture many of the features of the experimental data, as shown on Figure 3.9. For instance, the model predicts the asymptotic behavior of the harvesting rate curves at high amplitudes. It also correctly follows the behavior seen at low amplitudes (e.g., 0.1 L) and high frequencies (e.g., 90 BPM), displaying the lowest voltages and harvesting rates.

These effects can be explained in physical terms thanks to the model. At low amplitudes, the deflections of the piezoelectric beam are small, which lead to low harvesting rates at all frequencies. At high amplitudes, the deflection saturates (i.e., the beam reaches its maximum range of motion), further increases in amplitude beyond this point have little effect on the produced voltage. Furthermore, the lower frequencies lead to more leaked charge per breath. Breathing patterns in between these extremes, produce the most power.

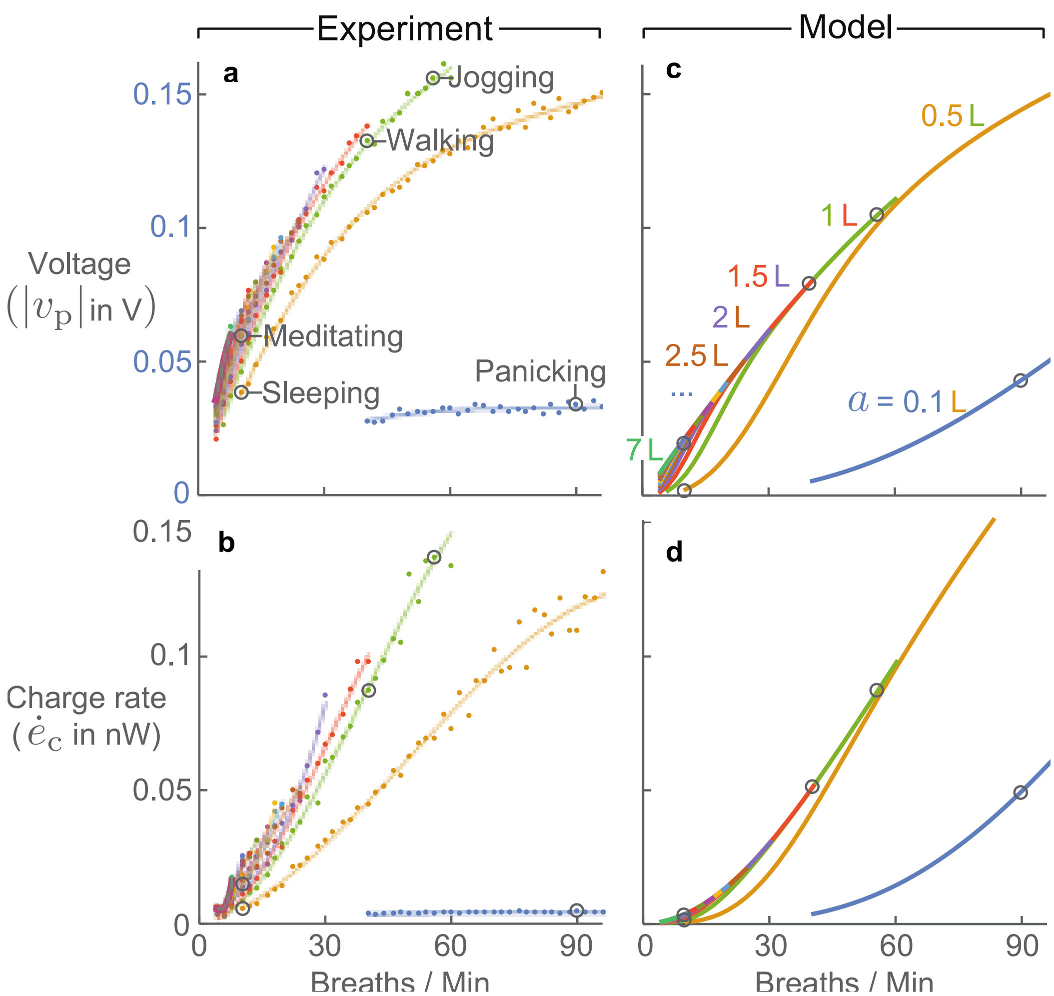

Figure 3.9 | Validation of the model against the experimental data. a, b) Experimental results. Solid circles: raw data; solid lines: fitted 3rd-order polynomials to help visualize trends. Colors indicate breath amplitude in L. Five sample breath types from Figure 3.6 located as indicated. **c, d)** Model predictions. Color scheme and labeled breaths as in a, b.

The model has some limitations. This can be observed when the model cannot capture some some of the features from the experimental data. For example, the low value of the one fitted coefficient ($\alpha = 0.01$; Figure 3.9) shows that the model significantly overpredicts the absolute magnitude of the voltage and harvesting rate. Some overprediction is expected given the assumptions in the model. The model assumes perfect voltage rectification from ideal diodes, whereas the real system has to deal with the losses from real diodes in the bridge rectifier. The model also assumes a perfectly symmetrical loading, when in fact slight misalignments and leakages in the real system cause a voltage offset in the piezoelectric cantilever (~30 mV registered with no airflow). Nevertheless, the model does well at explaining the relative values for voltage and harvesting rate.

For the design of self-powered sensors based on piezoelectric devices, the model presents the potential of accelerating the process of energy profiling when evaluating piezoelectric cantilevers in more complex flows.

Chapter 4

System-Level Power Optimizations

Power optimizations in energy neutral harvesting systems are critical to guarantee the self-powered operation of the device. The main goal of these optimizations is to reduce the overall energy losses and, therefore, improve the system's energy efficiency. In the context of this dissertation, and at a system level, these optimizations are done through the appropriate selection of components and implementation of techniques used for the system's power management. Here we explore four different techniques: system power modeling, energy storage for harvesting droughts, harvester sizing, and maximum power extraction.

4.1. System Power Modeling

4.1.1. Introduction

With the widespread adoption of personal computing devices and wireless communication systems, power consumption has become an important design constraint alongside processing performance, area or form factor, and other similar metrics relevant to microelectronic systems. Power modeling is a technique that analyzes the architecture of any given system and captures the power contributions of each element in the architecture with the goal of identifying potential areas for power reduction.

As the development of integrated circuits closely followed Moore's law at the end of the last century, this approach became commonly applied to the design of digital integrated circuits [78]–[80]. Furthermore, with the interest of researchers and designers expanding to power estimation, synthesis and optimization, Electronic Design Automation (EDA) tools were developed to create a design environment that integrated power modeling as one of its core components. These novel tools helped shorten the development time for integrated circuits, and positively impacted the cost of the devices. As a result, embedded systems expanded to more applications and power modeling became relevant at a higher level of abstraction.

Multiple works looking at power modeling and power estimation for embedded systems have been presented in the literature. In [81], Talarico et. al. developed a framework to evaluate power consumption of embedded systems in early stages of the design process for faster execution time. Li et. al. used power modeling to select the optimal power modes for power management of embedded systems [82]. Similarly, in [83], the authors propose a modeling technique based on power profiles corresponding to different tasks executed by an embedded system, and use this approach to make power estimations for different embedded systems. Other works on the same matter have looked at improving accuracy of the power estimation, the automation of the power modeling process, and even modeling the power consumption of the software running in the embedded system for a more complete model [84]–[86].

In this dissertation, power modeling is similarly adopted as a power optimization technique. We demonstrate how the technique is transferable to self-powered system design and its potential in assisting in system integration and achieving self-powered operation.

4.1.2. System Operation Considerations

To illustrate the implementation of power modeling in the design of self-powered sensors, we considered the Vigilant Cardiac Monitoring case study presented in Chapter 2. In this instance, the model had the purpose of assisting in the selection of components, the definition of specifications for the design of custom electronics, and as a mean to assess the effect of different sensing conditions in the total system power consumption and self-powered operation. The model was based on a general architecture of the system and a duty-cycled operation scheme common to self-powered systems.

Regardless of the application and the power source, most sensor systems are integrated by three main sub-systems: sensing, power management, and data acquisition and transmission.

The components in each sub-system are defined by initial requirements constrained by the application. In the sensing sub-system, it is common to find the sensor and additional circuitry for signal conditioning (e. g. amplifiers, filters, etc.) in order to prepare the sensed signal before display or further processing. The power management block has the purpose of providing the appropriate voltage levels and deliver power to all the other components in the system to operate adequately. In a battery-powered system, this block normally includes voltage regulators since the energy source is assumed to be constant. However, for self-powered or energy harvesting systems, this unit increases in complexity due to the need for energy storage elements and voltage conversion. Finally, although data acquisition and transmission entail two very different tasks, they are normally grouped together given the evolution of highly integrated digital circuits such as microcontrollers (MCUs) and System-on-Chip (SoCs). These circuits not only are able to capture, digitize and store information, but also offer the capability to communicate with other devices directly wired or wirelessly. For the vigilant cardiac system, we adopted a general architecture as presented in Figure 4.1.

Duty cycling schemes have been adopted by the majority of remote sensing devices due to the power saving benefits that this mode brings by switching between different operation states. In general, a device with this operation mode is normally in a low-power mode (sleep) and

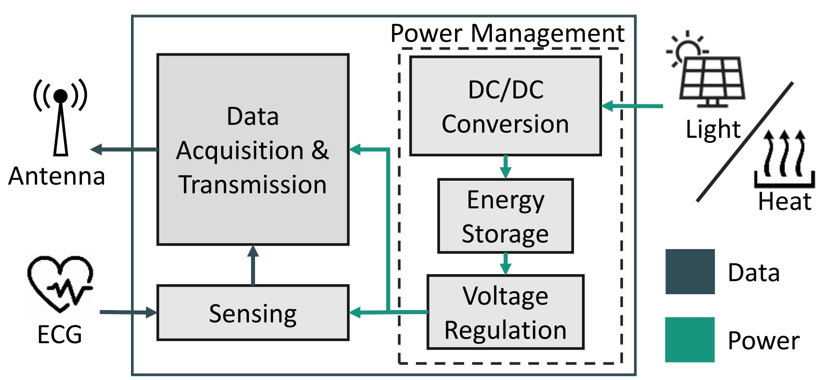

Figure 4.1 | System architecture of the vigilant cardiac system. The architecture integrates three main subsystems: power management, data acquisition and transmission, and sensing. The system can be powered by solar cells or TEGs.

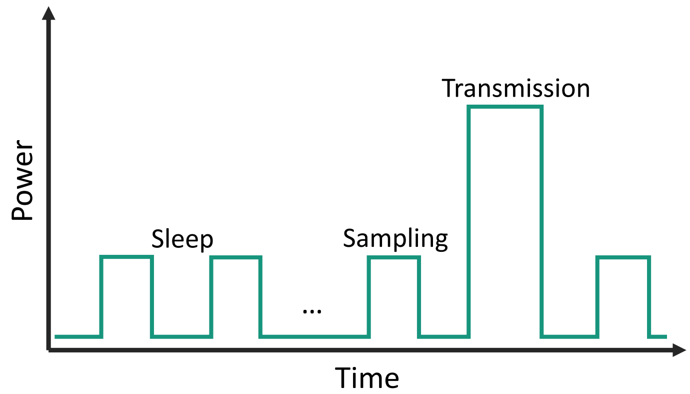

Figure 4.2 | Duty-cycled scheme of the vigilant cardiac system. The system's operation scheme switches between three states to reduce the average power consumption. The best components to integrate the system and the optimal duration of each state to reduce power consumption can be determined through power modeling.

switches to a higher power mode for a shorter period of time to perform a specific task; e.g., acquire data (sampling), do an operation to the data (processing) or send the data to an aggregator (transmission). For total power estimation, a power model considers the power consumption of the system in each of the states and the time that it takes the system to perform such given task. If more accuracy in the model is required, the tasks can be divided in sub-tasks and follow the same procedure.

For the vigilant cardiac system, we assume three main operation states: sleep, sample, and transmission. In sleep mode, the system achieves the lowest power consumption and it switches to sampling mode multiple times until enough data has been acquired to be transmitted. For wireless systems, transmission is the task that presents the highest power consumption. A representation of this duty-cycled scheme is presented in Figure 4.2.

4.1.3. Power Model

To develop the power model, we considered all the elements in the system from the energy storage down to the consumers, following the power path. Additionally, we assume that these components can be grouped into those that are always on and those that switch states. With these considerations, the total average power of the system can be expressed as

$$P_T = P_{St} + P_{Sw} , \tag{4.1}$$

where P_T corresponds to the system's total average power, P_{St} is the power consumption of the components that are always on and are required for the subsystems to operate (e.g., regulators, crystal oscillators, etc.), and P_{Sw} is the power consumption of the components that switch between states (e.g., sensors, microcontrollers, radios, etc.). In the majority of the cases, P_{St} is considerably lower than P_{Sw} and it sets the baseline for the total power consumption. P_{Sw} then can be then expressed as

$$P_{Sw} = P_{smpl}D_{smpl} + P_{tx}D_{tx} + P_{slp}D_{slp}, \tag{4.2}$$

having P_{smpl}, P_{tx}, and P_{slp} as the power consumption during sampling, transmission, and sleep, respectively. D_{smpl}, D_{tx}, and D_{slp} correspond to the duty cycle of each state in that same order. In this context, the duty cycle is the portion of time that the device spends in a given state with respect to the total period of the operating state in consideration. In other words, this is the ratio of the time *on* state with respect to the addition of time *on* state plus time *off* state, and it is written as

$$D_{state} = \frac{t_{on-state}}{T_{state}} = \frac{t_{on-state}}{t_{on-state} + t_{off-state}}. \tag{4.3}$$

For any periodic signal, the period is the inverse of the frequency of the signal ($T = 1/f$). Thus, the duty cycle for the sampling and transmission states in our system expressed in terms of sampling frequency can be defined as

$$D_{smpl} = f_s t_{smpl} \text{ and } D_{tx} = \frac{f_s}{N} t_{tx}, \tag{4.4}$$

where f_s is the sampling frequency, t_{smpl}, and t_{tx} are the time duration of a single sampling and transmission events, respectively; and N is the number of samples in a single transmission packet bounding the duration of the period between transmission events. What this term represents is that the transmission event does not occur every time a sample is collected, instead it occurs until a transmission packet is full, aligning with the representation of the duty cycle scheme in Figure 4.2. Moreover, the duty cycle for the sleep state can be derived as the complement of the duty cycles for sampling and transmission, this is

$$D_{slp} = 1 - D_{smpl} - D_{tx} = 1 - f_s t_{smpl} - \frac{f_s}{N} t_{tx}. \tag{4.5}$$

Finally, the total average power consumption for the sensing system as a function of sampling frequency can be expressed as

$$P_T = P_{St} + f_s t_{smpl} P_{smpl} + \frac{f_s}{N} t_{tx} P_{tx} + \left(1 - f_s t_{smpl} - \frac{f_s}{N} t_{tx}\right) P_{slp} \; . \tag{4.6}$$

This expression offers a mechanism to effectively and efficiently evaluate potential components to integrate in the system. Similarly, the model allows for the analysis of different sensing specifications such as sampling frequency and bit depth as a mean for additional power optimizations; this is discussed in further detail in Chapter 5. Figure 4.3 shows the evaluation of different power management elements and radios to be integrated into the system.

Although this example evaluation only considers one variable or element at the time, and the behavior is fairly linear, the full analysis during the design process turns rapidly into a multidimensional analysis that is more complex to represent in a 2-D plot and that the model can capture. Overall, the model provides an environment to rapidly assess different operational

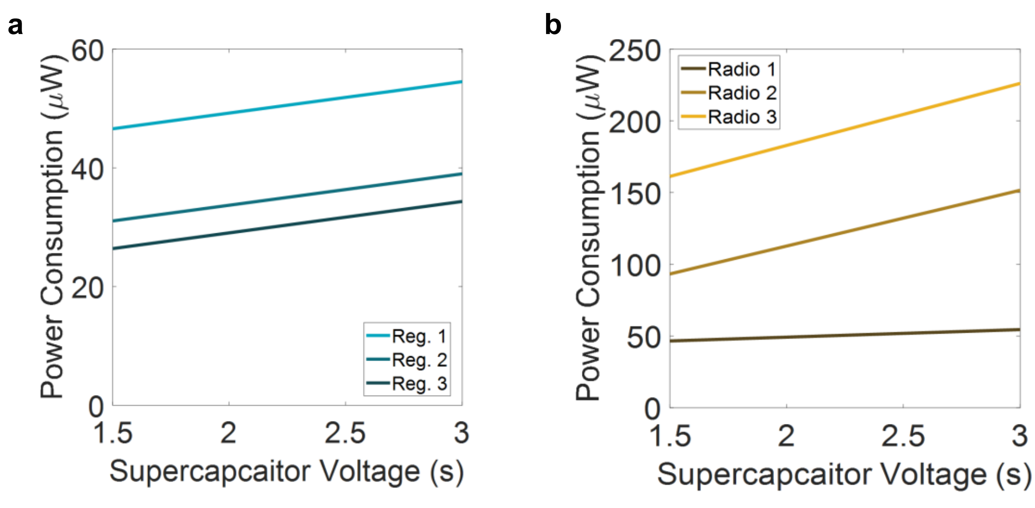

Figure 4.3 | Example power evaluations using the developed power model. a) Evaluation of three COTS voltage regulators and their impact in total power consumption. **b)** Evaluation for three Bluetooth low energy (BLE) radios and their impact in the total power consumption. Although the final decision to use one component over the other may not solely depend on power, the developed power model is a tool for the quick assessment and information during the system design.

scenarios (e.g., components in the system, sensing specifications, transmission conditions, etc.) and determine the effects on the system's power consumption, a key consideration to achieve self-powered operation in dynamic low harvesting environments.

4.2. Energy Storage for Harvesting Droughts

4.2.1. Introduction

As discussed in Chapter 3, low energy harvesting environments common to several self-powered sensing applications are highly dynamic, and the developed energy profiles are a demonstration of this behavior. In comparison, battery-powered wireless sensor nodes do not face such a challenge given the steady and continuous delivery of power during the battery lifetime. While variations in power that are short in duration can be filtered using standard storage elements such as capacitors, episodes of longer duration require a more precise evaluation in the design of self-powered sensors.

For self-powered sensors, there are two long-duration harvesting events that are important to consider for the operation of the system: high energy harvesting events and no/low harvesting events (i.e., harvesting droughts). In the case of the former, the excess of harvested energy is not a threat to the system's operation, but it represents a missed opportunity to improve the sensing performance of the device. A self-powered sensor that often operates in this scenario can be considered as inefficient as one that loses power and stops operation for long periods of time when the application requires it otherwise. Aware of this, researchers have developed adaptive power management schemes that adjust the sensing conditions of the node based on current and forecasted energy harvesting levels [87]. However, this is out of the scope of this dissertation.

Energy harvesting droughts are relevant to self-powered sensors because if they are prolonged enough, the system has the risk of completely stop operating. In these situations, not only valuable information for the sensing application is lost, but also additional service to restart the device may be required. Since this type of sensors are commonly used in applications where the nodes cannot be easily accessible after deployment, mechanisms to prevent such scenarios are necessary. This section of the manuscript discusses the appropriate selection and sizing of energy storage elements in self-powered sensos to deal with energy harvesting droughts.

4.2.2. Batteries vs. Supercapacitors

The two most common large capacity storage elements used in energy harvesting systems are rechargeable batteries and supercapacitors. Both devices are effective alternatives to store the instantaneous excess of harvested energy in the system to be used when not enough harvestable energy is available. To assist in the selection of storage elements best suited for a given application, we discuss these devices considering four characteristics: energy density, power density, cycle life, self-discharge rate.

Energy density refers to the amount of charge that a storage device can hold per unit mass or unit volume (gravimetric energy density for mass and volumetric energy density for volume). Their units are Watt-hour per liter or Watt-hour per kilogram. Power density is the maximum amount of power a storage element can deliver per unit volume or unit mass. Similar to the energy density, the terms used respectively are volumetric or gravimetric and the units correspond to Watts per liter or Watts per kilogram. Cycle life is a measure of the storage element's ability to support repetitive charging and discharging while providing a minimum required capacity for a given application. The cyclic charge and discharge testing can be done at various rates and depths for the discharge to simulate conditions similar to the target application. Finally, self-discharge rate defines how long a storage element can be left unused and still provide a minimum required capacity and be recharged to rated capacity. Self-discharge rate is normally measured in terms of percentage capacity loss per month or per year in term of energy lost (Watt-hour).

Considering these four characteristics, supercapacitors present an appealing combination of energy density and power density. Additionally, these energy storage devices have a higher cycle life than batteries, but their drawback is in the self-discharge rate. Supercapacitors show higher leakage than batteries, undermining the capacity for long-term energy storage. It is worth noting that the leakage is very specific to the device in consideration, and novel advances in materials and processes have shown a considerable reduction in leakage, bringing these devices closer to some batteries [88].

Current battery research has put special focus on lithium batteries since this technology has demonstrated the highest combination of energy density and power density for batteries [89]. Nonetheless, as discussed above their cycle life can be an important limiting factor for some applications that charge and discharge frequently. To address this limitation, topologies that use a capacitor or supercapacitor in parallel with a battery have been presented in the literature [90]. Furthermore, their low self-discharge rate places batteries as the main alternative when long-term storage is heavily weighted in an application. In table 4.1, we summarize this discussion, indicating the typical characteristics for the two storage elements considered in this section [91].

4.2.3. Energy Storage Sizing

To demonstrate a method to appropriately size the storage element in an energy harvesting system, we considered the vigilant cardiac monitoring case study. For this application, a supercapacitor was selected as the best technology to deal with energy harvesting droughts and achieve self-powered operation. The two main reasons for that are the form factor of the device, which relates to energy and power density, and the cycle life of supercapacitors given the highly dynamic characteristics of energy harvesting in wearable applications.

The sizing method is a combination of empirical and theoretical procedures, and an important consideration in this case study is that energy harvesting droughts are expected to last up to 12

Feature	Supercapacitor	Lithium-Based Battery
Energy Density (Wh/kg)	1 – 10	30 – 200
Power Density (W/kg)	< 10,000	< 1,000
Cycle Life	> 500,000	~ 1,000
Leakage/Self-discharge rate	3 μA after 72 hours	1 – 2% per month

Table 4.1 | Comparison between supercapacitor and battery technologies. Adapted from [80].

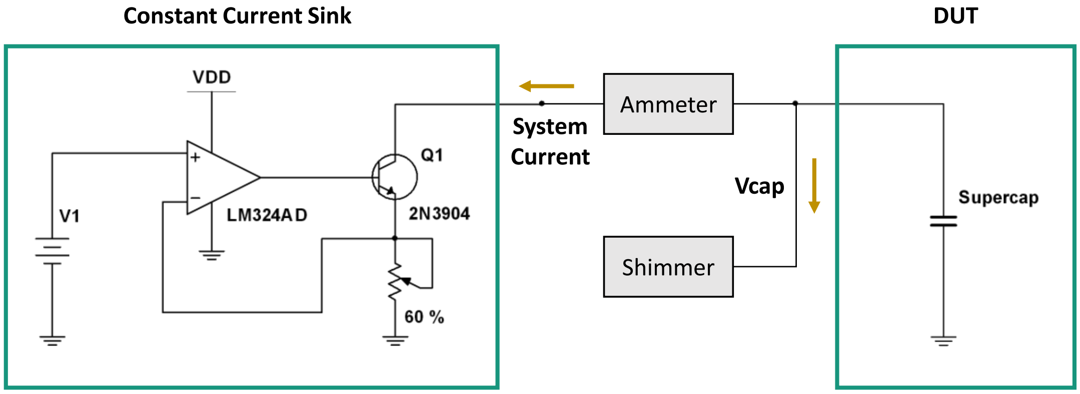

Figure 4.4 | Supercapacitor discharge test setup. Experimental setup for the runtime evaluation using fully charged supercapacitors. The devices were discharged at a constant rate equivalent to the average power consumption of the vigilant cardiac monitoring system.

hours, approximately. This represents when the user is sleeping at night. In addition, the total system power consumption was estimated to be 100 μW, as a worst-case scenario. With these assumptions, we conducted a set of experiments to map the required time between charges (energy harvesting drought duration) and supercapacitor size. Using COTS supercapacitors, we tested four capacitance values: 82 mF, 164 mF, 246 mF and 328 mF. These values were chosen based on previous knowledge acquired during other projects. The experiments consisted in charging the supercapacitors to 3 V and monitoring the discharge time until 1.5 V with a constant load of 33 μA, which corresponded to the 100 μW assumption. In Figure 4.4, we show a diagram of the testing setup for the discharge evaluation. An ammeter was added to the setup to monitor the current of the system, which was set using the potentiometer in the current sink. Additionally, a Shimmer node was used to monitor and log the voltage in the capacitor during the discharge process.

From the experimentation, for each capacitance value the respective recorded runtimes were 53 minutes, 115 minutes, 207 minutes, and 247 minutes. Using this information, we performed a linear fitting with an R^2 = 0.9713, and followed with an extrapolation technique to estimate the required capacitance to meet a specific runtime. For our application, the required capacitance value for a 12-hour runtime with no harvesting was determined to be 929 mF. This

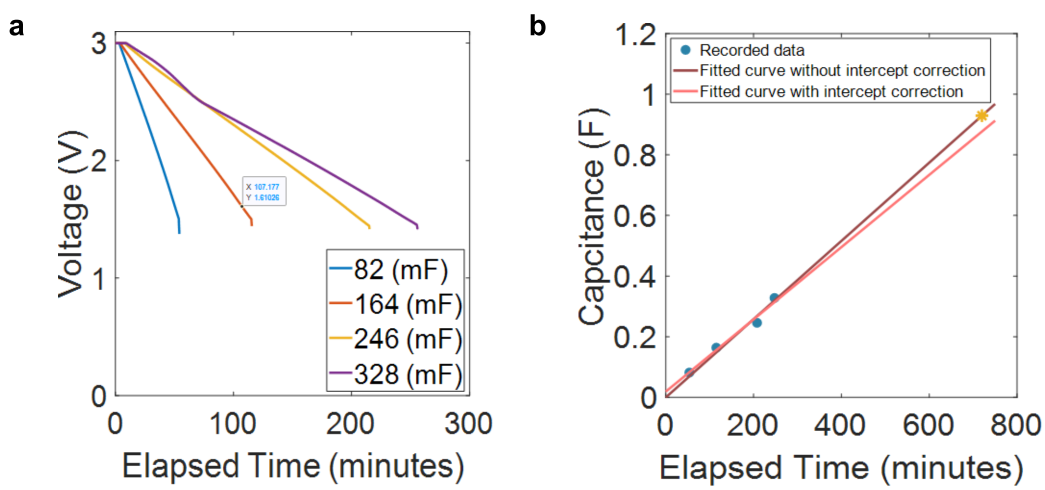

Figure 4.5 | Evaluation to determine supercapacitor size. a) Runtime evaluation for fully-charged supercapacitors. The discharge time from 3V to 1.5V with a constant load of 33 μA was recorded. **b)** Using the results from the runtime testing, a linear fitting was done to extrapolate the corresponding supercapacitor size for a 12-hour runtime under no harvesting conditions. The fitted curve was corrected to fit the physical behavior at time t=0.

calculated value, along with the leakage of the supercapacitors used in the experimentation, were turned into specifications for a custom supercapacitor that was designed for the vigilant cardiac monitoring system. Further details and discussion about this device are presented in Chapter 6.

4.3. Maximizing Harvested Power

4.3.1. Introduction

Considering the general architecture of a self-powered system as shown in Figure 4.6, system power modeling was applied to the System Load block in the architecture and then followed by the appropriate selection of energy storage elements to guarantee the self-powered

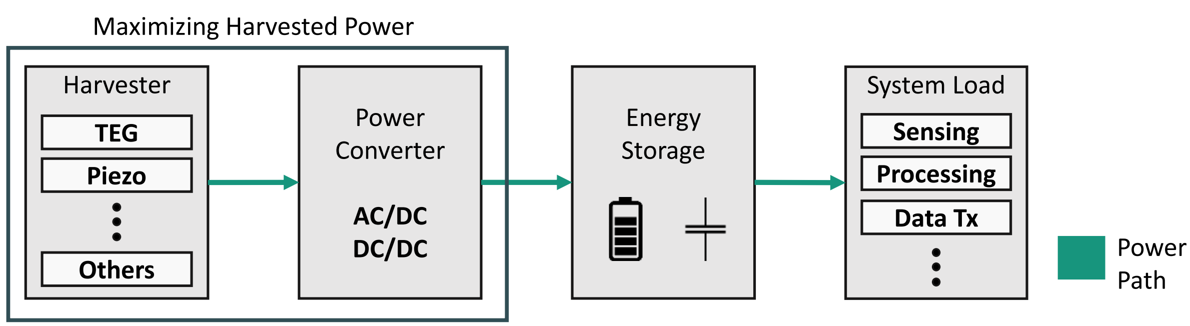

Figure 4.6 | General architecture of a self-powered system. The optimizations to maximize the harvested power in a given system have place at the harvester and/or the power converter.

operation during energy harvesting droughts. Continuing in that direction, opposite to the power path, maximizing harvested power looks at the two components left in the architecture: the harvester and the power converter.

In this section, we consider the respiratory health monitoring case study to present two methods for such power optimization. The first method focuses on the design of the harvester to be used in the application, and it is supported by the work presented in Chapter 3 about energy harvesting profiling. The second method consists on minimizing the losses from the harvestable power to the usable power during the power conversion process.

4.3.2. Harvester Design Optimizations

The mathematical model for piezoelectric cantilevers presented in Chapter 3 is a great mechanism to understand the behavior of the cantilevers for different flow conditions. However, its purpose is not to predict energy harvesting levels, but to present trends in the behavior of the device. Therefore, for a system implementation using these elements, additional work is necessary to define the harvester that can help achieving self-powered operation.

Intuitively, for most harvesters, a bigger surface area of the device represents a higher power output. This is true for solar cells and thermoelectric generators. Nonetheless, for piezoelectric cantilevers the statement does not always hold given that the additional area in these devices also represents a load for the harvester that can affect the power output. In addition, each

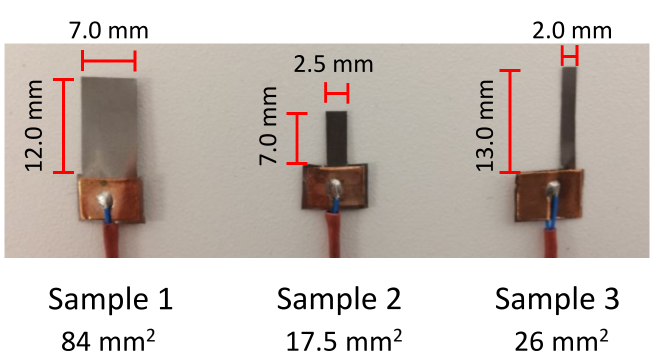

Figure 4.7 | Piezoelectric cantilever samples for size evaluation. The size of a harvester directly affects the power it can output; however, this does not apply to all types of harvesters.

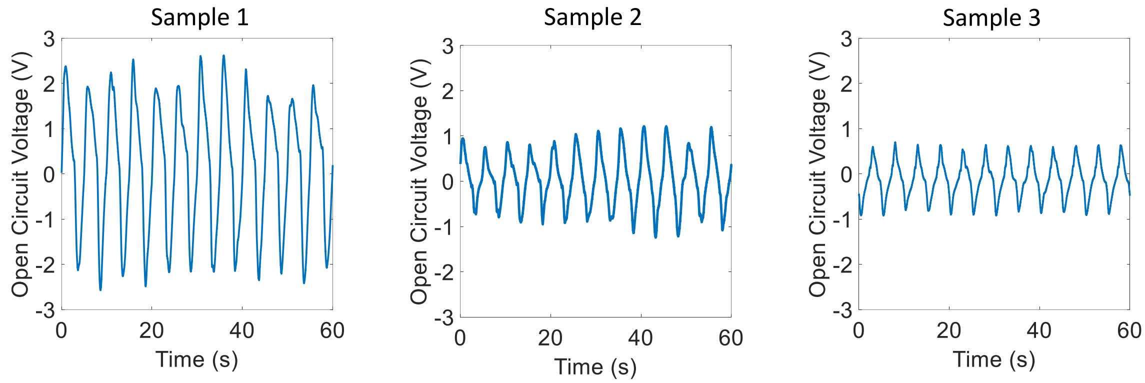

Figure 4.8 | Example of the response of the cantilevers during testing. The open circuit voltage of the cantilevers was used as an indicator of the potential output power for each device.

application presents space constraints that limit the size and/or shape that the harvester can adopt. To find the most suitable harvester for the respiratory health monitoring system, we conducted a set of experiments that looked at the size of the cantilevers.

To evaluate the effects of size in the cantilevers ability to harvest energy, we created three rectangular piezoelectric cantilever samples with different dimensions that corresponded to surface areas of 84 mm^2, 17.5 mm^2, and 26 mm^2., as shown in Figure 4.7. Then, the devices were incorporated to the test setup presented in Chapter 3 for piezoelectric characterization and tested under breathing conditions of 0.5 L and 1 L with rates that went from 12 BPM to 25 BPM. These parameters represent typical breathing conditions for adults at rest.

To analyze the potential for power output from the devices, the open circuit voltage of the cantilevers was used as an indicator and recorded over the entire test. In Figure 4.8, we present 60-second windows of the output voltage for the three samples in consideration at 0.5 L and 12 BPM. Sample 1 shows the highest amplitude of the three, as expected being the bigger device. Sample 2 on the other hand seemed to give a higher output than sample 3 despite the smaller surface area, which seems counterintuitive at first. However, looking at the structure of the cantilever and the harvesting environment in which the devices were operating, we can explain the behavior mainly due to the loading effect of the additional material in Sample 3 with respect

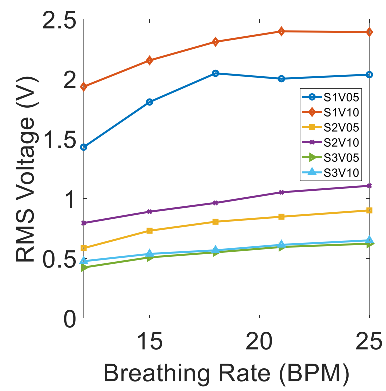

Figure 4.9 | RMS voltage of the piezoelectric cantilevers during testing. Sample 1 showed the highest open circuit voltage from the three samples, making it the better harvester. Sample 2 outperformed sample 3 despite the smaller surface area.

to Sample 2 and the fact that during the breathing cycle, this end section of the harvester does not suffer a big deformation to produce more power.

This behavior was verified for the entirety of the experiment, and it is summarized in Figure 4.9, where the RMS voltage for each cantilever and each breathing condition was calculated. In conclusion, Sample 1 showed to be the best harvester for the application and it was confirmed that the size of the harvester does not necessarily mean a higher power output.

4.3.3. Energy Harvesting Circuits for Piezoelectric Harvesters

In contrast with other harvesters such as solar cells and TEGs, piezoelectric devices produce an AC signal that needs to be converted to DC before it can power a sensor node. A very common circuit used for this conversion is the full bridge rectifier [92], [93]. This circuit is integrated by four diodes that are *activated* in pairs, and which conduct the current coming from the harvester always in the same direction to store the harvested energy into a capacitor. This circuit has the advantage of being simple, therefore making it easy to be successfully implemented in any given application. The limitation of this design is the non-negligible losses in the diodes related to the barrier at the P-N junction that forms the device and which is presented as a voltage drop across the diodes (forward voltage). Typical values for this voltage drop in commercially available devices is around 0.7 V, with low-forward diodes that show a voltage drop of ~100 mV. Although these voltage numbers can be negligible for several applications, in the case of self-powered devices, this can be a determinant to achieve self-powered operation or not.

An alternative circuit with better efficiency is the voltage doubler. This rectifying circuit uses only two diodes and adds an additional capacitor to deal with the half-wave that was rectified by the other pair of diodes in the full bridge circuit. The two main advantages of this circuit are 1) the reduced number of diodes for implementation and 2) the capacity of the circuit to output the maximum power at a higher output voltage: almost twice the output voltage of the full bridge circuit. As a result, the maximum output power of an energy harvesting circuit using a voltage doubler is higher than the one using a full bridge rectifier [94]. Figure 4.10 presents the topologies of both harvesting circuits and their Output Power vs. Output Voltage curves for a given circuit.

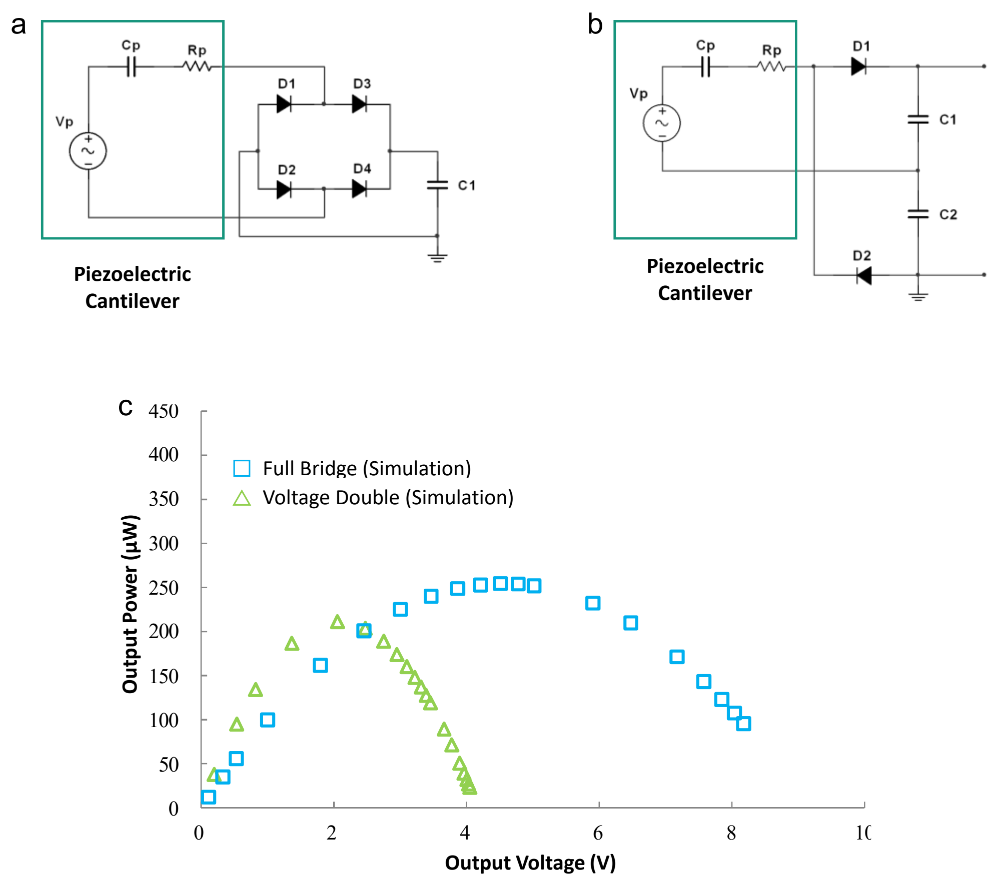

Figure 4.10 | Piezoelectric energy harvesting circuits. a) Full bridge rectifier, **b)** Voltage doubler, **c)** Typical Output Power vs. Output Voltage curve for the two circuits in discussion (adapted from [83]).

Researchers have developed additional harvesting circuits for piezoelectric energy harvesting with higher conversion efficiency by adding switching devices [94], [95]. These new topologies are a combination of the full bridge rectifier or voltage doubler in parallel with the switching circuit. Furthermore, maximum power point tracking is a technique where the harvesting circuit adapts the impedance seen by the harvester to match the value at which the harvester reaches the maximum power output. Latest contributions have added MPPT to the switched topologies for additional improvement [96].

For the respiratory health monitoring case study, a voltage doubler was adopted given the improved energy harvesting efficiency over the full bridge rectifier with minimized complexity for implementation. Although small, this improvement showed enough benefit in the realization of the desired self-powered prototype for the case study. In addition, since the purpose of this dissertation is the development of a framework that assists in the design of self-powered devices and not specific circuit design contributions, the study of more complex circuits is out of the scope of this work.

Chapter 5

Application-Specific Quality of Information Metrics

The definition of application-specific QoI metrics in the design of sensing systems shifts from the idea of providing all the information possible to instead presenting the required information in a given application. The advantages of this approach are that it allows for a more refined specification of requirements in the system and reduced data saturation, a problem faced by current information systems [97], [98].

The relevance of an appropriate definition of QoI metrics in achieving self-powered operation for systems operating in dynamic low harvesting environments can be better understood by looking at the relations among the three main components of a self-powered system: energy harvesting, power management, and sensing (related to QoI). To further help present this concept, we look at the two types of system discussed in this dissertation.

For an information-driven self-powered system, it is desired that the energy fluctuations that occur in the energy harvesting sub-system become *invisible* to the sensing sub-system. This means that the information generated by the device always meets the defined quality regardless of the energy harvesting levels. To achieve this, the power management sub-system acts as mediator that masks the activity in the energy harvesting subsystem from the sensing subsystem. On the other hand, in a harvesting-limited self-powered system, the activity in the energy harvesting sub-system is closely related to the information that the sensing sub-system generates, and the power management sub-system acts as a facilitator for a harmonious interaction between the two to provide useful information. In general, one can think of an

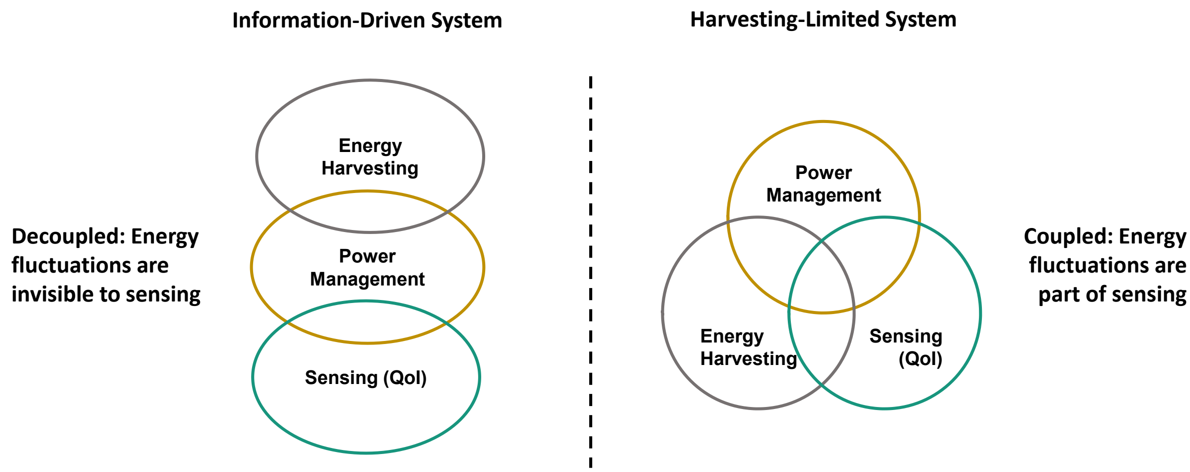

Figure 5.1 | Self-powered systems as coupled systems. The effects of appropriate QoI metrics and self-powered operation can be understood by looking at the relation between energy harvesting and sensing.

information-driven system and a harvesting-limited system as a coupled and decoupled self-powered system, respectively. Figure 5.1 helps illustrate this concept.

In this chapter we further discuss these relations and the benefits of adequate QoI metrics to achieve self-powered operation in dynamic low harvesting environments using the two case studies defined in Chapter 2.

5.1. QoI for Information-Driven Self-Powered Systems[3]

5.1.1. Introduction

Within the self-powered sensing systems, the information-driven approach is the most commonly adopted when designing a sensor for critical applications such as the vigilant cardiac monitoring case study in this dissertation, although oftentimes it is not identified as such. This is because traditional low-power embedded systems, the predecessors of self-powered sensors, are designed following the same principle. As a reminder, in this approach, the power budget is defined by the sensing requirements according to the application of interest. Following these requirements, the goal is to reduce the power consumption as much as possible and/or maximize

[3] The work in this section was done in collaboration with Dawei Fan.

the harvested power to meet those requirements. By definition, the QoI of these types of systems is assumed to be high.

In alignment with our cardiac case study, a look at low power systems for ECG monitoring reported in the literature demonstrates the adoption of the information-driven approach during the design process as a common practice. For instance, the work developed in [41] emphasizes the need for higher sensing capabilities (i.e., higher resolution, less noise, higher sampling frequency) to produce *better* information during long-term cardiac monitoring. Accordingly, the authors design the hardware catering to these sensing specifications as their design premise followed by power optimizations after those specifications have been established. Similarly, a low-power ECG sensing system introduced in [99] presents a design based on a COTS chip optimized for biopotential sensing. As such, the authors highlight the chip's high resolution, signal to noise ratio (SNR), and high sampling frequencies to support the selection of the component to integrate the core of their system. The authors of [100] and [101] present similar arguments for their designs, and the researchers in [102] build upon those ideas to emphasize the high-data transmission feature that their sensor has due to high sampling frequency and a compression algorithm.

All this type of systems are important contributions to wearable sensing technology. However, their full potential to achieve low-power operation is limited by following standard digital signal metrics established for signal reconstruction. In some cases, this is decided to meet certain regulations, and in some others with the goal of catering to multiple sensing applications. In the case of self-powered sensors, this represents a big tradeoff that requires further analysis to guarantee the usefulness of the information provided by the system despite not following those same metrics. In our cardiac case study, we present this analysis by looking at sampling frequency and bit resolution to determine the minimum optimal specifications to perform AFib detection. Furthermore, we correlate this analysis to the self-powered operation of the vigilant cardiac monitoring system using the power model derived in Chapter 4, and illustrate the design space for this system according to different sensing conditions.

5.1.2. Vigilant Atrial Fibrillation Sensing

Given the characteristics of AFib described in Chapter 2, the analysis of R-R intervals and atrial activity waveforms are two of the main methods for AFib detection. In a comparative study for AFib detection reported in [103], the algorithm performance for both approaches was evaluated, and it was concluded that the R-R interval-based approach provided better results. Therefore, an R-R interval approach was adopted for the analysis performed in this dissertation.

Multiple techniques for AFib detection using R-R interval variations have been reported in the literature. In [104], a normalized R-R interval variation threshold is set to classify AFib events. In other works, both R-R interval and its change are used for detection of AFib [105]. In [106], the

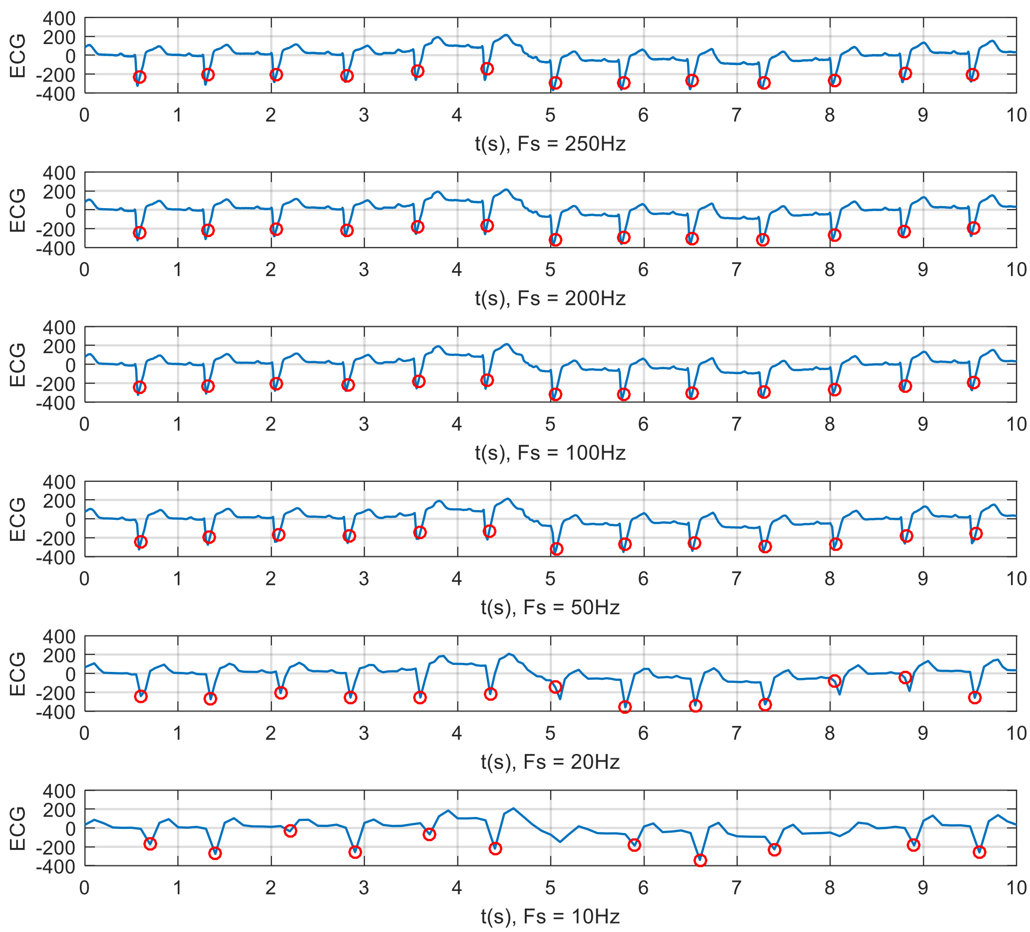

Figure 5.2 | R-peak detection on ECG signals from MIT-BIH database. R-peak detection (red circles) was performed on the original ECG signal and several down-sampled versions. With the decrease in sampling rate, the ECG signal becomes distorted, but the R peak detection works well until a minimum sampling rate of 20Hz.

Kolmogorov-Smirnov test is used to detect AFib episodes. For our application, we used the method in [104] for its simplicity and high performance. For R-R interval calculation, we used the curve length transform introduced in [107] and a wavelet transform [108]. The advantage of using a curve length transform algorithm is that it has the capacity to deal with baseline changes using a dynamic threshold.

The original ECG data employed in the exploration was retrieved from the MIT-BIH AFib database [109], number 05121. The data was collected using ambulatory Holter monitors with a sampling frequency of 250 Hz. The total length of the recordings corresponds to 10.23 hours, which contains 26 AFib events and junctional premature episodes that comprise 6.51 hours out of the total length. For the assessment, the raw ECG signal was down-sampled to simulate low sampling rate scenarios. Then the AFib detection with R-R interval calculation algorithm was executed using the down-sampled ECG signals as the input. The R-R interval calculation algorithm was reimplemented from [107] to tune the parameters for dealing with low sampling frequency scenarios. Figure 5.2 shows a 10 second window of ECG data at the original sampling frequency and five down-sampled versions.

To quantitatively evaluate the performance of the AFib detection algorithm with respect to the sampling frequency, the receiver operating characteristic (ROC) curve was created considering

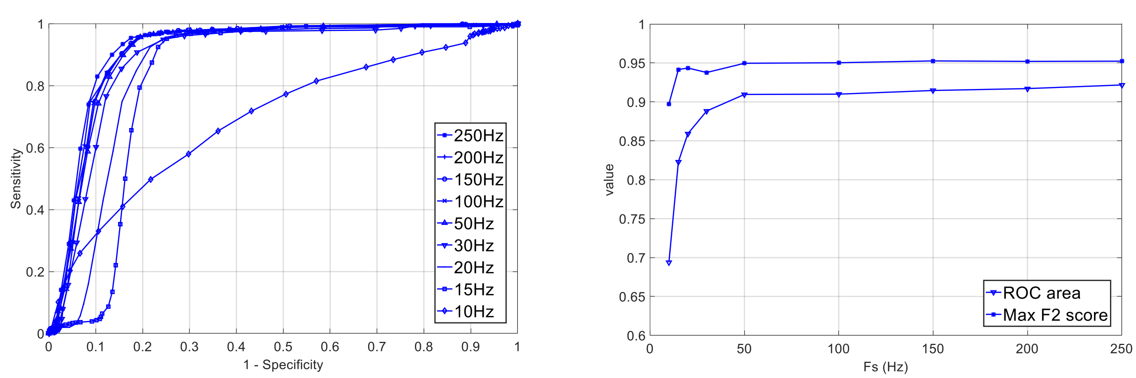

Figure 5.3 | Algorithm performance evaluation with respect to sampling frequency. a) The receiver operating characteristic (ROC) curve of AFib detection under 9 sampling rates. The curve is moving inwards as the sampling rate decreases, **b)** The ROC area and maximum F2 score across different sampling rates of ECG data.

9 different sampling rates from 250 Hz to 10 Hz. The resultant family of curves is presented in Figure 5.3a. In general, the curve moves inwards as the sampling rate decreases. Furthermore, to expand the evaluation, the ROC area and the maximum F2 scores were calculated. The results are illustrated in Figure 5.3b. The ROC area corresponds to the area under the ROC curve, and the F2 score considers both classification recall/sensitivity and precision, and weights recall higher to reduce the false negative rate (failed to detect AFib). For each sampling rate, the maximum F2 score was calculated over the set threshold.

For both curves, the value generally increases with higher sampling rate. For the ROC area, the performance increases fast when the sampling rate is low, and it sees diminishing returns when the sampling rate is higher. In addition, from the curves it is possible to see that the performance almost reaches saturation after 50 Hz, which makes it the minimum sampling rate for vigilant AFib monitoring.

A similar analysis looking at the effects of bit depth on the sampled ECG signal was conducted. For this matter, the ROC, ROC area, and F2 score were computed over different quantization depths going from the original 12 bits to 6, as illustrated in Figure 5.4. For completeness, the ROC area results for sampling rate and bit depth were combined to determine the minimum sensing specifications for vigilant AFib detection. Thse results are presented in

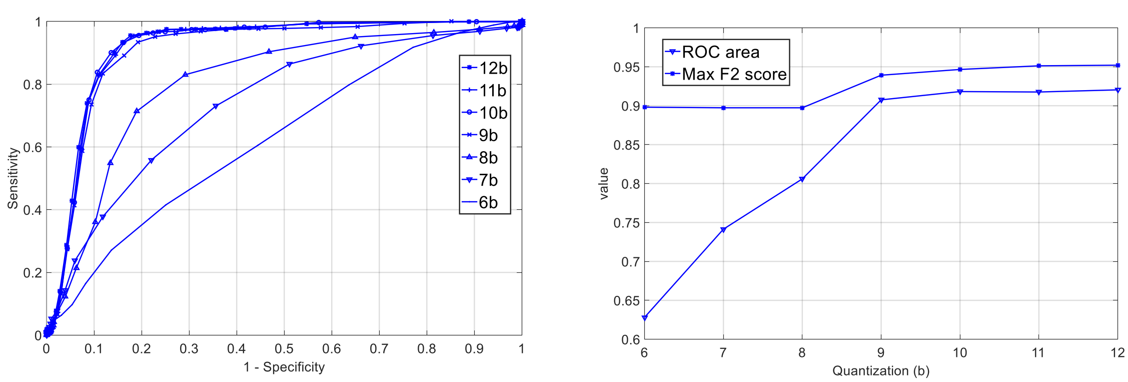

Figure 5.4 | Algorithm performance evaluation with respect to bit resolution. a) The receiver operating characteristic (ROC) curve of AFib detection corresponding to seven bit depths. The curve is moving inwards as the bit depth decreases, **b)** The ROC area and maximum F2 score across different bit depths of ECG data.

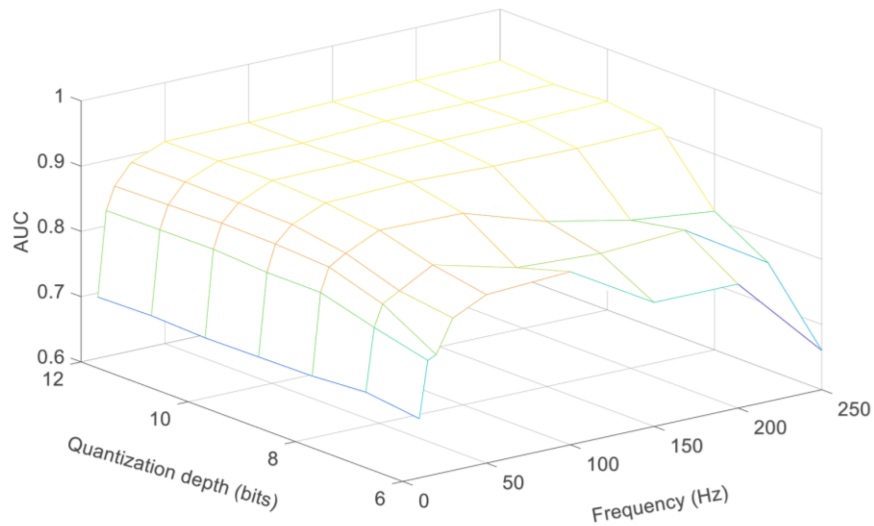

Figure 5.5 | ROC area versus bit depth and sampling rate. The ROC area for different sensing specifications.

Figure 5.5. It is possible to see that the ROC area, representing the performance of the system, is directly proportional to the sampling rate and bit depth. However, some irregularities when the bit depth is below 8 bits are identified. Under these conditions, the above relation does not hold. The main reason for this behavior is that the initial classification result is smoothed using a majority vote. Under the low bit depth scenarios, the R-R interval computation performs poorly, but the smoothing may increase the performance regardless of the sampling rate.

With the interpretation of the results from this analysis, it is possible to establish that sensing conditions below 50 Hz and 8 bits does not provide useful information for AFib detection and therefore it is not considered for real-world monitoring. Furthermore, from equation (4.6), it is possible to see that these two sensing parameters (i.e., sampling frequency and bit depth) have a considerable impact in the total power consumption of an embedded system. Therefore, determining the minimum sampling frequency and bit depth for vigilant AFib monitoring will reflect in important power savings. Most cardiac systems use high sampling frequencies and bit depths (>100 Hz and >10 bits) to capture ECG with the goal of faithfully recreate the signal, however for vigilant AFib detection, signal recreation may not be necessary.

5.1.3. Information-Driven Approach and Self-Powered Operation

System power modeling was introduced in Chapter 4 as a mechanism to identify and evaluate areas of opportunity for power optimizations. The implications of finding the appropriate sensing specifications in power levels and therefore in achieving self-powered operation can be demonstrated using this power modeling technique and considering a specific sensing system. In this case, the sensing system to examine is the vigilant cardiac monitoring system paired with the sensing conditions used in the analysis in section 5.1.2.

For completeness, we start by rewriting equation (4.6), previously defined as

$$P_T = P_{St} + f_s t_{smpl} P_{smpl} + \frac{f_s}{N} t_{tx} P_{tx} + \left(1 - f_s t_{smpl} - \frac{f_s}{N} t_{tx}\right) P_{slp}. \tag{5.1}$$

In this equation we can directly identify the sampling frequency represented by f_s and see a directly proportional relationship to power. However, the bit resolution is hidden in the variable N, which again represents the number of samples in a transmission packet. Let us then define N as

$$N = \frac{K_{sz}}{L_{sz}}, \tag{5.2}$$

where K_{sz} and L_{sz} represent packet size and sample size, respectively. Both with units expressed in terms of bits. This is

$$K_{sz}: \left[\frac{\#\ of\ bits}{1\ packet}\right] \quad \text{and} \quad L_{sz}: \left[\frac{\#\ of\ bits}{1\ sample}\right], \tag{5.3}$$

then substituting N in equation (5.4) with equation (5.2), the expression for total power consumption can be rewritten as

$$P_T = P_{St} + f_s t_{smpl} P_{smpl} + \frac{f_s L_{sz}}{K_{sz}} t_{tx} P_{tx} + \left(1 - f_s t_{smpl} - \frac{f_s L_{sz}}{K_{sz}} t_{tx}\right) P_{slp}. \tag{5.4}$$

Furthermore, considering that the power consumption in the system during sleep (P_{slp}) is much smaller than the power consumption in any of the other switching states (P_{smpl}, P_{tx}), equation 5.1 can be simplified as

$$P_T \approx P_{St} + f_s t_{smpl} P_{smpl} + \frac{f_s L_{sz}}{K_{sz}} t_{tx} P_{tx}, \tag{5.5}$$

where one can see more clearly that the total power consumption of the system is directly proportional to both variables -sampling frequency and bit resolution. Additionally, K_{sz} is defined by the wireless communication protocol used, in our case Bluetooth, and it is a constant value. Consequently, for a given set of hardware components integrating the vigilant cardiac monitoring system, which are discussed in Chapter 6, the design space considering sensing specifications and power consumption is represented by the plot shown in Figure 5.6.

By computing the slopes of the lines, it is possible to determine the rate of change in power per Hz or bit in the system. At the minimum sampling rate of 10 Hz considered in the vigilant AFib analysis, the power increases with bit resolution at a rate of 1.23 μW/bit while at the maximum sampling rate of 250 Hz, the growing rate of power is 30.75 μW/bit. On the other hand, for the minimum bit resolution of 6 bits, the power consumption of the system increases by 1.28 μW/Hz, while the slope for a 12-bit resolution corresponds to 2.02 μW/Hz.

Finally, by combining the power model from Chapter 4 and the vigilant AFib analysis, it is also possible to establish the power budget that needs to be met by the energy harvester, and inform the selection and/or design of this device. The red marker in Figure 5.6 represents the power budget for the vigilant cardiac monitoring system in this dissertation operating at the

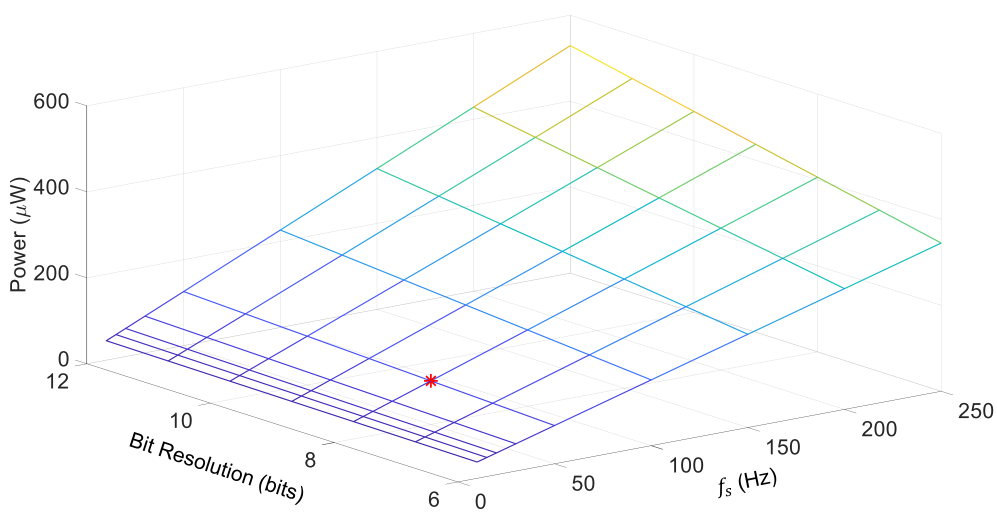

Figure 5.6 | System design space with respect to sensing specifications. The surface condenses the set of power consumption estimations for all the sensing conditions considered for the vigilant AFib analysis. The red marker indicates the estimated power consumption for 50 Hz and 8 bits.

minimum sensing specifications for AFib detection, which is estimated to be 101.3 μW. This number was used in Chapter 4 for the appropriate sizing of the storage element as a way to deal with harvesting droughts.

5.2. QoI for Harvesting-Limited Self-Powered Systems

5.2.1. Introduction[4]

The value of a self-powered system with harvesting-limited operation highly depends on the usefulness of the information that it can provide. Therefore, it is fundamental to develop a method to provide meaningful data for systems following this design approach. As a reminder, in the design of harvesting-limited systems, the first step is to establish a power budget according to the harvester being used and the environment where it will be operating. Once this step is completed, power optimizations are performed, and the information provided is the result of a best-effort approach.

Even though there are no strict sensing requirements that need to be met by these types of systems, it is necessary to establish a minimum acceptable information threshold. This threshold is particular to the target application and can be set based on several factors such as previous sensing experiences, criticality of the application, or even the lack of any previous sensing information. For instance, we know that outdoor ambient temperature does not change drastically in a short period of time, thus for a person to plan their day outside, providing temperature readings in the morning, afternoon, and evening might be enough. In contrast, in an industrial application monitoring the temperature of some machinery, that same frequency of readings is very likely insufficient since any issue with the equipment may not be detected in time to prevent any higher complication. Moreover, for a recently discovered fish, a sensor harvesting energy from the animal natural swimming and reading its body temperature once a day could represent a big contribution for marine wildlife researchers.

[4] The work in this section was done in collaboration with Prof. Dan Quinn and Lucy Fitzgerald

For the development of this section and to guide the discussion around this type of systems, we will consider the respiratory health monitoring case study introduced in Chapter 2. The final goal for this system is to provide continuous information about the airways in patients with chronic respiratory conditions as an alternative to sporadic and burdensome spirometry tests. For this application, guaranteeing even a reading per day represents more information than what is currently collected in the majority of cases for patients suffering these conditions.

In this section, we will look at the feasibility of extracting and presenting information from the airways through indirect sensing that searches for a relation between the harvested energy and the conditions in the airway.

5.2.2. Indirect Sensing Through Harvesting Levels and Ping Rate

Based on the findings of our study on energy profiling for piezoelectric cantilevers discussed in Chapter 3, power levels in the order of nW represent a challenge to perform continuous active sensing using commercially available technology. As an alternative, we explored the possibility of using the harvester as the sensor at the same time, where the harvesting levels serve as a proxy to the flow conditions in the airway. We refer to a device operating in these conditions as a *sharvester*.

To present a first order analytical approximation, let us consider the architecture shown in Figure 5.6 for the respiratory health monitoring system. The sharvester delivers an AC signal generated from the oscillating flow in the airway, then the AC/DC conversion occurs and the harvested energy is stored until a certain threshold is reached, when the switch S closes and

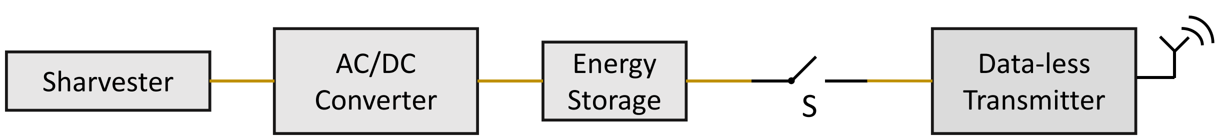

Figure 5.7 | Architecture of the respiratory health monitoring system. In this system, the harvester has a dual purpose: to provide energy to the system and act as a sensor. Therefore, the name of sharvester.

powers the data-less transmitter that generates an RF ping. The RF ping can be detected by an external receiver. Then let P_{pz} be the power delivered by the piezoelectric sharvester at the input of the AC/DC converter, whose power conversion efficiency is denoted by η and defined as

$$\eta = \frac{P_{DC}}{P_{pz}}, \tag{5.6}$$

where P_{DC} represents the output power after the AC/DC conversion. We called this the usable power. Solving for P_{DC}, we can see that

$$P_{DC} = \eta * P_{pz}. \tag{5.7}$$

From this point on, the rest of the system can be represented by the equivalent circuit shown in Figure 5.8 and P_{DC} can be expressed in terms of voltage and current as

$$P_{DC} = V_{DC} * I_{DC}. \tag{5.8}$$

Furthermore, R_p represents all the parasitic resistance in the circuit and C_s the storage element. With this configuration, the current coming from the AC/DC converter (I_{DC}) and the voltage in the capacitor (V_{Cs}) can be modeled by the charging equations of the RC circuit expressed as

$$I_{DC} = \frac{V_{DC}}{R_p} e^{-t/R_pC_s} \text{ and } V_{Cs} = V_{DC}(1 - e^{-t/R_pC_s}). \tag{5.9}$$

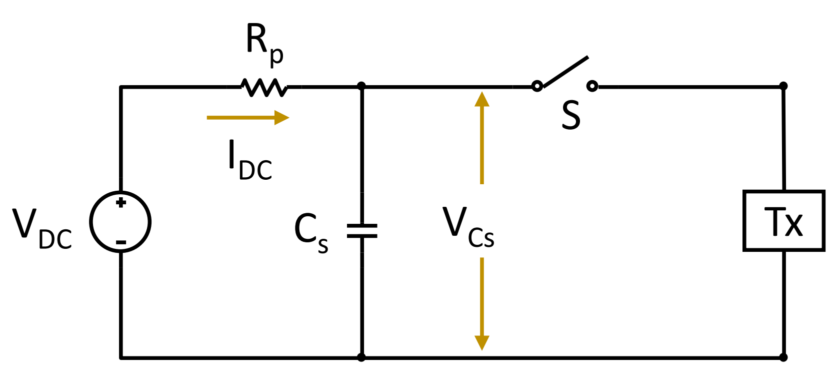

Figure 5.8 | Equivalent circuit after AC/DC conversion. By considering the equivalent RC circuit, an expression for the time required to generate an RF ping can be derived.

To determine the average power coming from the converter and therefore the piezo cantilever during the time until a ping occurs, we can start by looking at the energy consumed during this process written as

$$E = \int_0^{t_p} V_{DC} * I_{DC}(t)dt = V_{DC} \int_0^{t_p} I_{DC}(t)dt, \tag{5.10}$$

where t_p is the time until the circuit pings. Then substituting I_{DC} from equation (5.9) and solving the integral in equation (5.10), we have

$$E = \frac{V_{DC}{}^2}{R_p}\left(-R_p C_s e^{-t/R_p C_s}\right) \Big|_0^{t_p} = V_{DC}{}^2 C_s \left(1 - e^{-t_p/R_p C_s}\right). \tag{5.11}$$

Since the power is the energy per unit time, the average power from the converter until a ping occurs can be derived as

$$\overline{P_{DC}} = \frac{V_{DC}{}^2 C_s}{t_p}\left(1 - e^{-t_p/R_p C_s}\right), \tag{5.12}$$

and using the expression for V_{Cs} in equation (5.9) considering that $V_{Cs} = V_{th}$, with V_{th} being the threshold voltage in the capacitor at which the switch S closes to produce a ping, the average power from the converter as a function of t_p and V_{th} is written as

$$\overline{P_{DC}} = \frac{V_{DC} C_s}{t_p} * V_{DC}\left(1 - e^{-t_p/R_p C_s}\right) = \frac{V_{DC} C_s V_{th}}{t_p}. \tag{5.13}$$

Finally, we use equation (5.6) to derive an expression for the average power delivered by the cantilever, which is written as

$$\overline{P_{pz}} = \frac{1}{\eta} * \frac{V_{DC} C_s V_{th}}{t_p}. \tag{5.14}$$

This expression serves the purpose of demonstrating that a relation between ping rate and harvested power can be established, but we need to acknowledge the limitations it presents, many of which are related to the non-idealities of devices in the real world. Let's think about the test setup for piezoelectric cantilevers introduced in Chapter 3. The expression assumes a symmetric signal coming from the cantilever, but as we can remember from Figure 4.8, this is never the case since the deflection in the cantilever that occurs during exhalation is normally different during inhalation. In the case of the capacitor C_s, the equivalent circuit does not consider the leakage from the capacitor and the switch, which at very low power levels can have an important impact in the transmission events and self-powered operation. This will be better illustrated in Chapter 6. Finally, and perhaps more importantly, the harvesting levels coming from the cantilever do not only depend on the airflow in the airway, but also other physical factors such as temperature, humidity, etc. Therefore, a 1:1 function that considers all these variables requires additional work in profiling and modeling that is beyond the scope of this dissertation.

5.2.3. Broadband Sensing with Harvesting-Limited Sensor Arrays

To expand the potential alternatives to provide valuable information in harvesting-limited sensor systems, we looked at the possibility of using arrays of harvesting-limited sensors to capture signals with different frequencies. This exploration was done within the respiratory health monitoring case study but can be easily extrapolated to other fluid sensing applications. The hypothesis for this approach is that piezoelectric cantilevers with different geometries also present different resonant frequencies (i.e., the frequency at which they are more efficient) [110]. Therefore, in a complex flow with multiple frequency components, some elements will produce a ping rapidly while others stay dormant. The set of pings will also now contain information about the flow's frequency if the cantilevers that were excited are known. A sketch of this hypothesis is shown in Figure 5.9. It is worth noting that a similar principle is used in other applications such as cochlear implants, where different electric stimulators in the ear are activated based on specific frequencies that are perceived by the implant [111].

Our first step in this exploration consisted of a simulation that allowed us to establish a circuit to carry an experimental validation of our hypothesis using the setup developed and introduced in Chapter 3. The circuit is shown in Figure 5.10 and it was based on the design of a single harvesting-limited sensor that is discussed in detail in Chapter 6. The circuit to validate integrates

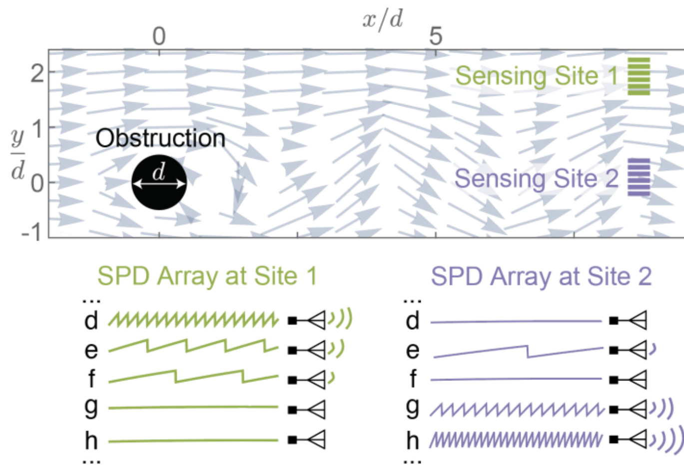

Figure 5.9 | Broadband sensing for harvesting-limited flow sensors. Using an array of sharvesters it may be possible to capture more information from complex flows whose behavior is not purely laminar.

three harvesting-limited sensors powered by three different sharvesters. The sharvesters in the simulation are configured to produce signals with different characteristics in terms of voltage and current, which directly correlate to their output power. This setting represents different excitations from the flows where the devices are deployed. The output coming from the switches in the circuit (S_1, S_2, S_3) was connected to a single load emulating the data-less transmitter.

If three identical harvesting-limited sensors were used, it would be almost impossible to map the ping generation to the corresponding sensor without an identifier. An option to overcome this challenge is to use different data-less transmitter that operate at different transmission frequencies. However, this increases the complexity of the design and potentially the power consumption of the electronics. As a solution, we used different capacitor sizes for each sensor as the identifier since the size of the equivalent capacitor is directly correlated to the duration of the ping.

The results of the simulation showed that the topology of the circuit array could effectively operate to produce identifiable pings, which could be later related to a specific location in the airway and conditions of the surrounding environment. A snippet of the results is presented in Figure 5.11. An interesting result was the fact that even when two or more sensors pinged, it was possible to identify the group of sensors that were activated.

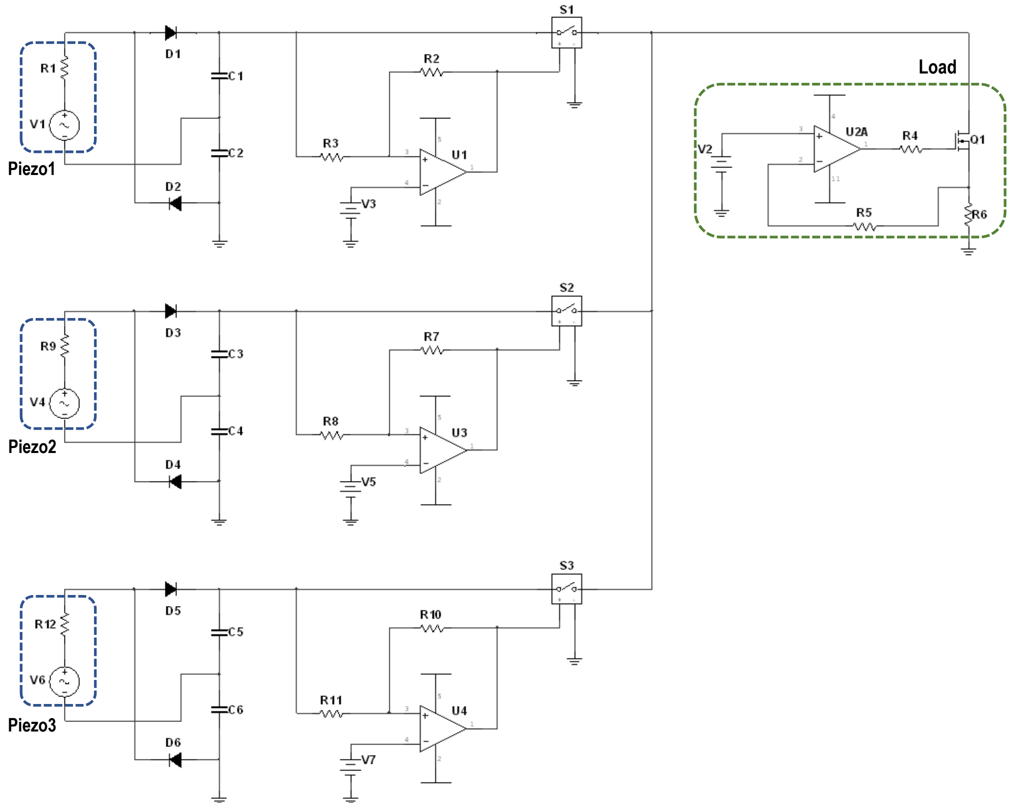

Figure 5.10 | Proposed circuit for broadband sensing with harvesting-limited sensor arrays. The circuit is intended to generate pings as a result of complex flows.

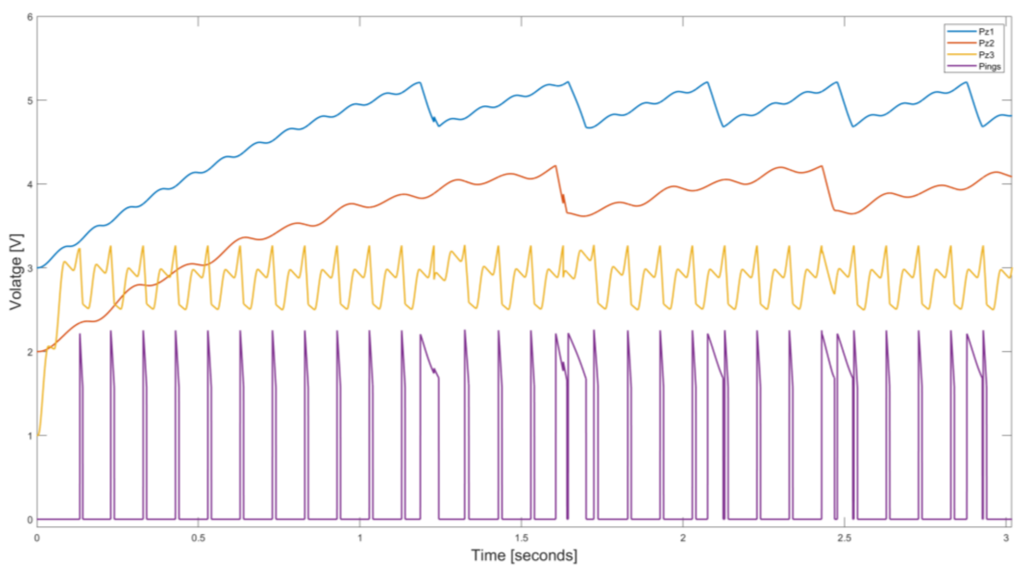

Figure 5.11 | Simulation results for the harvesting-limited array circuit. The circuit is effective at identifying the sensor that is activated by the flow as a mechanism to capture multifrequency information contained in a complex flow.

To complete the validation of our hypothesis we implemented a similar circuit to the one in Figure 5.10 and incorporated it into the test setup describe in Chapter 3 for piezoelectric cantilever characterization. Each sensor was powered by a rectangular cantilever with different widths and lengths. The array was tested following a similar procedure as the one described in Chapter 6 for a single harvesting-limited sensor with a sweep in breathing rate and tidal volume. From the results of this experimentation, we verified that an array of harvesting-limited sensors has the potential to increase the QoI of a sensor system using this approach compared to a single sensor. In Figure 5.11, we show a sketch of the cantilevers employed with their corresponding dimensions, and short sample of two of the sensors pinging seen from the charge and discharge process of the capacitors in each sensor.

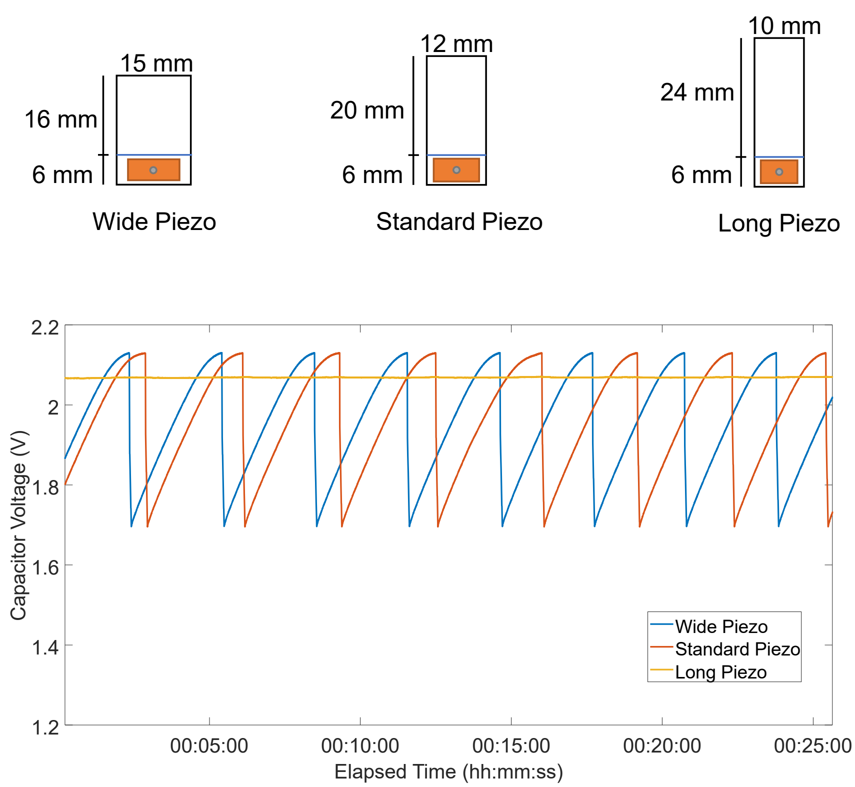

Figure 5.11 | Experimental demonstration of the harvesting-limited array circuit. The circuit for broadband sensing was implemented and tested using three piezoelectric cantilevers with different geometries and resonance frequencies.

Chapter 6

Self-Powered Sensor Systems for Health Monitoring

The growing synergy between engineering and medicine has yielded a new paradigm known as mobile health (mHealth) that enables continuous remote monitoring for a variety of health and wellness applications [26], [112]. The mHealth framework enables the transition from the discrete data healthcare model with time and location-limited samples to a continuous data model that captures critical data anytime and anywhere. This new approach not only enables the detection of rare events but also the delivery of just-in-time and personalized interventions [113].

Wearable sensors are a critical component of mHealth given their continuous connection to the wearer and their increasing ability to track relevant physiological, behavioral, and ambient factors. But despite their demonstrated potential to improve health outcomes, their adoption by physicians and acceptance by users have been limited [28], [114]. One issue is the big data problem, where the large amount of often-noisy data can be hard to decipher into actionable information and knowledge [115]. But for the data even to be generated, user compliance issues have to be addressed, as form factor, comfort, and battery life have all posed challenges to wearables [116]. The methodical integration of advancements in materials, sensing, low-power electronics, wireless communication, and system design represent an opportunity to help with these challenges.

Several efforts in those individual areas have focused on the development of specific technologies targeted to wearable sensors, shrinking the devices, integrating them with standard clothing and accessories, and extending battery life. Bridging the gap among these endeavors can result in a new generation of wearable sensors that are self-powered from the body to help propel the mHealth framework to a new realm that improves access to quality care for all. This new class of self-powered wearable sensors has several key benefits. Operating from energy harvested on the body in a clothing-integrated form factor means that the system can produce data continuously whenever it is worn without any user actions required. In contrast, each operation performed by a battery-powered system shortens its subsequent lifetime, leading to either less continuous data collection or the need for a user to recharge the battery, which can reduce compliance over the long term.

In this chapter, we present two self-powered sensing systems for health monitoring following the case studies introduced in Chapter 2. The design of each system adopted a different approach that uses the proposed framework from this dissertation. These approaches are discussed in further detail within each system's subsection. The end-to-end functionality achieved with the systems demonstrates the potential of the framework to assist in the synergistic integration of individual sensing technologies to achieve self-powered operation in dynamic low harvesting environments.

6.1. Vigilant Cardiac Monitoring System Powered by Body Heat

6.1.1. Introduction[5]

User compliance and battery life represent two major challenges for the widespread adoption of wearable technology. The implications of these issues are commonly reflected in the willingness of the user to wear the device, the system losing power during the deployment, or the effects of the latter on the former by having the user frequently recharge the device. To address user acceptance, researchers have made innovations related to form factor, operation and maintenance [28]. In addition, multiple efforts have been made to develop ultra-low power electronics to increase battery life or even to replace the battery itself by harvesting energy from

[5] The cardiac system was a collaboration among multiple universities as part of the ASSIST Center.

the environment or the body [117]. However, achieving these operating conditions typically requires reduced sampling rates and duty cycling, which may result in missed critical cardiac and activity events, relegating the system incapable of providing vigilant monitoring.

Achieving long-term vigilance in a self-powered system requires continuously maintaining a positive energy balance. Energy harvesters have been developed for BSNs to scavenge solar energy from the environment, and heat and motion from the body, but form factors, low conversion efficiencies, and variable energy availability have proven to be difficult challenges. Several approaches to efficiently administer the harvested energy have been presented from a hardware and software perspective. In the case of the former, the individual blocks of the energy harvesting and power management unit (PMU) have been optimized for self-powered applications [118]. In the latter, dynamic power management (DPM) techniques have been developed to adjust the operation of the system based on workload, available energy, and required data quality [119], [120]. Even though previous works have investigated the relationship of data quality and power consumption, many of these approaches consider digital signal metrics that may or may not relate to application-level information metrics, such as critical event detection vigilance.

6.1.2. Related Work

The miniaturization of technology has enabled the development of sensor systems that can be attached to the body with purposes that range from disease diagnosis and tracking to physical rehabilitation and behavior modification. For instance, in [117] the authors discuss the design of a system intended for improving the understanding of the impact of increased ozone levels and other pollutants on chronic asthma conditions. Similarly, the authors Han et al. reported in [121] a piezoelectric based system embedded in a shoe sole to identify different forms of human motion. Furthermore, a system designed for motion monitoring during physical rehabilitation is presented in [122]. Given this wide range of efforts in wearables for health applications, Witte et al. conducted a systematic literature review of state-of-the-art devices reported from 2013 to 2018 [123]. The authors conducted an extensive search on four different research literature databases, selecting 200 papers from each database as a representative sample based on relevance for their fields. After multiple filters using a predefined criterion, 97 papers were selected for the systematic review. To analyze the reported works, the authors classified the papers based on disease treatment, application area, vital parameter measurement and target patients. From this evaluation, five potential research areas were identified: application scenarios for widespread diseases, expansion of wearable systems functionality, diversity of vital parameters measurement, proactive analysis of sensor data for preventive purposes and promoting patient adoption through enhanced usability.

A comparable exercise done by Pevnick et al. in [124] for cardiac monitoring proposed a taxonomy to classify wearable sensor systems in the general context of health applications based on the data collection mechanism. Such classification was established according to the patient engagement required (passive vs. active), the data acquisition mode (continuous vs. intermittent) and the data management mode (streaming vs. storing). As a result, each reported wearable device could be categorized based on the patient engagement and the data acquisition and management modes employed. However, a limitation of this categorization is the broad definition of continuous collection, which does not differentiate between continuous monitoring and vigilant monitoring.

A different approach taken by researchers has been the development of application specific integrated circuits (ASIC) with subsystems designed, optimized, and highly integrated on a single chip or package for wearable and health applications. For instance, a system-on-chip (SoC) presented in [125] proposes an event-driven architecture that allows for clockless operation and power reduction. The SoC has an ultra-wideband transmitter for wireless communication and it consumes 2.89 μW when operating at 1.2V. A comparable effort was proposed in [126] where an ASIC front-end for biosensing was optimized for noise, power, and area. These optimizations give the chip the flexibility of sensing different biopotentials by adjusting parameters such as gain and filter cutoff frequency. The chip consumes 5.74 μW plus 306 nW for the power management unit and it is all packed in an area of 0.0228 mm^2. Another example of this approach is the work introduced in [7] where a highly integrated SoC incorporates subsystems for sensing, processing and control, wireless communication, energy harvesting and power management, and application-specific accelerators for wearable sensors. The SoC is able to operate from different harvesters with high efficiency without the need of additional energy sources and employs an ultra-wide band transmitter for wireless communication. The full system consumes 6.45 μW in a motion capture application, powered from indoor solar by the energy harvesting and power management unit.

6.1.3. System Overview

The proposed wearable is a fully custom system designed to perform vigilant, long-term, cardiac monitoring. It continuously samples and wirelessly streams one-lead ECG data to a smartphone for storage and display, locally and on the cloud. The system samples ECG data with an 8-bit resolution at 50 Sa/s following the QoI analysis presented in Chapter 5 to achieve an ultra-low power consumption of 65 μW while preserving vigilant operation.

The architecture of the system is constituted by three main subsystems: energy harvesting and storage, data acquisition and transmission, and sensing and textile integration. Flexible

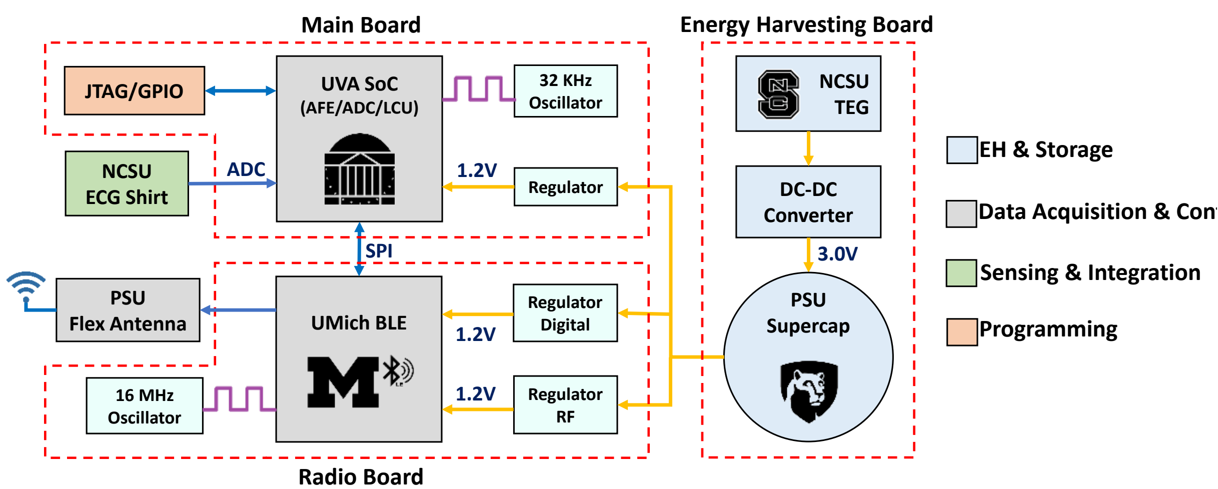

Figure 6.1 | System architecture. The system integrates multiple custom components that are the result of multiple efforts from different universities integrating the ASSIST center.

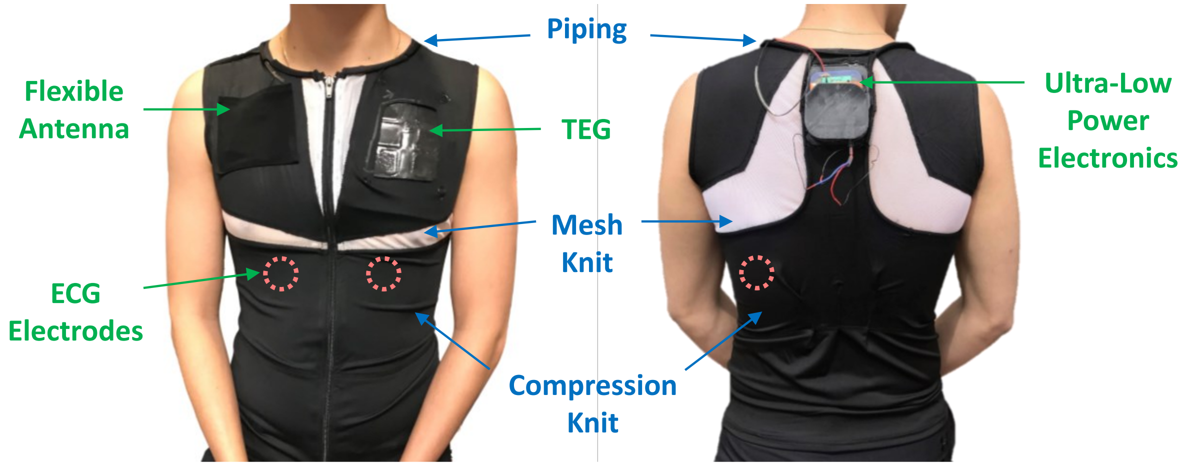

Figure 6.2 | ECG e-textile shirt and system integration. The ECG shirt has the purpose of serving as the sensing interface and as the hub to integrate the full system.

thermoelectric generators (TEGs) made of liquid metal interconnects and bulk bismuth chalcogenide p- and n-type legs connected to an Analog Devices DC-DC converter (ADP5090), and a custom ultra-low leakage 0.92 F supercapacitor comprise the energy harvesting and storage subsystem. Similarly, the data acquisition and transmission block incorporate an ultra-low power System-on-Chip (SoC), an ultra-low power Bluetooth Low Energy (BLE) compatible radio, and a flexible antenna designed to cope with the effects of human body dielectric loading seen on normal antennas. Finally, an e-textile ECG shirt made of a knitted compression fabric with embedded dry electrodes to address issues of user comfort, skin irritation and motion artifacts constitutes the sensing and textile integration block. All the electronics are incorporated onto three printed circuit boards (PCB) with a combined surface area of 32.58 cm2 and mounted on a 3D printed enclosure that magnetically attaches to the ECG shirt. Figure 6.1 shows the architecture of the system and Figure 6.2 display the integrated system with the ECG shirt.

The successful design and implementation of this system is the result of the collaboration of multiple universities as part of the Center for Advanced Self-Powered Systems of Integrated Sensors and Technologies (ASSIST).

6.1.4. Self-Powered Validation and Discussion

The system was deployed on multiple healthy subjects across different sessions with the goal of evaluating the performance of specific components and the fully integrated system.

The first evaluation was performed on the flexible TEGs under different activity conditions to guarantee a power-positive state of the system, even during long periods of reduced activity when no airflow is present. In a similar fashion, the power consumption of the system from the supercapacitor node was measured and three operational regions were identified. When the voltage of the capacitor is above 1.8 V and up to the maximum set voltage of 3 V, the system is fully-operational. In this region, the power consumption of the system goes from 54 μW to 90 μW, which makes our system the lowest reported wireless, wearable, vigilant cardiac monitoring system as presented in Table 1 (see Supplementary Information for system selection criteria).

If the voltage in the supercapacitor decreases from 1.8 V, the system enters a restricted region. Under this condition, the system can operate fully in terms of sensing and transmission, however the DC-DC converter shuts down the internal boost converter and a charge pump with lower efficiency takes over the energy harvesting unit. Operating in this region becomes a risk because if the energy available from the TEGs is not sufficient to charge the supercapacitor and the voltage keeps dropping below 1.4 V, the system will enter the non-operational region. In this non-operational region, the system shuts down and a manual restart that cannot be done by the user is required.

Based on the results of those deployments and characterizations, a patch containing 768 p-type and 768 n-type legs with a combined surface area, including surrounding elastomer, of 40 cm2 was optimized to be the power source for the system. The patch was placed on the chest of the ECG shirt to guarantee an optimal TEG/skin interface and maximize the air exposure of the device to maintain a temperature difference. With the system fully integrated, the power-neutral point was determined to be 65 μW, which occurs under no air conditions and with a supercapacitor voltage of 2.15 V. Furthermore, to determine the runtime of the system under no harvesting, the supercapacitor was pre-charged to the maximum 3 V and the system was left running until it stopped. If no energy is available and the supercapacitor is fully charged, the system can operate for almost 12 hours, from which 9.16 hours correspond to the fully operational region. With a voltage decay of 33.32 μV/s on the supercapacitor, these reported values represent the potential of our system to operate overnight without compromising the self-powered operation.

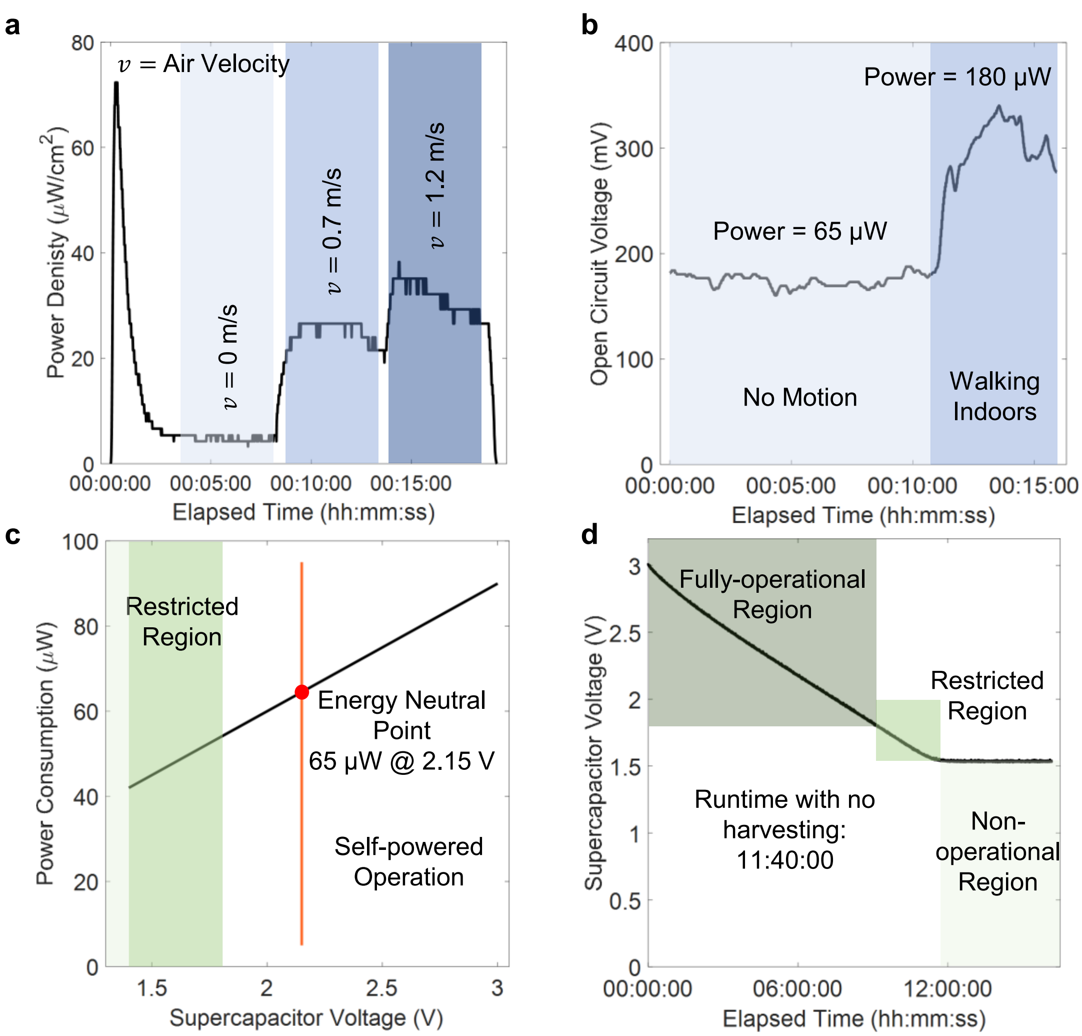

Figure 6.3 | Validation of the proposed self-powered wearable sensing system. a) Power density measured at rest and two walking speeds (0.7 and 1.2 m/s) at an ambient temperature of 24 °C. During walking, moving air provides cooling on the TEG cold side via forced convection. **b)** TEG open circuit voltage response at rest (no motion) and walking indoor (airflow presence). **c)** System power consumption over the operational voltage range. The energy neutral point corresponds to 65 μW. **d)** System runtime with no harvesting and a full supercapacitor. The system can operate for almost 12 hours with no harvesting.

Additionally, a study surveying national human activity patterns in the U.S. reported that the average American spends 87% of their time indoors, 6% in enclosed vehicles and 7% outdoors [127]. This last number represents 1 hour and 40 minutes under conditions where airflow is present and when the supercapacitor can be recharged. Figure 6.3 summarizes the results of the described deployments and validations.

6.1.5. State-of-the-Art Comparison.

To highlight the relevance of this work, the proposed system was compared to state-of-the-art cardiac monitoring devices [128], [41], [129]–[132] and commercially available solutions [153]. In order to present a fair comparison, the selected systems had to feature three main characteristics: low power operation, small form factor for wearability, and designed for long-term monitoring. Based on these criteria a set of 12 categories were defined, and the results were summarized in Table 6.1. From this comparison it is possible to notice how most of the devices operate at 3 V, have a relatively small form factor and present a single lead, 3-electrode configuration. The bigger differences among the solutions can be observed in the bit depth, sampling frequency, textile integration, and power consumption.

The strengths of the proposed system are the low power consumption (only 65 μW), its continuous vigilant operation, its wearability, and the end-to-end system integration for remote monitoring. While all of the compared solutions can operate continuously, none of them features a true vigilant characteristic for long-term monitoring given the limited battery lifetime. A special case is the Ultra-Low Power Sensor Evaluation Kit (ULPSEK) [132], where energy harvesting is used as the power source. The system can operate continuously, and it achieves the closest low power consumption to our work. However, a heavy duty-cycling scheme is required. Its implemented power management scheme wakes up the device to sample the sensor data for 31 seconds and then puts it to sleep for 12 minutes to reduce the average power consumption to 137 μW over the 12.5-minute window. Therefore, ULPSEK is a self-powered system with near-continuous operation but does not provide vigilant monitoring for cardiac event detection.

	This Work	[128]	[153]	[129]	[130]	[131]	[41]	[132]
No. of electrodes	3	3	2	3	3	3	2	3
ADC (bits)	8	8	8	10	13	12	16.5 (14 ENOB)	12
fs_{ECG} (Sa/s)	50	50	300	250	512	256	320	200
Voltage (V)	2.15	3	n/r	3	2.8	n/r	3	3
Power Consumption (μW)	65	683	n/r	4075	2018	n/r	12000	137
Communication Protocol	BLE Compatible	BLE	BT	BT	BLE	USB	ZigBee Pro	BLE
Multimodal Sensing	No	Yes	Yes	No	Yes	Yes	No	Yes
Textile Integration	Yes	Yes	No	No	No	No	No	No
Web Access	Yes	Yes	Yes	No	No	No	Yes	No
Vigilant Operation	Yes	Yes	Yes[1]	No	Yes[1]	Yes[1]	Yes[1]	No
Data Storage	Remote	Remote	Local / Remote	Remote	Local / Remote	Local	Remote	Remote
Power Source	TEG (Self-powered)	Photovoltaic + TEG (Self-powered)	Battery (48 hrs)	Battery (100.8 hrs)	Battery (586.6 hrs)	Battery (90 hrs)	Battery (160 hrs)	TEG (Self-powered)
Dimensions (mm)	64 x 62 x 22	28 x 23 x 12	90 x 40 x 16	n/r	n/r	38 x 38 x 7	65 x 34 x n/r	60 x 32 x n/r

Table 6.1 | State-of-the-art comparison of low-power cardiac monitoring systems. The systems compared are low power, wearable, ECG systems for long-term monitoring. [1]Vigilant operation only during battery lifetime.

Even though this work presents lower numbers in terms of bit depth and sampling frequency, these parameters were set based on the developed application-driven approach to optimize power consumption while ensuring data quality. Finally, comparing this work to our previous effort [128], which uses the same approach and mostly COTS components, the current system has an improvement in power reduction bigger than 10x while keeping a similar performance.

6.2. Piezoelectric-Based Continuous Monitoring System for the Airways[6]

6.2.1. Introduction

Wearable and implantable devices have shown the potential to transform healthcare by enabling continuous care outside the clinic [116]. Remote patient monitoring is a fundamental component in this new framework as it produces richer data sets that can help not only in the

[6] The respiratory monitroing system was a collaboration with Prof. Dan Quinn and Lucy Fitzgerald.

diagnosis and management of chronic diseases but also in preventing episodes that can threaten the patient's life [133].

Chronic respiratory diseases such as asthma or chronic obstructive pulmonary disease (COPD) are characterized by severe and potentially life-threatening respiratory exacerbations, which can occur regardless of the severity of the disease, and need to be detected early. However, this procedure requires professionally supervised monitoring in controlled settings and bulky instruments that are not suited for real-world use [52]. Airflow sensors embedded in the trachea and/or bronchi that could automatically detect an impending arrest would therefore have considerable clinical impact for patients with chronic respiratory conditions. Such a sensor could offer early warning to patients during their day-to-day life, thus triggering medical interventions that prevent the need for urgent care.

6.2.2. Related Work

Wearable technology in the context of respiratory health can be categorized into four different areas: pulse oximetry, pulmonary ventilation, activity tracking, and air quality monitoring [134]. For example, a two-electrode capacitive sensor was integrated into clothing in order to measure respiratory rate [135]. The electrodes were placed in the abdominal area and in the back. The changes in air volume during inhalation and exhalation produced a change in the permittivity of the medium between the electrodes and therefore a change in the capacitance. Through this method, the respiratory rate was directly inferred, and with further analysis, the air volume was also estimated. Another chest-mounted device used a novel material based on silver nanoparticles that changed its resistive properties when stretched [136]. Using this principle, the respiratory rate was determined by evaluating the changes in resistance of the device.

Chu et al. developed a sensor that was able to measure respiratory rate and also tidal volume [137]. The sensor had a form factor similar to a band-aid and was meant to be disposable. It relied on a similar principle as other sensors that measure the thoracic displacement using strain gauges. A very different approach was taken by Sharma et al. who created a wearable that uses radio-frequency (RF) to measure respiratory rate, respiratory volume, and heart rate [138]. The device uses a near-field coherent sensing principle: it transmits a low-power RF signal into the body, then evaluates the signal's coupling to the internal dielectric motion of the heart and lungs. While all these efforts are pointed in the right direction, these devices present limitations common to wearable technology – limited battery life, form factor, difficulty for adoption [27], [29], [139].

Implantable technology has focused primarily on cardiac applications. An implantable device intended to guide strategies for anticoagulation in atrial fibrillation was developed by Medtronic and cleared by the FDA [140]. Another example is the system for ambulatory monitoring developed by Angel Medical Systems used to detect ischemia and provide early alerts to the user [141]. The battery-life for these devices is up to 3 years, and 4-8 years respectively. Nonetheless, implantable devices for the airways have limited space to accommodate batteries, which poses additional challenges to power these devices for extended periods.

Some efforts looking into alternative power sources for implantable technology have explored solar cells and thermoelectric generators for subcutaneous implants [142], [143]. Others have looked at harvesting energy from the motion of the heart, lungs and diaphragm using piezoelectric films [144]. Nevertheless, specific implantable airway sensors have some precedent. An implantable device used ultrasonic transmitters mounted in the trachea and looked at the phase shift produced in the ultrasonic beam to estimate the air velocity [145]; another work used an implantable catheter with two hot-film sensors to measure flow rate [146]. These devices surround the airflow and require major surgery to install.

6.2.3. System Overview

Our proposed system is designed to provide continuous sensing of airway conditions in respiratory health applications. The system is integrated by a set of PVDF piezoelectric cantilevers serving as the harvester and the sensor simultaneously. The cantilevers are mechanically stressed by the airflow in the airway, producing an electrical potential with every deflection that occurs. The energy resulting from this phenomenon is stored into a capacitor

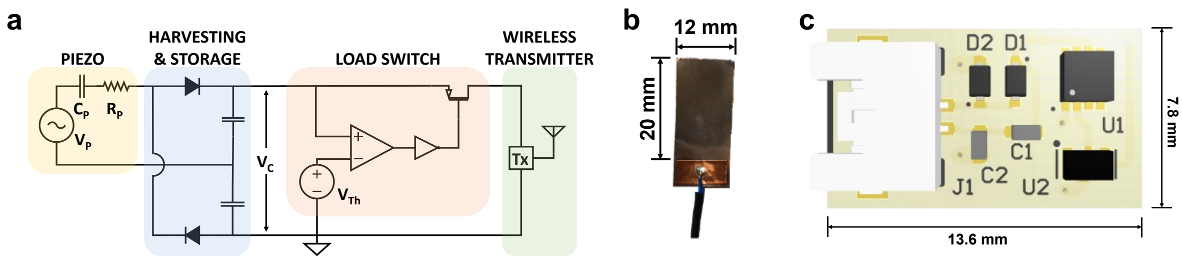

Figure 6.4. Proposed self-powered system. a) System's architecture highlighting the corresponding subsystems. **b)** PVDF cantilever. **c)** 3D rendering of the flexible PCB incorporating the functional electronics of the self-powered system.

connected to an ultra-low power load switch that controls when a data-less transmission event occurs. The transmission rate is later correlated with breathing parameters that define the status of the airway conditions. This process is done on the premise that the breathing conditions are reflected in the amount of harvested energy and therefore have an effect on the transmission rate.

The system architecture can be divided in three subsystems: energy harvesting and storage, control, and wireless transmission. The energy harvesting and storage unit incorporates a full-wave voltage multiplier made of two diodes (1N4001) and two capacitors that rectify the AC signal produced by the piezoelectric cantilevers and convert it into a DC signal that powers the rest of the electronics.

The control unit is fully integrated in an ultra-low power load switch from Semtech (TS12001). The device integrates a comparator that contrasts the voltage level of the capacitor to an internal regulated threshold and outputs a signal to drive a P-Channel transistor that acts as the switch in the circuit. The comparator presents a hysteresis that defines the window in which the switch remains closed. This window is factory preset to 500 mV and for our application the lower threshold was chosen to be 1.7 V. These specifications state that the capacitor needs to be charged to 2.2 V for the switch to close, and it remains in this state until the voltage drops to 1.7 V. In our experiments we found that the actual upper threshold was approximately 2.13 V, while the lower threshold remained at 1.7 V.

Finally, the wireless transmission unit is formed by a low-power oscillator from SiTime (SiT1533). The oscillator has a fixed output frequency of 32.768 kHz, which is suited for implantable devices [147]. Figure 6.4 presents the architecture of the proposed self-powered system and the printed circuit board (PCB) integrating the functional electronics.

Given the ultra-low energy harvesting levels from the piezoelectric cantilevers, a characterization of the leakage current of the electronics was fundamental for the successful implementation of our system. For the proposed architecture, the load switch represents the biggest leakage contributor. Semtech states that the device presents an “off-active” quiescent current of 100 pA, which includes the leakage of the device. This is correct while the voltage at the input is below the lower threshold voltage (1.7 V), but as this voltage increases to reach the upper threshold voltage (2.13 V) for the switch to close, the “off-active” current grows exponentially up to 35 nA as seen in Figure 6.5a.

Based on this information and the energy harvesting profiling from human breathing previously discussed in Chapter 3, we were able to define the size and number of cantilevers required to achieve self-powered operation. The array consists of five PVDF piezoelectric

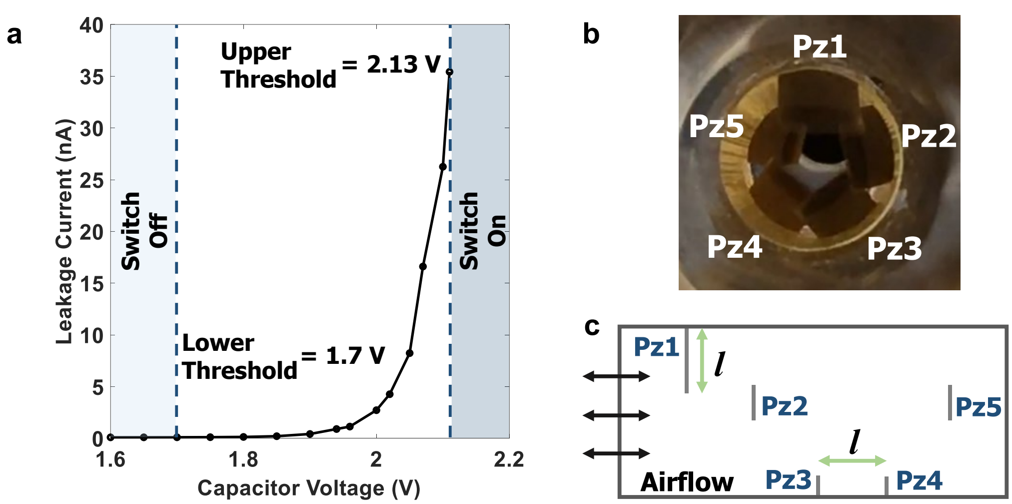

Figure 6.5 | Leakage characterization and cantilever array. a) The leakage increases exponentially as the voltage in the capacitor increases. The harvesting levels from a single cantilever are not sufficient to overcome the leakage. **b)** Picture of the actual array mounted in the tube showing the cross-sectional distribution of the cantilevers. **c)** Longitudinal distribution of the cantilevers.

elements (20 mm x 12 mm x 28 μm, TE Connectivity 1-1003702-7) connected in parallel and separated along the airway by a distance l that is equal to the height of a single cantilever (20 mm). The elements are each offset by a 72-degree rotation about the airway's central axis (Figure 6.5b,c). This layout prevents the cantilevers from impeding each other when mechanically stressed.

6.2.4. Self-Powered Validation and Discussion

To validate the self-powered sensing system, we created a new experimental setup that consisted of a tube (25 mm in diameter) attached to the lung simulator on one end and open on the other end to emulate the human airway. In the middle of the tube, a 3D printed mount was incorporated to suspend the piezoelectric cantilevers. The cantilevers were connected to the printed circuit board (PCB) holding the electronics, and the DAQ was also used to monitor the voltage levels in the capacitor.

The initial experiment we conducted was aimed at validating the end-to-end functionality of the system, i.e., for a given set of flow conditions, receive and detect a series of pings on the SDR. The initial flow conditions were established at 30 BPM and 4 L per breath based on the knowledge acquired during the profiling tests. For this experiment the SDR was placed 1 cm away from the wireless transmitter. With a fully discharged 5 μF equivalent capacitor as the storage element, the first transmission event (ping) took over 3 h and 30 min to occur. After that, the time interval between consecutive pings was approximately 4 min and 40 s. Each ping has a duration of 1.55 s and it is preceded by a start-up time of 140 ms, where the oscillator goes through an initialization process before outputting a stable signal. The size of the capacitor was determined empirically based on the energy demands of the oscillator during this process. The average power consumption of the system when transmitting was determined to be 7.31 μW. A close up to the behavior of the system during each ping is presented in Figure 6.6.

The following experiments were conducted to validate the hypothesis that the ping rate is affected by the energy harvesting levels and, therefore, the flow conditions. To study this relation,

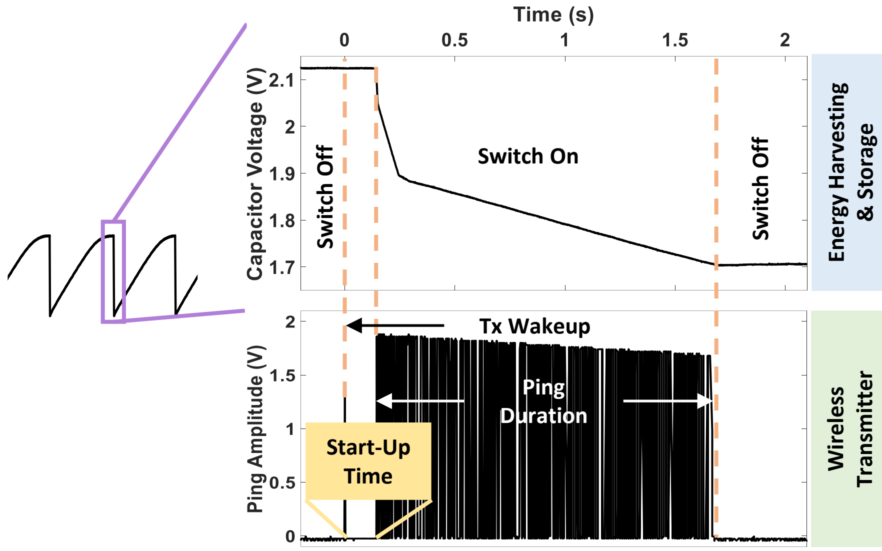

Figure 6.6 | Data-less transmission event. Close up to a transmission event (ping) observed at the storage element and the wireless transmitter.

we kept the volume at 4 L and varied the breathing rate. 28 BPM was found to be the lowest breathing rate able to consistently generate continuous pings at a constant rate. As shown in Figure 6.7, 28 BPM yielded a ping every 5 minutes between pings – 20 s more than the ping period at 30 BPM, demonstrating that the breathing conditions affect the ping rate in our system.

While the results of the experimentation validated our hypothesis, it is important to acknowledge that the testing setup and breathing conditions do not represent realistic values for human breathing, and the current form factor is not viable for deployment. However, our work expands the study of alternative energy sources and functional designs for implantable technology, it bridges the gap between individual efforts intended for self-powered technology

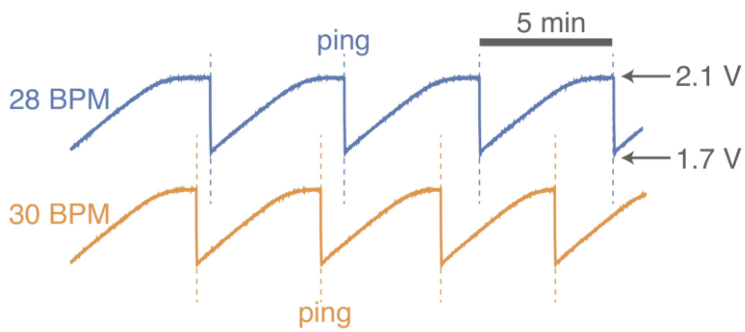

Figure 6.7 | Ping rate and breathing rate. Capacitor voltage showing the ping rate for two different breathing conditions, demonstrating how the ping rate is affected by the flowrate in the airway.

(e.g., energy harvesting, ultra-low power electronics, etc.), and it presents a technique for the design of self-powered flow sensors.

With optimized geometries that concentrate piezo near the base [148], or optimized materials such as recent single crystal piezo electric devices [149], future sensors could potentially use our technique to offer self-powered implantable flow sensing solutions. These new sensors with smaller form factor and higher power densities could provide day-by-day monitoring of breath activity in patients with long term diseases like COPD or Cystic Fibrosis, and even do hour-to-hour monitoring to potentially give asthma patients early warning of incoming exacerbations.

Chapter 7

Closing Remarks

Ubiquitous sensing is a fundamental component of the IoT. As the number of sensing devices for diverse applications increases, a mechanism to effectively and sustainable power these sensors is necessary for the full realization of the IoT. Energy harvesting and self-powered operation represent potential solutions to this challenge. However, successful demonstrations of these approaches have been limited to applications with more relaxed constraints. In this dissertation, I have presented a framework that aims to assist and facilitate the development of self-powered sensing technology even in applications where energy availability is highly dynamic and in smaller magnitudes with respect to the power consumed of a typical sensor normally used for such application.

The framework incorporates three main components that are fundamental to any self-powered sensing application: energy harvesting profiling, system power optimizations and QoI. The development of the framework was done around two medical case studies that aim to provide continuous and/or vigilant monitoring of chronic conditions for better health outcomes. For each case study, a different design approach was followed. For the vigilant cardiac monitoring case study, the sensing system design followed an information-driven approach that needs to meet specific sensing requirements. On the other hand, the respiratory health monitoring case study followed a harvesting-limited approach, which has the purpose of providing a reliable alternative to sporadic and burdensome spirometry tests performed in the diagnosis and management of chronic respiratory conditions.

Both design approaches are founded in the three methods integrating the framework, and their successful implementation resulted in self-powered sensing systems for each of the case studies.

7.1. Contributions and Open Problems

The specific contributions of this dissertation include:

1. An energy harvesting and data collection (EHDC) platform for energy harvesting profiling of solar cells and thermoelectric generators (TEGs) under wearable conditions. This platform was one of the first efforts at enabling the development of energy harvesting datasets beyond solar cells in static locations. The EHDC has served as the foundation for other energy harvesting profilers currently used in energy harvesting research. The hardware and firmware files for the implementation of the platform are available to the research community in a public repository in GitHub.
2. A study of piezoelectric cantilevers excited by oscillating complex flows and their ability to harvest energy under non-ideal conditions (sub-Hz and non-resonance). The study comprised a characterization of these devices in conditions similar to the human airways and was complemented by the development of a mathematical model that gives the opportunity to assess the effects of physical parameters related to the design of the harvester and their implications in the harvesting performance of the device. This work was a very close collaboration with Prof. Dan Quinn and Lucy Fitzgerald from the Smart Fluids Lab at UVA.
3. An information-driven design approach for self-powered systems that are required to meet specific QoI metrics or sensing requirements. This design approach uses the elements of the proposed framework in the following order: 1) definition of application-specific QoI metrics, 2) system power optimizations based on a selected architecture

and operation scheme, and 3) harvester design and/or selection using information from energy harvesting profiling.

4. A harvesting-limited design approach for self-powered sensors as an alternative to the limited or lack of sensing solutions that can provide continuous or vigilant sensing. In this approach, sensing, harvesting and power management are closely related; thus, they methods in the framework oftentimes are followed in parallel during the design of this type of systems.
5. A demonstration of the potential of the framework and design approaches through the successful implementation of self-powered sensing systems intended for the case studies described in the dissertation.

As every other research effort, this dissertation leaves the following open problems as potential options for the advancement of self-powered sensing technology:

- Extended energy harvesting datasets for multi-modal harvesting from the body. We have demonstrated the usefulness of energy profiles in the design of wearable self-powered sensors, but the amount of harvesting data available from actual wearable conditions remains very limited. Conducting studies to collect longer energy profiles and diversify the individuals in the study to better represent the larger population in our society can benefit the widespread adoption of self-powered sensing technology.
- Piezoelectric cantilever energy harvesting in more complex fluids. The work in this dissertation regarding piezoelectric energy harvesting in fluids considered environments where the flows were mostly laminar and barely touched the concept of turbulence as way to improve energy harvesting from these devices. In addition, the developed mathematical model was not analyzed for this type of environments.
- Ultra-low power energy harvesting circuits with MPPT for piezoelectric harvesters. The availability of integrated circuits intended for piezoelectric harvesting that can operate from µW levels and below is very limited. Recent successful efforts have

been reported in the literature, but the scarcity of devices supporting applications with very low harvesting levels undermines the proliferation of piezoelectric-based self-powered sensing.

- Increasing QoI for harvesting-limited self-powered sensors. This dissertation explored the feasibility of extracting useful information using harvesting-limited sensors and showed that indirect sensing has the potential to achieve that goal. However, the work here presented had the purpose of starting paving the path that can lead to well established methods correlating harvesting levels and sensing. Continuing the work on broadband sensing represents a great opportunity to advance this effort.

7.2. Publications

During my time as a Ph.D. student at the University of Virginia, I have had the opportunity to collaborate and conduct research with experts from many fields of study and from multiple renowned academic institutions. Below are the lists of my publications during the Ph.D. and planned after graduation.

7.2.1. Completed

[1] D. Fan, **L. L. Ruiz**, J. Gong and J. Lach, "Profiling, modeling, and predicting energy harvesting for self-powered body sensor platforms," 2016 IEEE 13th International Conference on Wearable and Implantable Body Sensor Networks (BSN), 2016, pp. 402-407, doi: 10.1109/BSN.2016.7516295.

[2] D. Fan, **L. Lopez Ruiz**, J. Gong and J. Lach, "EHDC: An Energy Harvesting Modeling and Profiling Platform for Body Sensor Networks," in IEEE Journal of Biomedical and Health Informatics, vol. 22, no. 1, pp. 33-39, Jan. 2018, doi: 10.1109/JBHI.2017.2733549.

[3] **L. L. Ruiz**, M. Ridder, D. Fan, J. Gong, J. Lach and J. Strohmaier, "SCAVM: A self-powered cardiac and activity vigilant monitoring system," 2017 IEEE Biomedical Circuits and Systems Conference (BioCAS), 2017, pp. 1-4, doi: 10.1109/BIOCAS.2017.8325126.

[4] D. Fan, **L. L. Ruiz** and J. Lach, "Application-driven dynamic power management for self-powered vigilant monitoring," 2018 IEEE 15th International Conference on Wearable and Implantable Body Sensor Networks (BSN), 2018, pp. 210-213, doi: 10.1109/BSN.2018.8329695.

[5] **L. J. L. Ruiz** et al., "Self-Powered Cardiac Monitoring: Maintaining Vigilance With Multi-Modal Harvesting and E-Textiles," in IEEE Sensors Journal, vol. 21, no. 2, pp. 2263-2276, 15 Jan.15, 2021, doi: 10.1109/JSEN.2020.3017706.

[6] **L. L. Ruiz** et al., "Piezoelectric-Based Respiratory Monitoring: Towards Self-Powered Implantables for the Airways," 2021 IEEE 17th International Conference on Wearable and Implantable Body Sensor Networks (BSN), 2021, pp. 1-5, doi: 10.1109/BSN51625.2021.9507022.

[7] **L. J. L. Ruiz** et al, “Capacitive Sensing for Monitoring Stent Patency in the Central Airway,” 2021 43rd Annual International Conference of the IEEE Engineering in Medicine & Biology Society (EMBC), 2021, in press.

[8] **L. J. L. Ruiz** et al, “Achieving Vigilant Health Wearables with Self-Powered Operation.” In IEEE Transactions in Biomedical Circuits and Systems (TBioCAS), submitted.

7.2.2. Planned

[1] “Towards Self-Powered Piezoelectric Fluid Flow Sensing.” Paper for Physical Review Letters, working on revision.

[2] “Self-Powered Broadband Sensing for Continuous Respiratory Health Monitoring,” Expansion journal paper from BSN 2021 for TBioCAS

[3] “Self-Powered Sensing Systems: A Taxonomy for Energy Harvesting Systems.” Work in progress.

References

[1] L. Mainetti, L. Patrono, and A. Vilei, “Evolution of wireless sensor networks towards the Internet of Things: A survey,” *2011 Int. Conf. Software, Telecommun. Comput. Networks, SoftCOM 2011*, pp. 16–21, 2011.

[2] S. H. Shah and I. Yaqoob, “A survey: Internet of Things (IOT) technologies, applications and challenges,” in *2016 4th IEEE International Conference on Smart Energy Grid Engineering, SEGE 2016*, 2016, vol. i, pp. 381–385.

[3] H. Jayakumar, K. Lee, W. S. Lee, A. Raha, Y. Kim, and V. Raghunathan, “Powering the internet of things,” in *Proceedings of the 2014 international symposium on Low power electronics and design*, 2014, vol. 29, no. 7, pp. 375–380.

[4] Cisco, “Cisco Annual Internet Report (2018-2023),” 2018.

[5] V. Gazis *et al.*, “Short Paper: IoT: Challenges, projects, architectures,” in *2015 18th International Conference on Intelligence in Next Generation Networks*, 2015, pp. 145–147.

[6] H. Jayakumar, K. Lee, W. S. Lee, A. Raha, Y. Kim, and V. Raghunathan, “Powering the internet of things,” in *Proceedings of the 2014 international symposium on Low power electronics and design*, 2014, pp. 375–380.

[7] A. Roy *et al.*, “A 6.45 μ W Self-Powered SoC with Integrated Energy-Harvesting Power Management and ULP Asymmetric Radios for Portable Biomedical Systems,” *IEEE Trans. Biomed. Circuits Syst.*, vol. 9, no. 6, pp. 862–874, 2015.

[8] C. J. Lukas *et al.*, “A 1.02 μw Battery-Less, Continuous Sensing and Post-Processing SiP for Wearable Applications,” *IEEE Trans. Biomed. Circuits Syst.*, vol. 13, no. 2, pp. 271–281, 2019.

[9] J. A. Khan, H. K. Qureshi, A. Iqbal, and C. Lacatus, “Energy management in Wireless Sensor Networks: A survey,” *Comput. Electr. Eng.*, vol. 41, no. C, pp. 159–176, 2015.

[10] W. K. G. Seah, W. K. G. Seah, Z. A. Eu, and H. Tan, “Wireless Sensor Networks Powered by Ambient Energy Harvesting (WSN-HEAP) - Survey and Challenges Wireless Sensor Networks Powered by Ambient Energy Harvesting (WSN-HEAP) – Survey and Challenges,” *Wirel. VITAE*, no. JUNE, pp. 1–5, 2009.

[11] J. Martin, “The 17 great challenges of the twenty-first century,” *Futurist*, vol. 41, no. 1. pp. 20–24, 2007.

[12] World Health Organization, “a Vital Investment,” *World Health*, p. 202, 2005.

[13] W. Raghupathi and V. Raghupathi, “An empirical study of chronic diseases in the united states: A visual analytics approach,” *Int. J. Environ. Res. Public Health*, vol. 15, no. 3, pp. 10–12, 2018.

[14] P. Boersma, L. I. Black, and B. W. Ward, “Prevalence of multiple chronic conditions among US adults, 2018,” *Prev. Chronic Dis.*, vol. 17, pp. 2–5, 2020.

[15] J. S. Wright, H. K. Wall, and M. D. Ritchey, “Million Hearts 2022,” *JAMA*, vol. 320, no. 18, p. 1857, Nov. 2018.

[16] W. Yang *et al.*, “Economic costs of diabetes in the U.S. in 2017,” *Diabetes Care*, vol. 41, no. 5, pp. 917–928, 2018.

[17] G. M. Massetti, W. H. Dietz, and L. C. Richardson, “Excessive weight gain, obesity, and cancer: Opportunities for clinical intervention,” *JAMA - J. Am. Med. Assoc.*, vol. 318, no. 20, pp. 1975–1976, 2017.

[18] B. M. Kuehn, “News from the Centers for Disease Control and Prevention,” *JAMA - J. Am. Med. Assoc.*, vol. 325, no. 20, p. 2040, 2021.

[19] S. Kumar *et al.*, “Mobile Health Technology Evaluation,” *Am. J. Prev. Med.*, vol. 45, no. 2, pp. 228–236, Aug. 2013.

[20] M. Luna-Delrisco *et al.*, “Adoption of Internet of Medical Things (IoMT) as an opportunity for improving public health in Latin America,” in *Iberian Conference on Information Systems and Technologies, CISTI*, 2018, vol. 2018-June, pp. 1–5.

[21] D. K. Ming *et al.*, “Continuous physiological monitoring using wearable technology to inform individual management of infectious diseases, public health and outbreak responses,” *Int. J. Infect. Dis.*, vol. 96, pp. 648–654, Jul. 2020.

[22] Montgomery, Chester, and Kopp, “Health Wearables: Ensuring Fairness, Preventing Discrimination, and Promoting Equity in an Emerging Internet-of-Things Environment,” *J. Inf. Policy*, vol. 8, pp. 35–77, 2018.

[23] R. K. Pathinarupothi, P. Durga, and E. S. Rangan, “IoT-based smart edge for global health: Remote monitoring with severity detection and alerts transmission,” *IEEE Internet Things J.*, vol. 6, no. 2, pp. 2449–2462, 2019.

[24] A. K. Yetisen, J. L. Martinez-Hurtado, B. Ünal, A. Khademhosseini, and H. Butt, “Wearables in Medicine,” *Adv. Mater.*, vol. 30, no. 33, 2018.

[25] E. A. Carroll *et al.*, “Food and mood: Just-in-time support for emotional eating,” *Proc. - 2013 Hum. Assoc. Conf. Affect. Comput. Intell. Interact. ACII 2013*, pp. 252–257, 2013.

[26] J. Dunn, R. Runge, and M. Snyder, “Wearables and the medical revolution,” *Per. Med.*, vol. 15, no. 5, pp. 429–448, 2018.

[27] P. C. Shih, K. Han, E. S. Poole, M. B. Rosson, and J. M. Carroll, "Use and Adoption Challenges of Wearable Activity Trackers," *iConference 2015*, no. 1, pp. 1–12, 2015.

[28] J. H. M. Bergmann and A. H. McGregor, "Body-Worn Sensor Design: What Do Patients and Clinicians Want?," *Ann. Biomed. Eng.*, vol. 39, no. 9, pp. 2299–2312, Sep. 2011.

[29] J. H. M. Bergmann, V. Chandaria, and A. McGregor, "Wearable and implantable sensors: The patient's perspective," *Sensors (Switzerland)*, vol. 12, no. 12, pp. 16695–16709, 2012.

[30] Y. M. Choi, M. G. Lee, and Y. Jeon, "Wearable biomechanical energy harvesting technologies," *Energies*, vol. 10, no. 10, 2017.

[31] G. W. Taylor, J. R. Burns, S. M. Kammann, W. B. Powers, and T. R. Welsh, "The energy harvesting Eel: A small subsurface ocean/river power generator," *IEEE J. Ocean. Eng.*, vol. 26, no. 4, pp. 539–547, 2001.

[32] H. Sharma, A. Haque, and Z. A. Jaffery, "Modeling and optimisation of a solar energy harvesting system for wireless sensor network nodes," *J. Sens. Actuator Networks*, vol. 7, no. 3, 2018.

[33] W. Hwang *et al.*, "Watts-level road-compatible piezoelectric energy harvester for a self-powered temperature monitoring system on an actual roadway," *Appl. Energy*, vol. 243, no. March, pp. 313–320, 2019.

[34] Y. Yuan, M. Liu, W.-C. Tai, and L. Zuo, "Design and experimental studies of an energy harvesting backpack with mechanical motion rectification," *Sensors Smart Struct. Technol. Civil, Mech. Aerosp. Syst. 2017*, vol. 10168, no. April 2017, p. 1016825, 2017.

[35] J. Zhao *et al.*, "Self-Powered Implantable Medical Devices: Photovoltaic Energy Harvesting Review," *Adv. Healthc. Mater.*, vol. 9, no. 17, pp. 1–22, 2020.

[36] Y. K. Tan and S. K. Panda, "Energy harvesting from hybrid indoor ambient light and thermal energy sources for enhanced performance of wireless sensor nodes," *IEEE Trans. Ind. Electron.*, vol. 58, no. 9, pp. 4424–4435, 2011.

[37] V. Leonov, "Thermoelectric Energy Harvesting of Human Body Heat for Wearable Sensors," *IEEE Sens. J.*, vol. 13, no. 6, pp. 2284–2291, Jun. 2013.

[38] S. Roundy and S. Trolier-Mckinstry, "Materials and approaches for on-body energy harvesting," *MRS Bull.*, vol. 43, no. 3, pp. 206–213, 2018.

[39] S. H. Kondapalli, Y. Alazzawi, M. Malinowski, T. Timek, and S. Chakrabartty, "Feasibility of Self-Powering and Energy Harvesting Using Cardiac Valvular Perturbations," *IEEE Trans. Biomed. Circuits Syst.*, vol. 12, no. 6, pp. 1392–1400, 2018.

[40] Y. Du, J. Xu, B. Paul, and P. Eklund, "Flexible thermoelectric materials and devices," *Appl. Mater. Today*, vol. 12, pp. 366–388, 2018.

[41] E. Spanò, S. Di Pascoli, and G. Iannaccone, “Low-Power Wearable ECG Monitoring System for Multiple-Patient Remote Monitoring,” *IEEE Sens. J.*, vol. 16, no. 13, pp. 5452–5462, 2016.

[42] I. Maghami, V. A. Victor, M. M. Morsy, J. C. Lach, and J. L. Goodall, “Exploring the complementary relationship between solar and hydro energy harvesting for self-powered water monitoring in low-light conditions,” *Environ. Model. Softw.*, vol. 140, no. March, 2021.

[43] F. Regan *et al.*, “A demonstration of wireless sensing for long term monitoring of water quality,” *Proc. - Conf. Local Comput. Networks, LCN*, no. October, pp. 819–825, 2009.

[44] A. Awawdeh, S. T. S. Bukkapatnam, S. R. T. Kumara, C. Bunting, and R. Komanduri, “Wireless sensing of flow-induced vibrations for pipeline integrity monitoring,” *2006 IEEE Sens. Array Multichannel Signal Process. Work. Proceedings, SAM 2006*, pp. 114–117, 2006.

[45] S. Dagtas, Y. Natchetoi, H. Wu, and A. Shapiro, “An integrated wireless sensing and mobile processing architecture for assisted living and healthcare applications,” *Heal. Proc. 1st ACM SIGMOBILE Int. Work. Syst. Netw. Support Healthc. Assist. Living Environ.*, pp. 70–72, 2007.

[46] C. Y. Lee and C. Toumazou, “Ultra-low power UWB for real time biomedical wireless sensing,” *Proc. - IEEE Int. Symp. Circuits Syst.*, pp. 57–60, 2005.

[47] D. Becker, T. D. King, and B. McMullen, “Big data, big data quality problem,” *Proc. - 2015 IEEE Int. Conf. Big Data, IEEE Big Data 2015*, pp. 2644–2653, 2015.

[48] A. Katal, M. Wazid, and R. H. Goudar, “Big data: Issues, challenges, tools and Good practices,” *2013 6th Int. Conf. Contemp. Comput. IC3 2013*, pp. 404–409, 2013.

[49] S. B. Dunbar *et al.*, “Projected Costs of Informal Caregiving for Cardiovascular Disease: 2015 to 2035: A Policy Statement From the American Heart Association,” *Circulation*, vol. 137, no. 19, pp. e558–e577, 2018.

[50] G. Giamouzis *et al.*, “Hospitalization Epidemic in Patients With Heart Failure: Risk Factors, Risk Prediction, Knowledge Gaps, and Future Directions,” *J. Card. Fail.*, vol. 17, no. 1, pp. 54–75, 2011.

[51] C. Davis, M. Bender, T. Smith, and J. Broad, “Feasibility and Acute Care Utilization Outcomes of a Post-Acute Transitional Telemonitoring Program for Underserved Chronic Disease Patients,” *Telemed. e-Health*, vol. 21, no. 9, pp. 705–713, 2015.

[52] S. Papiris, A. Kotanidou, K. Malagari, and C. Roussos, “Clinical review: Severe asthma,” *Critical Care*, vol. 6, no. 1. pp. 30–44, 2002.

[53] C. Dagdeviren *et al.*, “Conformal piezoelectric energy harvesting and storage from motions

of the heart, lung, and diaphragm," *Proc. Natl. Acad. Sci. U. S. A.*, vol. 111, no. 5, pp. 1927–1932, 2014.

[54] F. Yahya *et al.*, "A Battery-less 507nW SoC with Integrated Platform Power Manager and SiP Interfaces," in *IEEE Symposium on VLSI Circuits, Digest of Technical Papers*, 2017, pp. C338–C339.

[55] C. Seshan, "Cell efficiency dependence on solar incidence angle," in *Conference Record of the IEEE Photovoltaic Specialists Conference*, 2010.

[56] C. Viehweger, M. Baldauf, T. Keutel, and O. Kanoun, "Energy Profile Analysis by Simulation for the Design of Energy Harvesting Systems," *Int. Multi-Conference Syst. Signals Devices, SSD 2012 - Summ. Proc.*, pp. 1–3, 2012.

[57] V. Leonov, T. Torfs, P. Fiorini, and C. Van Hoof, "Thermoelectric converters of human warmth for self-powered wireless sensor nodes," *IEEE Sens. J.*, vol. 7, no. 5, 2007.

[58] D. C. Hoang, Y. K. Tan, H. B. Chng, and S. K. Panda, "Thermal energy harvesting from human warmth for wireless body area network in medical healthcare system," in *Proceedings of the International Conference on Power Electronics and Drive Systems*, 2009.

[59] V. Leonov, "Thermoelectric energy harvesting of human body heat for wearable sensors," *IEEE Sens. J.*, vol. 13, no. 6, pp. 2284–2291, 2013.

[60] S. Joshi, M. Parmar, and K. Rajanna, "A novel gas flow sensing application using piezoelectric ZnO thin films deposited on Phynox alloy," *Sensors Actuators, A Phys.*, vol. 187, 2012.

[61] D. Roche, C. Richard, L. Eyraud, and C. Audoly, "Piezoelectric bimorph bending sensor for shear-stress measurement in fluid flow," *Sensors Actuators, A Phys.*, vol. 55, no. 2–3, 1996.

[62] S. Lee *et al.*, "Super-flexible nanogenerator for energy harvesting from gentle wind and as an active deformation sensor," *Adv. Funct. Mater.*, vol. 23, no. 19, pp. 2445–2449, 2013.

[63] J. W. Sohn, S. B. Choi, and D. Y. Lee, "An investigation on piezoelectric energy harvesting for MEMS power sources," *Proc. Inst. Mech. Eng. Part C J. Mech. Eng. Sci.*, vol. 219, no. 4, 2005.

[64] M. J. Ramsay and W. W. Clark, "<title>Piezoelectric energy harvesting for bio-MEMS applications</title>," in *Smart Structures and Materials 2001: Industrial and Commercial Applications of Smart Structures Technologies*, 2001, vol. 4332.

[65] N. V Viet, N. Wu, and Q. Wang, "A review on energy harvesting from ocean waves by piezoelectric technology," *J. Model. Mech. Mater.*, vol. 1, no. 2, 2017.

[66] J. D. Hobeck and D. J. Inman, “Artificial piezoelectric grass for energy harvesting from turbulence-induced vibration,” *Smart Mater. Struct.*, vol. 21, no. 10, p. 105024, 2012.

[67] H. D. Akaydin, N. Elvin, and Y. Andreopoulos, “Energy harvesting from highly unsteady fluid flows using piezoelectric materials,” in *Journal of Intelligent Material Systems and Structures*, 2010, vol. 21, no. 13, pp. 1263–1278.

[68] H. Li *et al.*, “An Energy Harvesting Underwater Acoustic Transmitter for Aquatic Animals,” *Sci. Rep.*, vol. 6, p. 33804, 2016.

[69] H. Liu, S. Zhang, R. Kathiresan, T. Kobayashi, and C. Lee, “Development of piezoelectric microcantilever flow sensor with wind-driven energy harvesting capability,” *Appl. Phys. Lett.*, vol. 100, no. 22, p. 223905, 2012.

[70] N. R. Alluri, B. Saravanakumar, and S. J. Kim, “Flexible, hybrid piezoelectric film (BaTi(1-x)ZrxO3)/PVDF nanogenerator as a self-powered fluid velocity sensor,” *ACS Appl. Mater. Interfaces*, vol. 7, no. 18, pp. 9831–9840, 2015.

[71] H. Y. Wang, X. B. Shan, and T. Xie, “An energy harvester combining a piezoelectric cantilever and a single degree of freedom elastic system,” *J. Zhejiang Univ. Sci. A*, vol. 13, no. 7, pp. 526–537, 2012.

[72] C. Sun, J. Shi, D. J. Bayerl, and X. Wang, “PVDF microbelts for harvesting energy from respiration,” *Energy Environ. Sci.*, vol. 4, no. 11, pp. 4508–4512, 2011.

[73] M. R. Mhetre and H. K. Abhyankar, “Human exhaled air energy harvesting with specific reference to PVDF film,” *Eng. Sci. Technol. an Int. J.*, vol. 20, no. 1, pp. 332–339, 2017.

[74] R. Palanki, J. Poiroux, and S. Palanki, “Design and evaluation of a low-cost piezoelectric device for remote diagnosis of respiratory diseases,” *Int. J. Bioautomation*, vol. 19, no. 4, pp. 521–530, 2015.

[75] M. T. Chorsi *et al.*, “Piezoelectric Biomaterials for Sensors and Actuators,” *Advanced Materials*, vol. 31, no. 1. 2019.

[76] E. Lefeuvre, A. Badel, C. Richard, L. Petit, and D. Guyomar, “High Efficiency Piezoelectric Vibration Energy Reclamation.” pp. 1–9.

[77] M. Lallart, L. Garbuio, L. Petit, C. Richard, and D. Guyomar, “Double synchronized switch harvesting (DSSH): A new energy harvesting scheme for efficient energy extraction,” *IEEE Trans. Ultrason. Ferroelectr. Freq. Control*, vol. 55, no. 10, pp. 2119–2130, 2008.

[78] E. Macii, M. Pedram, and F. Somenzi, “High-level power modeling, estimation, and optimization,” *IEEE Trans. Comput. Des. Integr. Circuits Syst.*, vol. 17, no. 11, pp. 1061–1079, 1998.

[79] F. Li, Y. Lin, L. He, D. Chen, and J. Cong, “Power modeling and characteristics of field

programmable gate arrays," *IEEE Trans. Comput. Des. Integr. Circuits Syst.*, vol. 24, no. 11, pp. 1712–1723, 2005.

[80] W. Liao, L. He, and K. M. Lepak, "Temperature and supply voltage aware performance and power modeling at microarchitecture level," *IEEE Trans. Comput. Des. Integr. Circuits Syst.*, vol. 24, no. 7, pp. 1042–1053, 2005.

[81] C. Talarico, J. W. Rozenblit, V. Malhotra, and A. Stritter, "A new framework for power estimation of embedded systems," *Computer (Long. Beach. Calif).*, vol. 38, no. 2, pp. 71–78, 2005.

[82] D. Li, P. H. Chou, and N. Bagherzadeh, "Mode selection and mode-dependency modeling for power-aware embedded systems," *Proc. - 7th Asia South Pacific Des. Autom. Conf. 15th Int. Conf. VLSI Des. ASP-DAC/VLSI Des. 2002*, pp. 697–704, 2002.

[83] V. Konstantakos, A. Chatzigeorgiou, S. Nikolaidis, and T. Laopoulos, "Energy Consumption Estimation in Embedded Systems," *IEEE Trans. Instrum. Meas.*, vol. 57, no. 4, pp. 797–804, Apr. 2008.

[84] A. Varma, E. Debes, I. Kozintsev, P. Klein, and B. Jacob, "Accurate and fast system-level power modeling: An XScale-based case study," *Trans. Embed. Comput. Syst.*, vol. 7, no. 3, 2008.

[85] A. Mohsen and R. Hofmann, "Power modeling, estimation, and optimization for automated co-design of real-time embedded systems," *Lect. Notes Comput. Sci. (including Subser. Lect. Notes Artif. Intell. Lect. Notes Bioinformatics)*, vol. 3254, pp. 643–651, 2004.

[86] R. P. Dick, G. Lakshminarayana, A. Raghunathan, and N. K. Jha, "Power analysis of embedded operating systems," *Proc. - Des. Autom. Conf.*, pp. 312–315, 2000.

[87] D. Fan, L. L. Ruiz, and J. Lach, "Application-driven dynamic power management for self-powered vigilant monitoring," *2018 IEEE 15th Int. Conf. Wearable Implant. Body Sens. Networks, BSN 2018*, vol. 2018-Janua, no. March, pp. 210–213, 2018.

[88] A. R. Aref, C. C. Chou, R. Rajagopalan, and C. Randall, "Bimodal porous carbon electrodes derived from polyfurfuryl alcohol/phloroglucinol for ionic liquid based electrical double layer capacitors," *J. Mater. Res.*, vol. 33, no. 9, pp. 1189–1198, 2018.

[89] E. N. and O. a. . Oyewobi S.S.; Onwuka, "Mobile Terminals' Energy: A Survey of Battery Technologies and Energy Management Techniques," *Int. J. Eng. Technol.*, vol. 3, no. 3, pp. 282–286, 2013.

[90] L. Gao, R. A. Dougal, and S. Liu, "Active power sharing in hybrid battery/capacitor power sources," *Conf. Proc. - IEEE Appl. Power Electron. Conf. Expo. - APEC*, vol. 1, pp. 497–503, 2003.

[91] D. Newell and M. Duffy, “Review of Power Conversion and Energy Management for Low-Power, Low-Voltage Energy Harvesting Powered Wireless Sensors,” *IEEE Trans. Power Electron.*, vol. 34, no. 10, pp. 9794–9805, 2019.

[92] G. K. Ottman, H. F. Hofmann, A. C. Bhatt, and G. A. Lesieutre, “Adaptive piezoelectric energy harvesting circuit for wireless remote power supply,” *IEEE Trans. Power Electron.*, vol. 17, no. 5, pp. 669–676, 2002.

[93] G. K. Ottman, H. F. Hofmann, and G. A. Lesieutre, “Optimized piezoelectric energy harvesting circuit using step-down converter in discontinuous conduction mode,” *IEEE Trans. Power Electron.*, vol. 18, no. 2, pp. 696–703, 2003.

[94] Y. Kushino and H. Koizumi, “Piezoelectric energy harvesting circuit using full-wave voltage doubler rectifier and switched inductor,” *2014 IEEE Energy Convers. Congr. Expo. ECCE 2014*, pp. 2310–2315, 2014.

[95] J. Qiu, H. Jiang, H. Ji, and K. Zhu, “Comparison between four piezoelectric energy harvesting circuits,” *Front. Mech. Eng. China*, vol. 4, no. 2, pp. 153–159, 2009.

[96] S. Li, A. Roy, and B. H. Calhoun, “A Piezoelectric Energy-Harvesting System with Parallel-SSHI Rectifier and Integrated Maximum-Power-Point Tracking,” *IEEE Solid-State Circuits Lett.*, vol. 2, no. 12, pp. 301–304, 2019.

[97] T. Nasser and R. Tariq, “Big Data Challenges,” *Journal of Computer Engineering & Information Technology*, 2015. [Online]. Available: http://www.datastax.com/big-data-challenges.

[98] S. Shilo, H. Rossman, and E. Segal, “Axes of a revolution: challenges and promises of big data in healthcare,” *Nature Medicine*, vol. 26, no. 1. Springer US, pp. 29–38, 2020.

[99] Z. Ai, L. Zheng, H. Qi, and W. Cui, “Low-Power Wireless Wearable ECG Monitoring System Based on BMD101,” *Chinese Control Conf. CCC*, vol. 2018-July, pp. 7374–7379, 2018.

[100] E. Valchinov, A. Antoniou, K. Rotas, and N. Pallikarakis, “Wearable ECG system for health and sports monitoring,” *Proc. 2014 4th Int. Conf. Wirel. Mob. Commun. Healthc. - "Transforming Healthc. Through Innov. Mob. Wirel. Technol. MOBIHEALTH 2014*, pp. 63–66, 2015.

[101] A. B. Jani, R. Bagree, and A. K. Roy, “Design of a low-power, low-cost ECG & EMG sensor for wearable biometric and medical application,” *Proc. IEEE Sensors*, vol. 2017-Decem, pp. 1–3, 2017.

[102] L. H. Wang *et al.*, “A low-power high-data-transmission multi-lead ecg acquisition sensor system,” *Sensors (Switzerland)*, vol. 19, no. 22, 2019.

[103] N. L. Rubio, “Comparative Study of Algorithms for Atrial Fibrillation Detection,” 2011.

[104] B. Logan and J. Healey, “Robust Detection of Atrial Fibrillation for a Long Term Telemonitoring System,” *Comput. Cardiol.*, vol. 32, pp. 619–622, 2005.

[105] J. Lian, L. Wang, and D. Muessig, “A Simple Method to Detect Atrial Fibrillation Using RR Intervals,” *Am. J. Cardiol.*, vol. 107, no. 10, pp. 1494–1497, 2011.

[106] K. Tateno and L. Glass, “Automatic detection of atrial fibrillation using the coefficient of variation and density histograms of RR and ΔRR intervals,” *Med. Biol. Eng. Comput.*, vol. 39, no. 6, pp. 664–671, 2001.

[107] W. Zong, G. B. Moody, and D. Jiang, “A Robust Open-source Algorithm to Detect Onset and Duration of QRS Complexes,” in *Computers in Cardiology*, 2003, vol. 30, pp. 737–740.

[108] I. R. LEGARRETA *et al.*, “CONTINUOUS WAVELET TRANSFORM MODULUS MAXIMA ANALYSIS OF THE ELECTROCARDIOGRAM: BEAT CHARACTERISATION AND BEAT-TO-BEAT MEASUREMENT,” *Int. J. Wavelets, Multiresolution Inf. Process.*, vol. 03, no. 01, pp. 19–42, Mar. 2005.

[109] G. B. Moody and R. R. Mark, “A New Method for Detecting Atrial Fibrillation Using R-R Intervals,” in *Computers in Cardiology*, 1983, pp. 227–230.

[110] Y. Li, X. Hou, W. Qi, Q. Wang, and X. Zhang, “Modeling and Analysis of Multiple Attached Masses Tuning a Piezoelectric Cantilever Beam Resonant Frequency,” *Shock Vib.*, vol. 2020, 2020.

[111] F. G. Zeng, S. Rebscher, W. Harrison, X. Sun, and H. Feng, “Cochlear Implants: System Design, Integration, and Evaluation,” *IEEE Rev. Biomed. Eng.*, vol. 1, no. dc, pp. 115–142, 2008.

[112] L. Piwek, D. A. Ellis, S. Andrews, and A. Joinson, “The Rise of Consumer Health Wearables: Promises and Barriers,” *PLoS Med.*, vol. 13, no. 2, 2016.

[113] M. M. Baig, H. GholamHosseini, A. A. Moqeem, F. Mirza, and M. Lindén, “A Systematic Review of Wearable Patient Monitoring Systems – Current Challenges and Opportunities for Clinical Adoption,” *J. Med. Syst.*, vol. 41, no. 7, 2017.

[114] S. R. Steinhubl, E. D. Muse, and E. J. Topol, “The emerging field of mobile health,” *Sci. Transl. Med.*, vol. 7, no. 283, pp. 1–7, 2015.

[115] R. J. Shaw, J. P. Bonnet, F. Modarai, A. George, and M. Shahsahebi, “Mobile health technology for personalized primary care medicine,” *American Journal of Medicine*, vol. 128, no. 6. 2015.

[116] B. P. L. Lo, H. Ip, and G.-Z. Yang, “Transforming Health Care: Body Sensor Networks, Wearables, and the Internet of Things,” *IEEE Pulse*, vol. 7, no. 1, pp. 4–8, Jan. 2016.

[117] J. Dieffenderfer *et al.*, “Low-Power Wearable Systems for Continuous Monitoring of

Environment and Health for Chronic Respiratory Disease," *IEEE J. Biomed. Heal. Informatics*, vol. 20, no. 5, pp. 1251–1264, Sep. 2016.

[118] V. Misra *et al.*, "Flexible technologies for self-powered wearable health and environmental sensing," *Proc. IEEE*, vol. 103, no. 4, 2015.

[119] W. Dargie, "Dynamic power management in wireless sensor networks: State-of-the-art," *IEEE Sens. J.*, vol. 12, no. 5, 2012.

[120] B. Srbinovski, M. Magno, B. O'Flynn, V. Pakrashi, and E. Popovici, "Energy aware adaptive sampling algorithm for energy harvesting wireless sensor networks," in *SAS 2015 - 2015 IEEE Sensors Applications Symposium, Proceedings*, 2015.

[121] Y. Han *et al.*, "A self-powered insole for humanmotion recognition," *Sensors (Switzerland)*, vol. 16, no. 9, 2016.

[122] L. González-Villanueva, S. Cagnoni, and L. Ascari, "Design of a wearable sensing system for human motion monitoring in physical rehabilitation," *Sensors (Switzerland)*, vol. 13, no. 6, 2013.

[123] A. K. Witte and R. Zarnekow, "Transforming personal healthcare through technology - A systematic literature review of wearable sensors for medical application," in *Proceedings of the Annual Hawaii International Conference on System Sciences*, 2019, vol. 2019-January.

[124] J. M. Pevnick, K. Birkeland, R. Zimmer, Y. Elad, and I. Kedan, "Wearable technology for cardiology: An update and framework for the future," *Trends in Cardiovascular Medicine*, vol. 28, no. 2. 2018.

[125] X. Zhang, Z. Zhang, Y. Li, C. Liu, Y. X. Guo, and Y. Lian, "A 2.89 μw Dry-Electrode Enabled Clockless Wireless ECG SoC for Wearable Applications," *IEEE J. Solid-State Circuits*, vol. 51, no. 10, 2016.

[126] H. Bhamra, J. Lynch, M. Ward, and P. Irazoqui, "A Noise-Power-Area Optimized Biosensing Front End for Wireless Body Sensor Nodes and Medical Implantable Devices," *IEEE Trans. Very Large Scale Integr. Syst.*, vol. 25, no. 10, 2017.

[127] N. E. Klepeis *et al.*, "The National Human Activity Pattern Survey (NHAPS): A resource for assessing exposure to environmental pollutants," *J. Expo. Anal. Environ. Epidemiol.*, vol. 11, no. 3, 2001.

[128] L. J. L. Ruiz *et al.*, "Self-Powered Cardiac Monitoring: Maintaining Vigilance with Multi-Modal Harvesting and E-Textiles," *IEEE Sens. J.*, vol. 21, no. 2, pp. 2263–2276, 2021.

[129] N. Arora, B. Mishra, and Y. Vora, "A low power wearable device for real-time electrocardiogram monitoring and cardiovascular arrhythmia detection for resource

constrained regions," in *Journal of Low Power Electronics*, 2019, vol. 15, no. 2.

[130] S. Song *et al.*, "A 769 μW Battery-Powered Single-Chip SoC with BLE for Multi-modal Vital Sign Monitoring Health Patches," *IEEE Trans. Biomed. Circuits Syst.*, 2019.

[131] W. K. Lee, H. Yoon, and K. S. Park, "Smart ECG Monitoring Patch with Built-in R-Peak Detection for Long-Term HRV Analysis," *Ann. Biomed. Eng.*, vol. 44, no. 7, 2016.

[132] A. Tobola *et al.*, "Self-Powered Multiparameter Health Sensor," *IEEE J. Biomed. Heal. Informatics*, vol. 22, no. 1, 2018.

[133] M. Haghi, K. Thurow, and R. Stoll, "Wearable Devices in Medical Internet of Things: Scientific Research and Commercially Available Devices," *Healthc. Inform. Res.*, vol. 23, no. 1, p. 4, 2017.

[134] A. Aliverti, "Wearable technology: Role in respiratory health and disease," *Breathe*, vol. 13, no. 2, pp. e27–e36, 2017.

[135] S. K. Kundu, S. Kumagai, and M. Sasaki, "A wearable capacitive sensor for monitoring human respiratory rate," *Jpn. J. Appl. Phys.*, vol. 52, no. 4 PART 2, 2013.

[136] A. Al-Halhouli, L. Al-Ghussain, S. El Bouri, H. Liu, and D. Zheng, "Fabrication and evaluation of a novel non-invasive stretchable and wearable respiratory rate sensor based on silver nanoparticles using inkjet printing technology," *Polymers (Basel).*, vol. 11, no. 9, 2019.

[137] M. Chu *et al.*, "Respiration rate and volume measurements using wearable strain sensors," *npj Digit. Med.*, vol. 2, no. 1, pp. 1–9, 2019.

[138] P. Sharma, X. Hui, J. Zhou, T. B. Conroy, and E. C. Kan, "Wearable radio-frequency sensing of respiratory rate, respiratory volume, and heart rate," *npj Digit. Med.*, vol. 3, no. 1, pp. 1–10, 2020.

[139] P. Date *et al.*, "Internet of Things (IoT): A vision, architectural elements, and future directions," *Proc. 2015 Int. Conf. Compil. Archit. Synth. Embed. Syst.*, vol. 29, no. 7, p. 187, 2015.

[140] J. A. Walsh, E. J. Topol, and S. R. Steinhubl, "Novel wireless devices for cardiac monitoring," *Circulation*, vol. 130, no. 7, 2014.

[141] B. Hopenfeld, M. S. John, D. R. Fischell, P. Medeiros, H. P. Guimarães, and L. S. Piegas, "The Guardian: an implantable system for chronic ambulatory monitoring of acute myocardial infarction," *J. Electrocardiol.*, vol. 42, no. 6, pp. 481–486, 2009.

[142] Y. Yang, X. J. Wei, and J. Liu, "Suitability of a thermoelectric power generator for implantable medical electronic devices," *J. Phys. D. Appl. Phys.*, vol. 40, no. 18, pp. 5790–5800, 2007.

[143] S. Ayazian and A. Hassibi, “Delivering optical power to subcutaneous implanted devices,” *Proc. Annu. Int. Conf. IEEE Eng. Med. Biol. Soc. EMBS*, pp. 2874–2877, 2011.

[144] C. Dagdeviren *et al.*, “Conformal piezoelectric energy harvesting and storage from motions of the heart, lung, and diaphragm,” *Proc. Natl. Acad. Sci. U. S. A.*, vol. 111, no. 5, pp. 1927–1932, 2014.

[145] A. J. WOAKES and P. J. BUTLER, “An Implantable Transducer for the Measurement of Respiratory Air Flow,” in *A Handbook on Biotelemetry and Radio Tracking*, Elsevier, 1980, pp. 287–292.

[146] M. Shikida, T. Matsuyama, · Takayuki Yamada, M. Matsushima, and · Tsutomu Kawabe, “Development of implantable catheter flow sensor into inside of bronchi for laboratory animal,” *Microsyst. Technol.*, vol. 23, pp. 175–185, 2017.

[147] H. Hafezi, T. L. Robertson, G. D. Moon, K. Y. Au-Yeung, M. J. Zdeblick, and G. M. Savage, “An ingestible sensor for measuring medication adherence,” *IEEE Trans. Biomed. Eng.*, vol. 62, no. 1, pp. 99–109, 2015.

[148] Z. S. Chen, Y. M. Yang, and G. Q. Deng, “Analytical and experimental study on vibration energy harvesting behaviors of piezoelectric cantilevers with different geometries,” *1st Int. Conf. Sustain. Power Gener. Supply, SUPERGEN ’09*, pp. 1–6, 2009.

[149] C. Sun, L. Qin, F. Li, and Q. M. Wang, “Piezoelectric energy harvesting using single crystal Pb(Mg1/3Nb2/3)O 3-xPbTiO3 (PMN-PT) Device,” *J. Intell. Mater. Syst. Struct.*, vol. 20, no. 5, pp. 559–568, 2009.

[150] A. Holst, “IOT connected devices by use case 2030,” Statista, 19-Oct-2021. [Online]. Available: https://www.statista.com/statistics/1194701/iot-connected-devices-use-case/. [Accessed: 10-Aug-2021].

[151] A. Kunst, “EHealth Tracker / Smart Watch usage by brand in the United States 2021,” Statista, 24-Aug-2021. [Online]. Available: https://www.statista.com/forecasts/997195/ehealth-tracker-smart-watch-usage-by-brand-in-the-us. [Accessed: 10-Aug-2021].

[152] “AFIB: Atrial fibrillation symptoms and diagnosis,” Withings. [Online]. Available: https://www.withings.com/us/en/health-insights/about-afib. [Accessed: 21-Aug-2021].

[153] “Alive Bluetooth Heart & Activity Monitor,” Alive Technologies. [Online]. Available: https://www.alivetec.com/pages/alive-bluetooth-heart-activity-monitor. [Accessed: 13-Mar-2021].